Performance analysis and improvement of a small locally produced wind turbine for developing countries

N. Hosman

March 16, 2012

Master of Science Thesis

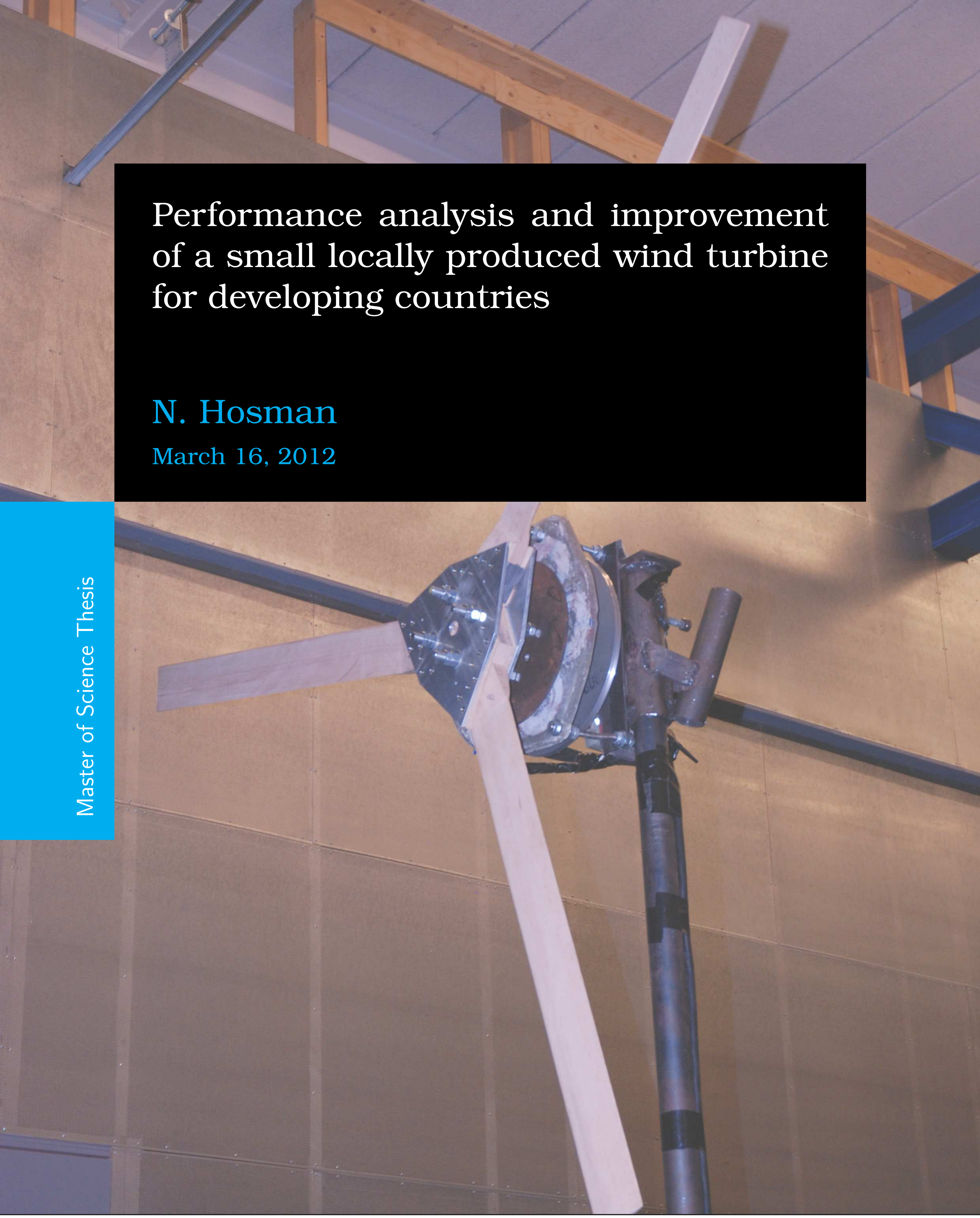

Faculty of Aerospace Engineering

TU Delft

Delft University of Technology

Performance analysis and improvement of a small locally produced wind turbine for developing countries

Master of Science Thesis

For obtaining the degree of Master of Science in Sustainable Energy Technology at Delft University of Technology

N. Hosman

March 16, 2012

Faculty of Aerospace Engineering · Delft University of Technology

STICHTING Energy Solutions For Humanity

Delft University of Technology

Cover picture: The new straight bladed rotor during wind tunnel experiments

Delft University Of Technology
Department Of
Aerodynamics and Wind Energy

The undersigned hereby certify that they have read and recommend to the Faculty of Applied Sciences for acceptance a thesis entitled **"Performance analysis and improvement of a small locally produced wind turbine for developing countries"** by **N. Hosman** in partial fulfillment of the requirements for the degree of **Master of Science**.

Dated: March 16, 2012

Professor: ______________________
prof.dr. G.J.W. van Bussel

Supervisors: ______________________
ir. J.J.H.M. Sterenborg

____
ir. W.A. Timmer

Reader: ______________________
dr. ir. J.C. Diehl

Abstract

In rural areas of Mali people depend on off-grid gasoline generators for the supply of electricity. Due to the import of expensive gasoline, electricity prices are very high and only few people can afford it. To make electricity cheaper and to stimulate the local economy, local renewable energy sources could be the solution. Due to the use of basic materials and tools for the production, home built wind turbines are one of the most promising alternatives in these regions. The wind turbine designs by Hugh Piggott are famous for this. Although there is a lot of knowledge by many home wind turbine builders about this type of wind turbines, there is a lack of good performance measurements that is required for the further improvement of these machines.

This thesis describes the performance identification of a small 1.8 m diameter wind turbine, based on the design of Hugh Piggott. It also presents a new rotor design as an alternative for the current rotor.

Wind tunnel experiments are conducted to identify the rotor performance, generator efficiency and furling behaviour of the 1.8 m turbine. Together with the manufacturability of the turbine this forms a complete overview of this type of wind turbines. Improvements can be gained in all before mentioned aspects. However, for operation and local production in developing countries with a low average wind speed like Mali it is most interesting to improve the power efficiency at low wind speeds and the ease of the production process of the rotor. For this reason it was decided to focus on a more simple design as an alternative to the current rotor.

Out of several design concepts a simple straight wooden rotor was found to be the most simple and efficient option. The rotor is a three-bladed rotor with untwisted and untapered blades that can be carved from wood using an airfoil template. The simplicity of the design makes production easier, lowering manufacturing errors and increasing the uniformity of the product. Furthermore, because of the smaller wood dimensions that are required, availability of the material has increased.

A second set of wind tunnel measurements has been conducted to test whether this new wind turbine rotor has an improved performance. The maximum performance of the new rotor is found to be only slightly better. However, since the new rotor is designed for a higher tip speed ratio it has a better generator matching at low wind speeds. This leads to significant improvements for operation in the Malian wind climate.

Preface

At the beginning of 2011, when I was looking for a thesis project, I was introduced to Piet Willem Chevalier and the i-love-windpower movement. The fact that a wind turbine could be built from scratch by just using simple tools and materials immediately caught my attention. Up till then I hadn't gained so much practical experience, and this project was the ultimate opportunity for this.

The project started with a workshop in May 2011, where we built the small wind turbine during a workshop of the i-love-windpower movement. I would like to thank everyone who helped me building the wind turbine and the experimental set-up for the wind tunnel tests.

Special thanks go to Piet and Joost. Piet, thank you for giving me the opportunity to start this project. Joost, I couldn't be more happy with you as a supervisor. Thank you so much for helping me with the wind tunnel tests and spending your precious time on giving me feedback. I wish Piet and Joost all the luck in the world to bring the project in Mali to a great success.

Furthermore I would like to thank Gerard van Bussel and Nando Timmer for their support and advice. The meetings where we discussed the progress of my work were a great help to me.

Finally I would like to thank my parents for supporting me all these years of my studies. And last but not least, Vincent, thank you so much for all your love, help and support.

Nienke Hosman
The Hague, February 29, 2012

"Simplicity is the ultimate sophistication"
— *Leonardo da Vinci*

Contents

Nomenclature

Latin Symbols

a	Axial induction factor	[-]
a'	Tangential induction factor	[-]
$a_{rotor,m}$	Measured rotor acceleration	[m/s^2]
B	Number of blades	[-]
c	Chord	[mm]
C_d	Drag coefficient	[-]
C_l	Lift coefficient	[-]
C_n	Normal load coefficient	[-]
C_P	Power coefficient	[-]
$C_{P,max}$	Maximum power coefficient	[-]
C_T	Thrust coefficient	[-]
C_t	Tangential load coefficient	[-]
d	Offset between rotor axis and yaw bearing	[m]
$D_{blade,c}$	Calculated drag for a single blade	[N]
$D_{blade,m}$	Measured drag for a single blade	[N]
d_p	Prony brake rope diameter	[mm]
E	Elasticity modulus	[MPa]
E_{month}	Monthly energy production for a given mean wind speed	[kWh]
f_{ax}	Axial force	[N]
F_f	Friction force in the prony brake pulley	[N]
F_l	Force of the prony brake rope measured in the load cell	[N]
f_{tan}	Tangential force	[N]

F_w	Force of the weights on the prony brake rope	[N]
I	Electrical current	[A]
I_x	Second moment of inertia	[mm^4]
L	Length of a beam	[mm]
M	Bending moment	[Nm]
m_{blade}	Blade mass	[kg]
M_{tail}	Tail moment	[Nm]
M_{yaw}	Yaw moment	[Nm]
P	Power	[W]
P_{aero}	Aerodynamic power	[W]
P_{bat}	Battery output power	[W]
P_{dump}	Dump load power	[W]
P_{gen}	Generator power	[W]
$P_{loss,Rc}$	Power loss by the resistance of the cables R_c	[W]
$P_{loss,rect}$	Power loss in the rectifier	[W]
P_{mean}	Wind turbine power at a given mean wind speed	[W]
P_{wt}	Wind turbine power	[W]
Q	Torque	[Nm]
$Q_{start-up}$	Start-up torque	[Nm]
r	Radius	[mm]
R_c	Resistance of ground cables, from rectifier to dump load	[Ω]
R_{coil}	Measured average resistance of a coil (+ extended wire to ground)	[Ω]
r_{drag}	Distance from blade root at which the resultant drag force acts	[m]
R_{dump}	Total dummy load resistance	[Ω]
Re	Reynolds number	[-]
R_p	Prony brake pulley radius	[mm]
R_r	Blade root radius	[m]
R_{stator}	Resistance of the stator	[Ω]
R_t	Blade tip radius	[m]
t	Thickness	[mm]
t	Time	[s]
U	Wind velocity	[m/s]
U_{cut-in}	Cut-in wind speed	[m/s]
U_m	Uncorrected wind speed	[m/s]
U_{mean}	Mean wind speed	[m/s]
U_{eff}	Effective blade velocity	[m/s]
$U_{start-up}$	Start-up wind speed, no load attached	[m/s]
V_{bat}	Battery voltage	[V]
V_{dump}	Dump load voltage	[V]

V_{wt}	Wind turbine voltage	[V]
W	Weight	[g]
y	Distance to neutral axis	[mm]
z	Rotor height	[m]
z_{ref}	Reference height	[m]
z_0	Roughness length	[m]

Greek Symbols

α	Angle of attack	[deg],[°]
γ	Yaw angle	[deg],[°]
δ	Deflection of a beam	[mm]
η_{dump}	Dump load power efficiency	[%]
η_{gen}	Generator efficiency	[%]
η_{match}	Efficiency of the generator-rotor matching	[%]
η_{wt}	Wind turbine efficiency	[%]
θ	Blade pitch angle	[deg],[°]
θ_c	Blade pitch angle correction for θ to θ_m	[deg],[°]
θ_m	Blade pitch angle, measured from flat pressure side	[deg],[°]
λ	Tip speed ratio	[-]
ρ	Air density	[kg/m^3]
σ	Bending stress	[N/mm^2]
σ_{max}	Ultimate bending stress	[N/mm^2]
ϕ	Inflow angle	[deg],[°]
ψ	Tail angle	[deg],[°]
ω	Rotational speed	[rpm]

Abbreviations

BEM	Blade Element Momentum
HP	Hugh Piggott
OJF	Open Jet Facility
SB	Straight bladed

Chapter 1

Introduction

This introductory chapter provides background information about the subject and describes the scope and incentive for this thesis project. Furthermore the research objectives are given and the structure of the report is described.

1.1 Background

Mali is considered to be one of the poorest countries in the world, being ranked 175th among the 187 countries on the United Nations Human Development Index [UNDP, 2011]. Most people live in rural areas where energy consumption is dominated by traditional sources such as wood and crop waste. The national power grid covers only a few urban areas, leaving 95% of the total population without access to electricity [REEEP, 2010].

People living in the rural areas are dependent mostly on batteries for electricity supply, which are usually charged by small gasoline driven generators which are run by local entrepreneurs. Due to rising gasoline prices the price of electricity per kWh is therefore extremely high in these regions, up to 85 eurocents per kWh [i-love-windpower, 2011]. For these regions a decentralized electricity production using renewable energy sources would be much more interesting.

For this reason in 2010 the foundation 'Energy Solutions for Humanity' was founded. This non profit organization will promote and setup energy solutions in developing countries thereby focusing on training disadvantaged people and on providing affordable electricity to the rural areas [i-love-windpower, 2011]. One of the movements of this organization is the i-love-windpower movement, which defines the following goals:

- Provide access to affordable electricity for the rural population of Mali
- Provide a renewable energy alternative rather than the current unsustainable methods of energy supply
- Provide technical training, employment and income to especially the uneducated population
- Provide energy security

Together with a Malian group of workers 6 wind turbines have been built in Mopti yet, of which one is currently operating. The other ones are almost finished, waiting for final wind turbine parts like the tower.

The design of the wind turbines is based on the open source wind turbine design by Hugh Piggott [Piggott, 2008]. Piggott provides a manual on how to build your own wind turbine using just basic tools and materials. This makes it a very attractive option for developing countries, since it gives local people the possibility to produce these turbines, eventually, on their own. Also other small wind turbine manuals exist, for example the book 'Homebrew Wind Power' [Bartmann and Fink, 2009], but most use the same kind of design as Piggott does.

Figure 1.1: The Hugh Piggott wind turbines that are built by the i-love-windpower movement in Mopti, Mali

1.2 Problem Statement

Piggott wind turbines are being built all over the world by many organizations that aim for energy supply in rural (developing) areas. One of those companies is RIWIK, founded by TU

Delft student Bart Fugers [RIWIK, 2011]. RIWIK is going to supply wind turbine kits based on the design by Piggott to local craftsman in rural Kenya. Recently the association 'Wind Empowerment' has also been founded, which is an international association that provides a knowledge sharing forum for the development of locally built small wind turbines for sustainable rural electrification. The open sharing of information is a good step forward in the improvement of small wind turbines.

Some organizations involved in building small wind turbines try to improve the wind turbine in order to fulfill their specific needs better. To determine what improvements would be most effective, the performance of the original wind turbine should be known. Despite the fact that many people are building these wind turbines and a lot of information can be found on the Internet, there is a lack of good performance measurements. Usually testing is limited to field testing, where operational conditions cannot be controlled.

The research objective of this thesis consisted of two parts. The first was to identify the performance of the Hugh Piggott wind turbine, as it is used by the i-love-windpower movement in Mali. The second part was to design a new wind turbine that has improved compared to the current wind turbine in one or more aspects.

The complete research objective was defined as follows:

1. Identify the performance of the Hugh Piggott wind turbine as it is used in Mali
    - Identify the performance of the wind turbine by means of literature and field research, a mathematical model and wind tunnel experiments
    - Compose a list of possible improvements for a new wind turbine
2. Design a new wind turbine that has improvements in one or more aspects
    - Choose one or several of the possible improvements to continue working on
    - Compose several design concepts and work out the most favorable concept in detail
    - Perform wind tunnel experiments to test whether the improvement was successful

1.3 Report outline

The contents of this report can be divided into three parts:

1. Identification - What could be improved?
2. Design - How could this be improved?
3. Evaluation - Is the improvement successful?

A more detailed structuring of the report is given in Figure 1.2.

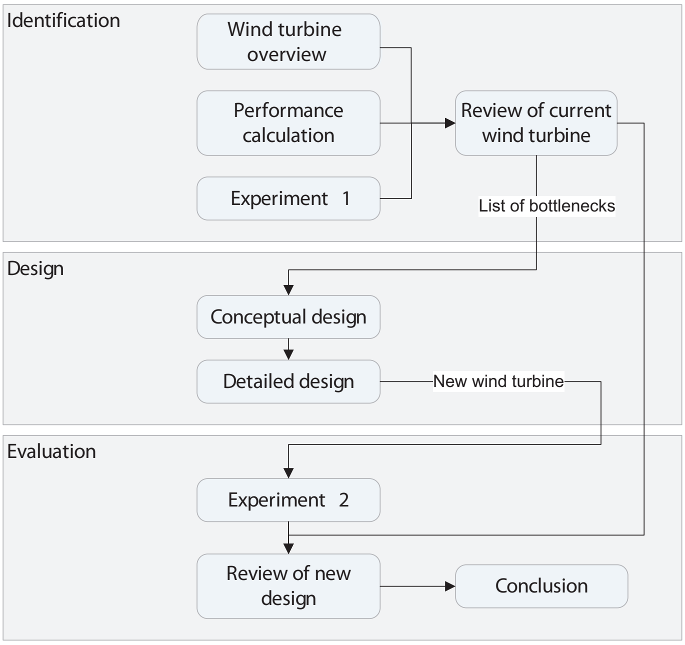

Figure 1.2: Report structure

The thesis starts with an overview of the current wind turbine for the specific location of Mali in Chapter 2. Using the rotor geometry of the current turbine and the Blade Element Momentum (BEM) model, the aerodynamic performance of the rotor is calculated in Chapter 3. Wind tunnel measurements are performed to measure the complete performance of the turbine, of which the set-up and results are described in Chapter 4. These first three chapters form the basis of the total identification of the current wind turbine. An evaluation of the current wind turbine based on these chapters, including a list of possible improvements, is given in Chapter 5.

Based on the improvements set in Chapter 5 the choice was made to make a new design for the rotor. Chapter 6 gives three possible design concepts and in Chapter 7 the most favorable concept is worked out in detail. To evaluate the performance of this new wind turbine and compare it with the original turbine, a second measurement campaign is performed, presented in Chapter 8. Chapter 9 gives an evaluation on the improvements of the new wind turbine rotor. Finally the conclusions for this thesis and recommendations for further research are given in Chapter 10.

Chapter 2

An overview of the Hugh Piggott 1.8m wind turbine

There are a few different wind turbine sizes available in the manual of Hugh Piggott [Piggott, 2008], with diameters ranging from 1.2 m to 4.2 m. In Mali currently the 3.0 m diameter turbine is built most often. However, the size of this turbine is too large to be tested in the Open Jet Facility wind tunnel at the TU Delft, as described in Chapter 4. Therefore, for this thesis the 1.8 m turbine will be investigated. Both turbines are based on the same design principle and it is therefore assumed that the performance of the 1.8 m turbine is representative for the performance of the larger turbine. The effects of the rotor size on the performance will be discussed in the evaluation of the test results. In this chapter a general overview of the Hugh Piggott turbine is given, as well as the specific details for the 1.8 m turbine that is built for this thesis.

In Figure 2.1 an overview of the wind turbine components is given. In this chapter the different parts of the wind turbine are discussed one by one. This includes the rotor, the generator (alternator), the furling system (the tail) and the support structure, presented in Section 2.1 to Section 2.4. An overview of wind turbine manufacturing and costs is given in Section 2.5. Since this thesis is concentrating on the wind turbine as it is built by the i-love-windpower movement in Mali, the wind climate in Mali is discussed in Section 2.6. In Section 2.7 the estimated power and monthly energy production according to the Piggott manual is given. The chapter is concluded with an overview of the different aspects that are important to consider when evaluating or designing a wind turbine for Mali and other developing countries.

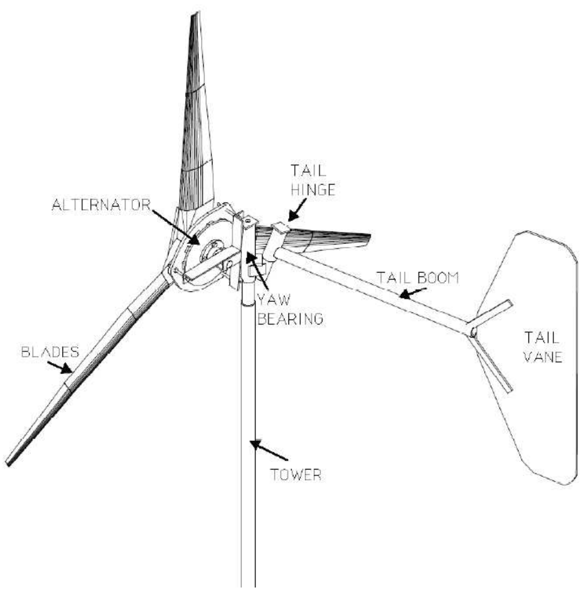

Figure 2.1: Wind turbine components, [Piggott, 2008]

2.1 The rotor

The rotor of the Hugh Piggott wind turbine is a three-bladed rotor with tapered and twisted wooden blades. In this section the advantages and disadvantages of the use of wood as a blade material are discussed first. After that the rotor geometry of the 1.8m turbine and modifications to the original design are described.

2.1.1 Wood as a blade material: advantages and disadvantages

The current rotor designed by Hugh Piggott is made of wood. Wood is a material that is widely used by home wind turbine builders all over the world. The advantages of wood as a blade material for building the current wind turbine in Mali can be listed as follows:

- Only simple tools are required to work with wood
- Wood has very good strength
- Wood is known to be durable
- The group of workers that is building the wind turbines in Mali now has some experience with wood working

The following disadvantages of the use of wood in Mali are known:

- Good quality wood in large dimensions is difficult to obtain in Mali
- Due to termites, wood storage is problematic in Mali
- For the current rotor design, with simple tools wood working costs a lot of time

Overall wood can be regarded as a suitable material for small scale usage, since it requires little tools to work with and it has good strength. The type of wood that is used to build the 1.8 m rotor for this thesis is Oregon pine wood, which is good quality wood which is comparable to the wood that is used in Mali for the 3.0 m turbine.

2.1.2 Rotor geometry

The rotor is produced according to the Hugh Piggott production manual [Piggott, 2008]. There are a few modifications to this, in order to install all the required testing equipment:

- A pulley that is required for the prony brake measurements (Section 4.3.1) is mounted on the hub between the frame and the alternator, see Figure 8.1
- The prony brake measurements require that the rotor is placed vertically, and not tilted by 4° as is described in the manual

Also, the nose (leading edge) of the blades is sharper than described in the manual. However, since the wind turbine is a hand-made product, similar errors in the production process will always occur, because there is a certain tolerance in the production process. For experiment 2 the nose will be rounded and the effect of this on the power that can be produced will be measured.

In Figures 2.2, 2.3 and 2.4 the designed geometry and the actual geometry for all three blades of the 1.8 m turbine is given. With the designed geometry the geometry according to the Hugh Piggott manual is meant. The actual geometry is the real geometry of the rotor, measured with an electronic caliper and a digital angle gauge. The geometry is expressed in blade angle θ_m, chord c and relative thickness t/c. The blade angle θ_m is measured from the straight pressure side of the airfoil.

It can be observed that the measured chord c only has a small error compared to the design. The blade angle θ_m shows a larger error, since this value can not be easily measured and checked

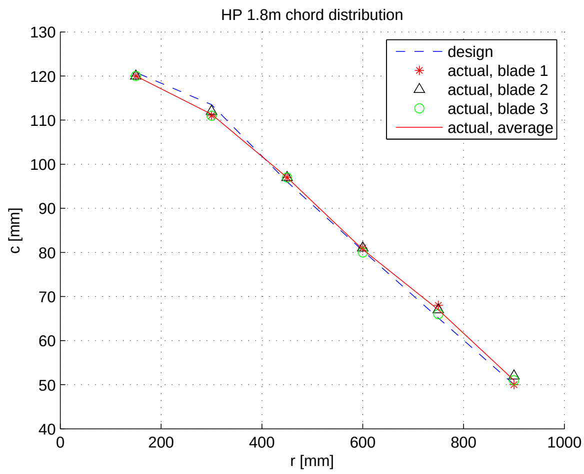

Figure 2.2: Chord distribution, for design and actual geometry of the HP 1.8m rotor

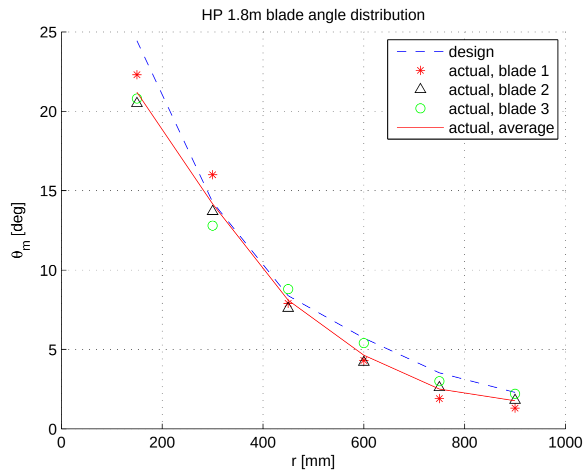

Figure 2.3: Blade angle distribution, for design and actual geometry of the HP 1.8m rotor

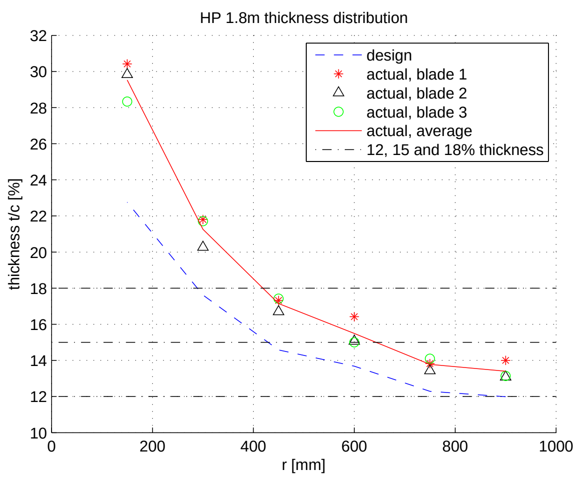

Figure 2.4: Thickness distribution, for design and actual geometry of the HP 1.8m rotor

during production. Also the thickness t/c shows a large error, which is mainly caused by the fact that the thickness dimensions are relatively small (only a few mm) and therefore mistakes are more easily made. The rotor geometry will be used to calculate the aerodynamic performance of the rotor, which is described in Chapter 3. In that chapter also the airfoils of the rotor are described.

2.2 The generator

The generator of the turbine (also called the alternator) is a permanent magnet axial flux generator. The magnets are mounted on a steel disk that is placed on the hub and rotates with the blades. For the 1.8 m turbine there is a steel disk facing the magnet disk, for larger turbines there are two magnet disks facing each other. There is a strong magnetic flux in the space between these two disks. In that space the stator is mounted, which is a disk consisting of copper coils. By rotating the steel disks, when a magnet passes a coil the magnetic flux will induce a voltage in that coil. When the copper coils are connected to an external circuit a current can flow and power can be produced. The stator and rotor disks are shown in Figure 2.5. After the copper coils are connected to each other (as described further in this section) they are cast in polyester resin. For the magnet disks this is done as well.

The generator of the wind turbine can be built for a 12 V, 24 V or 48 V system. For the 1.8 m turbine that is built a 12 V system is chosen. For the 12 V system the six coils in the stator are connected in parallel (star connection), which implies that six end wires come out of the wind turbine stator. These end wires are extended by 2 m to the ground. The total measured resistance of one copper coil + extended wire amounts $R_{coil} = 0.47\,\Omega$.

To convert the voltage from AC to DC a rectifier is used, which consists of a series of diodes. During normal operation the system would be connected to a 12 V battery. To protect the battery from overcharge a load controller (the Morningstar Tristar is currently used for this) is required.

The connecting circuit that will be used during experiment 1 (Chapter 4) also includes the rectifier, but the battery is replaced by a large dummy load resistance. Because overcharge is not

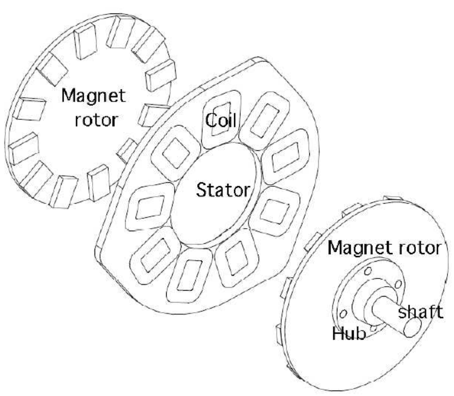

Figure 2.5: Exploded view of the generator [Piggott, 2008]: the rotor (magnet disks) and stator (coils). For the 1.8 m wind turbine the left magnet rotor disk is replaced by a steel disk.

a danger, a load controller is not required. The electrical circuit used for these tests is described in Section 4.3.2.

It is very important that the turbine is in open circuit at the start-up of the wind turbine, since otherwise the sticking force of the generator will increase the start-up speed. Therefore the turbine has to be connected to a rectifier and a battery, and cannot be connected directly to a load. When the turbine is connected to a battery the turbine will not experience a load until $V_{wt} > V_{bat}$ and therefore the turbine is free to start-up. A resistive load will also pose a load on the turbine during start-up and therefore the start-up speed will be higher.

The battery operation causes the wind turbine to operate at variable rotational speed and tip speed ratio. The tip speed ratio during operation at low wind speeds is high and decreases with increasing wind speed. The rotational speed increases with increasing wind speed.

Because the coils are connected in parallel, the total equivalent resistance of the stator is lower than the resistance of a single coil. In the manual [Piggott, 2008] Piggott gives the following equation to calculate the equivalent stator resistance:

$R_{stator} = 2 \cdot (\text{coils in series/coils in parallel}) \cdot R_{coil} = 2 \cdot (1/6) \cdot 0.47 = 0.16\,\Omega$

This resistance in the coil wires causes a loss in the stator, which is converted to heat. For this reason, when the generator is overloaded and the rotational speed becomes too high, the risk of burn out of the wires exists.

2.3 Overspeed protection

If the wind speed increases beyond a certain point, the danger of overload is present. This implies that the blades may overspeed, the generator may overheat, and the forces on the support structure may become too large. To prevent the turbine from overloading, a furling tail is mounted on the turbine.

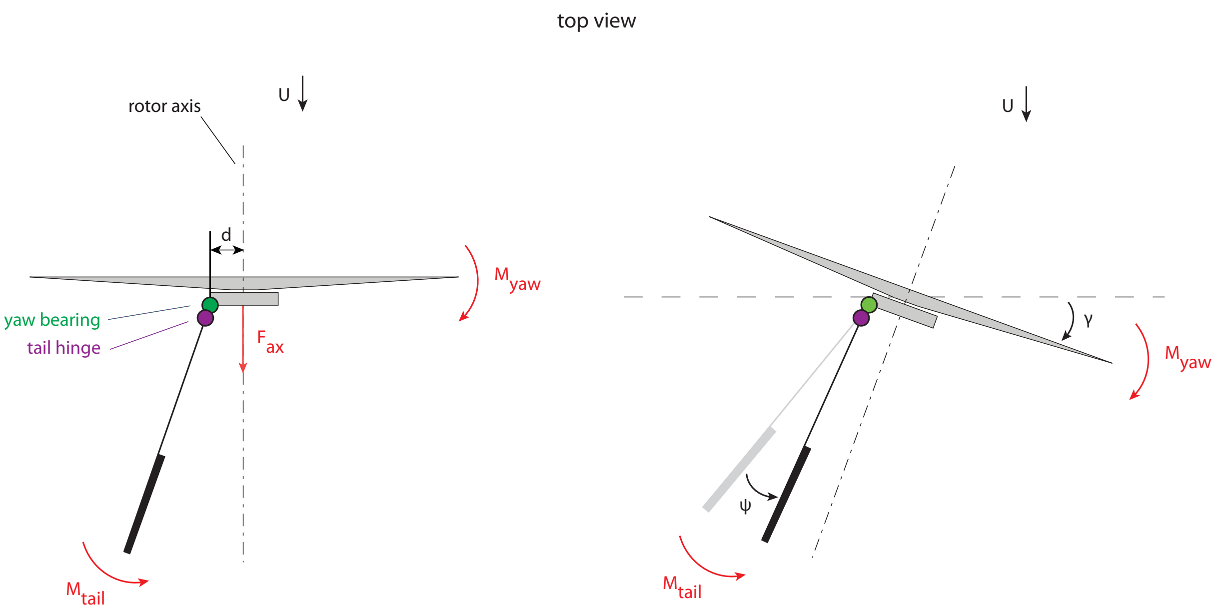

Figure 2.6: Drawing of the furling mechanism and definitions of the yaw angle γ and tail angle ψ

The principle of the furling system is shown in Figure 2.6 and can be explained as follows. The rotor axis is mounted offset from the yaw bearing by a distance d. By the thrust force F_{ax} of the rotor a yawing moment M_{yaw} around the yaw bearing is created, trying to turn the wind turbine out of the wind. The tail is mounted a little sideways, such that on the tail a restoring moment M_{tail} in opposite direction of the yaw moment is created. The tail hinge is 20 degrees off vertical (Figure 2.1). This means that the tail can only rotate around the tail hinge in positive tail angle ψ direction if the tail moment is large enough to lift the weight of the tail. At low wind velocities the tail moment is too small to lift the weight, and therefore the turbine is held in place. At higher wind speeds both the yaw moment and the tail moment will increase. At a certain point the moment of the furling tail will be high enough to move the tail sideways and slightly up around the tail hinge. This will allow the wind turbine to turn out of the wind. A new equilibrium will be established.

The definitions of the yaw angle γ and tail angle ψ are given in Figure 2.6.

In the most efficient case the wind turbine should have a zero yaw angle at low wind speeds and only start furling at wind speeds where the risk of overloading is present. The weight of the tail is important for correct furling. By making the tail heavier the furling can be delayed, because the tail moment has to be larger before the tail can be moved up and sideways. Also the area of the tail vane is an important parameter for correct furling. To optimize the tail, usually some trial and error on sizing the tail is required. The tail of the 1.8 m turbine built for this thesis is just built according to the manual, without additional tuning.

Both the yaw and tail bearing are very simple bearings that consist of two pieces of steel pipe, one inside the other. Therefore there is a considerable friction in the bearings which causes the yaw and tail movements to occur not smoothly but in steps, as we will see in the results of experiment 1 in Chapter 4.

2.4 The support structure

The support structure of the wind turbine consists of a steel frame on which the rotor, generator and tail are mounted, and a tower. The bearing hub is usually a rear wheel hub from a car, that can be obtained from the scrap yard. The tower is a thick steel pipe on which guy wires are attached. Normally two pipes of 6 m length are used for a small wind turbine tower, which make a total tower length of 12 m. In this thesis the support structure will not be discussed in much detail. However, some aspects of it are important to mention here. One of the main disadvantages of the use of a guyed tower is that the tower pipe material has to be very thick walled, which makes it an expensive material. The guy wires require a large ground area for the wind turbine. Furthermore maintenance on the wind turbine requires the wind turbine to be lowered to the ground.

It would be very interesting to investigate other options for a tower structure. One of those is a lattice tower, which can be both guyed or unguyed [Wood, 2011]. A lattice tower requires more pipe material, but the dimensions of the pipes are much smaller and therefore the price for one pipe is much cheaper. Because of the usage of more pipes the redundancy of the tower is also much better: when one of the pipes brakes the forces can be transferred to other pipes. A disadvantage of this system could be that the amount of workhours required to build the lattice tower is higher than for a guyed tower. Currently there is one lattice tower built for a wind turbine in Mali. However, an optimization of this lattice tower is required to improve this structure and increase cost savings further.

2.5 Wind turbine manufacturing and costs

In this section the wind turbine manufacturing process and time, material costs and availability of materials in Mali are discussed.

2.5.1 Wind turbine manufacturing

Since this wind turbine is a hand-made product, the manufacturing process is important to consider. In Table 2.1 the manufacturing times for the different components of the the 1.8 m wind turbine are given. The production time is expressed in man hours of the Malian working people, who have built a couple of wind turbines before. Often more than one person is needed to produce a part or assemble the wind turbine, which increases the production time. Working 8 hours a day, a group of 6 people would need 3 days to produce this wind turbine. It should be noted that these manufacturing times are only an estimation. The real manufacturing time is very dependent on the skills and pace of the group of workers.

From the table it can be seen that a large amount of the production time is spent on the production of the rotor. This is mainly caused by the wood carving of the blades into the twisted and tapered shape, which is quite time demanding. Also the production of the generator is quite time demanding, because the copper coils have to be winded and the stator and steel disks have to be cast in polyester resin.

Due to the fact that the wind turbine is hand-made, there is a large tolerance in the production process. This affects the uniformity of the wind turbine. One should keep in mind therefore that other wind turbines than the tested wind turbine in this thesis could perform better or worse. It is assumed that the test wind turbine represents an average wind turbine. One of the possible improvements for a new wind turbine could be to improve the uniformity of the product by simplifying or standardizing the production process.

Component	Material cost [euro]	Production time [man hours]	Production time [%]
Wind turbine components			
Rotor	80	50	36
Tail	40	10	7
Generator	170	40	29
Steel frame	40	20	14
Wind turbine assembly	-	20	14
Total wind turbine	330	140	100
Supporting components			
Charge controller (TriStar)	150	-	-
Electricals (cables and diodes)	50	-	-
Tower (12 m) and guy wires	250	-	-
Batteries (4x)	300	-	-
Total complete system	1080	140	100

Table 2.1: Overview of wind turbine cost and production time per component for the 1.8 m wind turbine. The costs are an estimation of Malian prices converted to euros. The production time is an estimation for the group of Malian workers.

2.5.2 Wind turbine material costs

From Table 2.1 it can be observed that a large part of the total system costs are caused by supporting components. The tower is a very expensive part, because the pipe material is an expensive material, as discussed in Section 2.4. Also the TriStar charge controller is expensive, because this is an off-the-shelf product. The i-love-windpower movement is currently working on a new design such that the charge controller can be produced locally as well. For the wind turbine itself the generator costs are the highest costs, which is caused by the use of strong permanent magnets that are very expensive. The costs presented in the table should be regarded as estimations of Malian prices converted to euros and depend very much on suppliers and quality of the material.

2.5.3 Availability of materials

Most components that are required for the wind turbine can be obtained in Mali itself. For some materials availability in Mali can be poor or even not present at all. Good quality wood is difficult to obtain for wind turbine dimensions larger than the 3.0 m turbine. The wood currently used for the 3.0 m turbine is good quality wood coming from Ivory Coast. Its quality is estimated to be comparable to the Oregon pine wood that is used for the wind turbine workshops in the Netherlands. As discussed before, the availability of large diameter pipes that are required for the current tower structure is also poor in Mali. The permanent magnets and off-the-shelf charge controller have to be imported from outside the country.

2.6 The wind climate in Mali

To determine how the wind turbine is performing in the wind regime that is most occurring, it is important to consider the wind climate at the wind turbine site in Mopti, Mali. Since measurements are not available from this site, a general windmap of Mali is used, taken from [Nygaard et al., 2008] and shown in Figure 2.7. From this wind map an average wind velocity for Mopti can be taken. However, this wind speed in the map is determined at 50 m height, whereas the wind turbine rotor height would be only 12 m. Since wind speed decreases with a decreasing altitude, it is important to consider the wind speed at the right altitude. Equation 2.1 [Manwell et al., 2009] can be used to convert the wind speed:

$$U(z) = U(z_{ref}) \frac{ln(\frac{z}{z_0})}{ln(\frac{z_{ref}}{z_0})} \tag{2.1}$$

where $U(z)$ is the wind velocity at the rotor height z, $U(z_{ref})$ the wind velocity at the reference height z_{ref} and z_0 the roughness length. From Figure 2.7 the reference wind velocity and corresponding reference height can be found, which are $U(z_{ref}) = 4.8$ m/s and $z_{ref} = 50$ m. When an open terrain exposure is assumed the roughness length is $z_0 = 0.03$ m. Using these values, the wind speed $U(z)$ at $z = 12$ m can be calculated and amounts 4 m/s. Therefore, when the Malian wind climate is referred to in this thesis, a mean wind speed of $U_{mean} = 4$ m/s is meant.

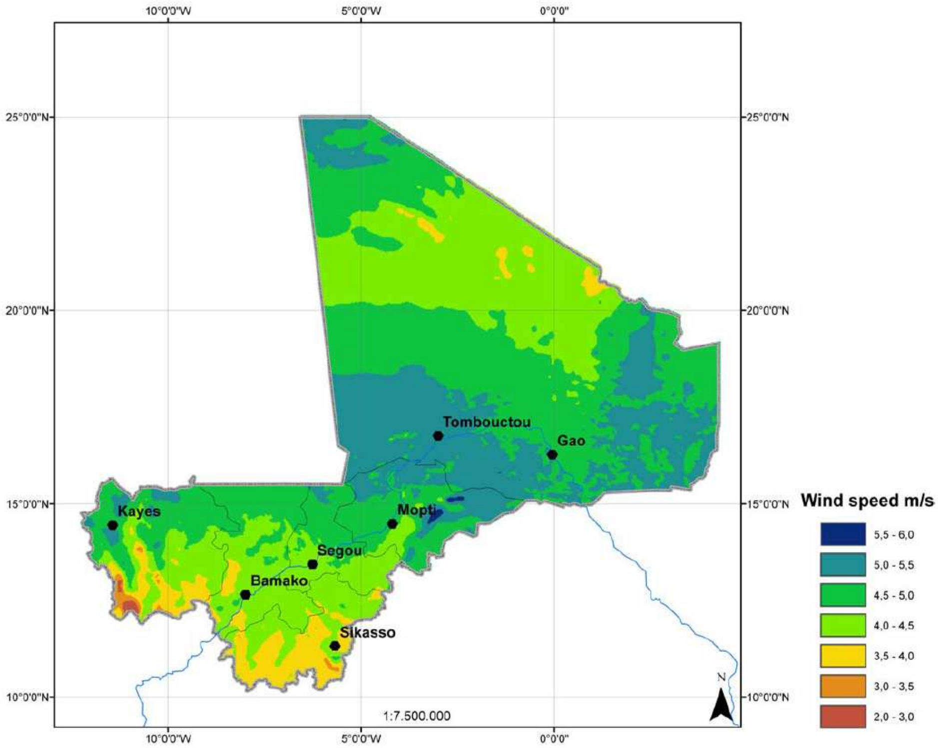

Figure 2.7: Annual mean wind speed for Mali at 50 m above ground level, generalized for a flat surface with roughness length z_0 =0.03 m, [Nygaard et al., 2008]

2.7 Estimated power output and monthly energy production

In the manual Piggott gives the estimated rated power P_{mean} and monthly energy production E_{month} at different mean wind speeds, for all turbine dimensions. In Table 2.2 these values are shown for the 1.8 m and 3.0 m turbines. The mean power P_{mean} can be calculated from the monthly energy production E_{month} and is shown in the table as well. At a mean wind speed of 4 m/s, which is characteristic for Mali, the power output for a 1.8 m turbine is estimated to be 42 W, giving a monthly energy production of 30 kWh. In this thesis the real power for the 1.8 m turbine will be measured.

Table 2.2: Estimated power and monthly energy production at different mean wind speeds, according to Piggott [Piggott, 2008]

Turbine diameter	1.8 m		3.0 m	
Rated power	350 W		800 W	
	P_{mean}	E_{month}	P_{mean}	E_{month}
$U_{mean} = 3$ m/s	17 W	12 kWh	47 W	34 kWh
$U_{mean} = 4$ m/s	42 W	30 kWh	118 W	85 kWh
$U_{mean} = 5$ m/s	74 W	53 kWh	203 W	146 kWh
$U_{mean} = 6$ m/s	103 W	74 kWh	285 W	205 kWh
$U_{mean} = 7$ m/s	128 W	92 kWh	356 W	256 kWh

2.8 Evaluation criteria for small wind turbines in developing countries

The following aspects are important for a wind turbine for developing countries in general and Mali in particular:

- **Performance**
  This aspect can be divided into the following parts:
  - Overall performance (Battery power P_{bat} versus wind speed U))
  - Performance in the Malian wind climate, where $U_{mean} = 4$ m/s
  - Start-up wind speed
- **Difficulty of production**
  An easy production process will minimize the possibility of production errors and ensure a uniform product. Furthermore, only simple production tools are available at the workshop in Mali. Easy production can be divided into the following parts:
  - Tolerance in the production process, affecting the uniformity of the product
  - Production time
  - Tools required for production
- **Availability of good quality materials in Mali**
  Good quality materials are important to ensure the quality and durability of the product. To stimulate the local economy local materials should be used as much as possible.
- **Material costs**
  Material costs should be limited to make the final electricity price as low as possible.

In the following chapters the 1.8 m wind turbine will be evaluated based on these criteria.

Noise production
Since small wind turbines are often placed in residential areas, closer to the user, noise production can also be an issue. In Mali noise production is not of major importance because there is enough space. However, at other locations in developing countries where these wind turbines are used it can be much more an issue. To ensure the relevance of this study for other applications than Mali, it is important to be aware of the noise production. Therefore noise production will be considered as an extra aspect of evaluation in experiment 2, presented in Chapter 8.

Chapter 3

Aerodynamic performance calculations

In this study the performance calculation will be limited to the aerodynamic performance of the 1.8 m rotor. For this the Blade Element Momentum (BEM) theory will be used, which is a fast and simple method, but has limited accuracy. However, as a design tool it is often used in industry and for this purpose it has proven to be a very useful tool. In Appendix A the BEM theory as well as the verification and validation of the model are described.

Before BEM can be applied, the input of the model needs to be defined. This is described in Section 3.1. The results of the BEM calculations are presented in Section 3.2. A sensitivity analysis is done to address the effect of changes in the input parameters on the model output. This is described in Section 3.3.

3.1 Input of the BEM model

As an input for the BEM model, the blade geometry (blade angle θ and chord c) and airfoil characteristics at each blade section are required. For the calculations two different geometries of the rotor are considered, which will be called actual and design geometry. The actual geometry is the measured geometry of the tested rotor. The design geometry is the designed geometry according to the Hugh Piggott manual. In Section 2.1 the blade angle θ_m and chord c distributions for both rotor geometries were shown.

To obtain the airfoil characteristics, the Reynolds number at which the rotor operates and the airfoil shape should be known. In Figure 3.1 the Reynolds numbers for the measured airfoil geometry are shown as a function of blade position, for different wind speeds.

In the catalogue of Hageman [Hageman, 1980] the lift and drag characteristics of airfoils for low Reynolds numbers can be found. To find the airfoils that approximate the shape of the real airfoils best, both the thickness of the blade and airfoil shape are important. The blade thickness was given in Section 2.1 and again shown in Figure 3.2. For the designed geometry thicknesses range from 12% to 22%. For the actual geometry thicknesses are slightly higher, because of the standard production errors.

Piggott based the design on the Naca 4412 airfoil. The Naca 4412 and Naca 4415 airfoils from the catalogue of Hageman are assumed to have the best approximation of the real blade airfoils.

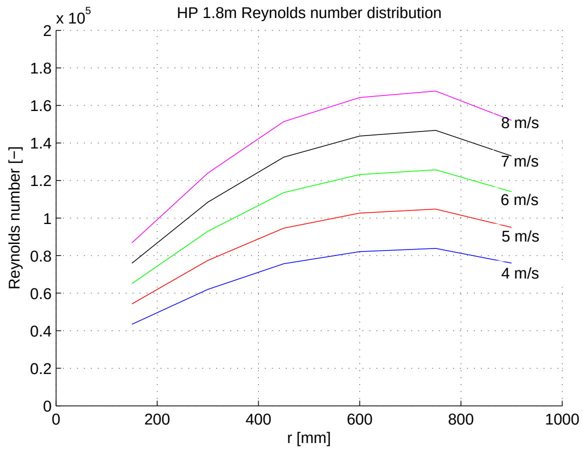

Figure 3.1: Reynolds number distribution for the actual geometry HP 1.8m rotor, for different wind velocities, at $\lambda = 5.5$

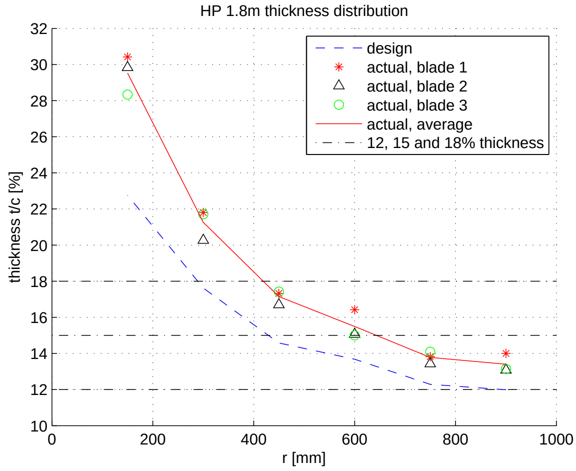

Figure 3.2: Thickness distribution, for design and actual geometry of the HP 1.8m rotor

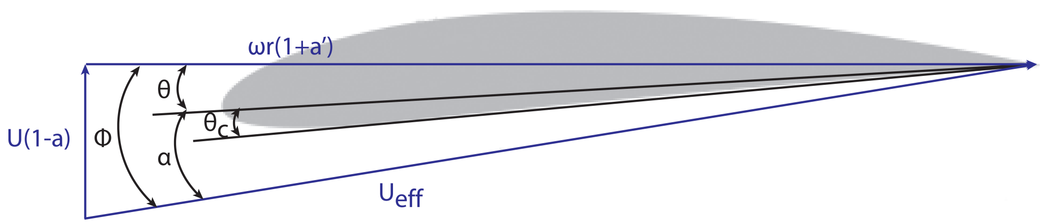

Figure 3.3: Airfoil geometry definitions

The thicknesses of these airfoils are shown in Figure 3.2. The lift and drag characteristics of these airfoils are available for a large range of angle of attack α. At the root a thicker airfoil, like the Naca 4418, would be better. However, since good data of this airfoil was not available for a large range of angle of attack, the root airfoils are also approximated by the Naca 4415.

The blade angles θ_m that are shown in Figure 2.3 are measured from the flat pressure side of the airfoil. However, the zero angle of attack line is defined as the chord line, from leading edge to trailing edge. Therefore, the measured blade angles θ_m have to be corrected to the Naca blade angles θ before they can be used in the BEM model. This is done by subtracting a correction angle θ_c which amounts 1.8° and 2.5° for respectively Naca 4412 and Naca 4415. The blade angles definitions are shown in Figure 3.3.

The Naca 4412 and 4415 data from the Hageman catalogue is taken from experiments from Jacobs and Sherman. The lowest Reynolds number Re for which lift and drag polars are available for this data is $Re = 1.1{\cdot}10^5$. Looking at Figure 3.1 this can be considered as an average for the lower wind velocities. The next Reynolds number for which data is available is $Re = 2.1 \cdot 10^5$, which is higher than the maximum relevant Reynolds number for this rotor. The airfoil characteristics at these two Reynolds numbers will be considered in the performance calculations. According to Figure 3.1 the performance at wind speeds of 5-10 m/s is assumed to lie within these boundaries. The polar plots for the relevant airfoils and Reynolds numbers are given in Figures 3.4 and 3.5.

For the analysis the performance will be expressed in power coefficient C_P versus tip speed ratio

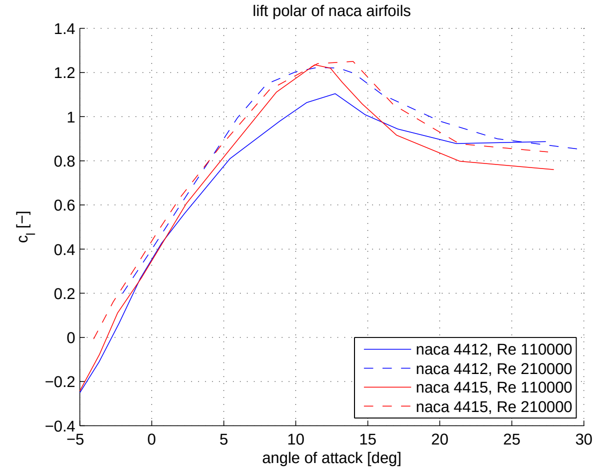

Figure 3.4: Lift polar for Naca 4412 and 4415 airfoils, obtained from [Hageman, 1980]

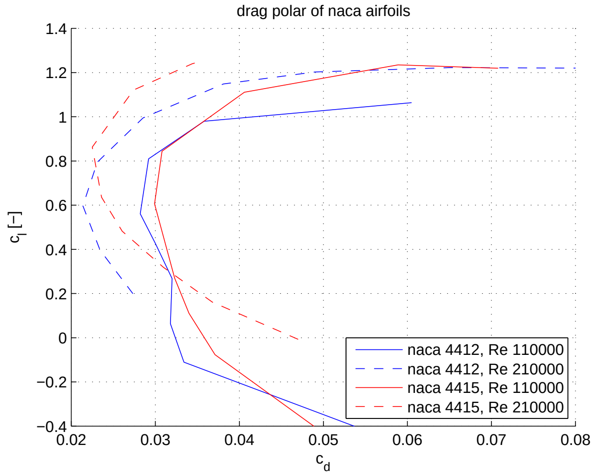

Figure 3.5: Drag polar for Naca 4412 and 4415 airfoils, obtained from [Hageman, 1980]

λ. The tip speed ratio λ in both non-yawed and yawed flow is defined as the ratio of the rotational speed ω and the freestream wind velocity U:

$$\lambda = \frac{\omega \cdot R_t}{U} \tag{3.1}$$

where R_t is the tip radius of the rotor.

3.2 Results of the BEM calculations

In Figure 3.6 the $C_P - \lambda$ curve for the actual and design geometries and Reynolds numbers $Re = 1.1 \cdot 10^5$ and $Re = 2.1 \cdot 10^5$ are given. The $C_P - \lambda$ curve is an important characteristic of wind turbines and can be used to compare the efficiency of different rotors. As can be expected, at higher Reynolds numbers better performance is obtained. This is due to the fact that at high Reynolds numbers lower drag and higher lift is obtained, which can also be observed from the lift and polar plots in Figures 3.4 and 3.5.

There is a drop in performance for the measured blade, due to the differences in actual and designed geometry. In Section 3.3 the influences of change in c and blade angle θ on the performance are described further.

The estimated performance of the rotor for the actual geometry at different yaw angles γ, according to the $\cos^3 \gamma$ rule (Appendix A), is shown in Figure 3.8. Since only the component of the wind velocity normal to the rotor plane is considered for the calculations, the power drops with increasing yaw angle.

3.3 Sensitivity analysis

Since the rotor blades are a handmade product, not every blade is exactly the same as the design. In Figures 2.2 and 2.3 the differences in designed and actual geometry were shown. Also

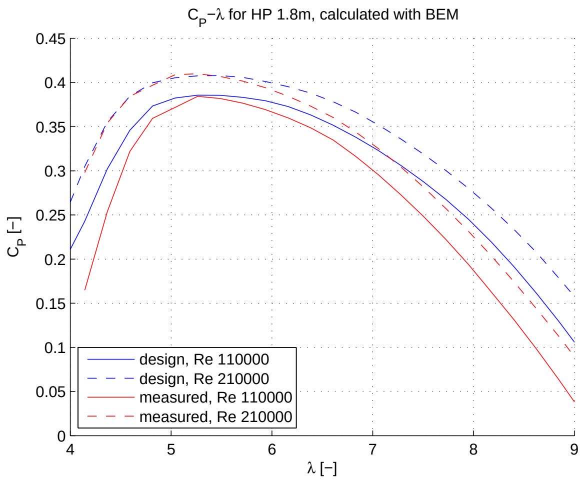

Figure 3.6: $C_P - \lambda$ for designed and actual geometry, calculated with BEM

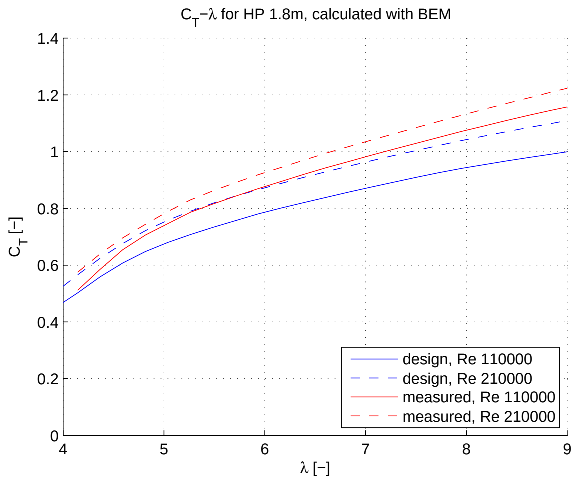

Figure 3.7: $C_T - \lambda$ for designed and actual geometry, calculated with BEM

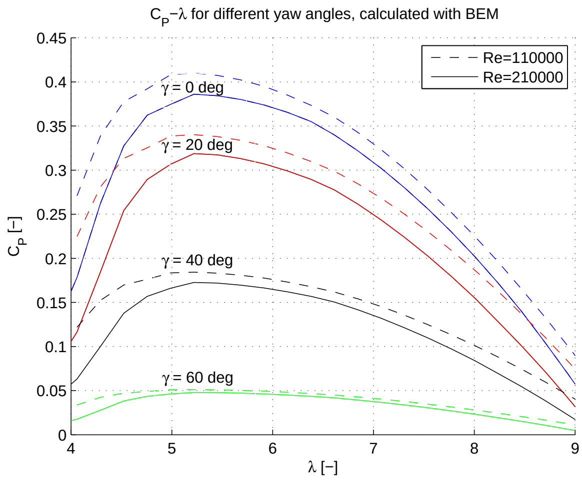

Figure 3.8: $C_P - \lambda$ at different yaw angles for the actual geometry, calculated with BEM and the $\cos^3 \gamma$ rule

the wind velocity at which the wind turbine operates has an influence on the (nondimensional) performance, since it affects the Reynolds number. To show which deviations will have the most influence on the rotor performance in general, a sensitivity analysis is done. The most important influences are listed below.

- Change in Reynolds number, due to a change in wind velocity
- Change in blade geometry
  - Chord c
  - Blade angle θ
  - Deviation in real airfoil shape from the Naca 4412 and Naca 4415 airfoils

The effect of change in Reynolds number was already shown in Figure 3.6. An increase in Reynolds number from $1.1 \cdot 10^5$ to $2.1 \cdot 10^5$ gives an increase in $C_{P,max}$ of around 5.5%.

The effect of change in blade geometry is shown in Figures 3.9 and 3.10. It can be seen that change in blade angle θ of $1°$ can already have a significant change in the $C_P - \lambda$ curve. It is expected that especially near the tip a small deviation in blade angle can be easily created by production errors. The chord dimensions are less prone to production errors, because this is easier to control during the production process using a simple ruler.

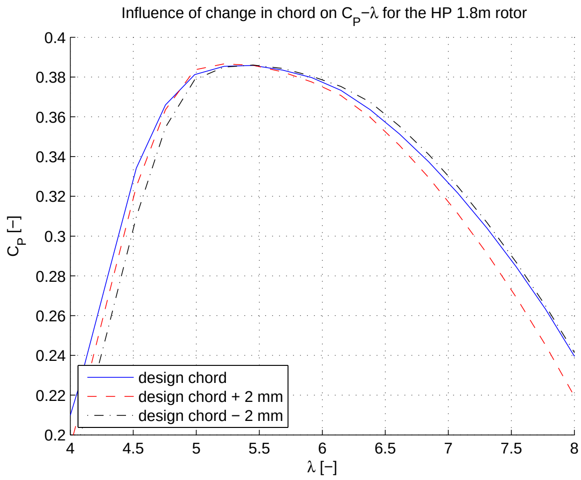

Figure 3.9: Effect of chord c on rotor performance, calculated on designed blade geometry and Re=110000

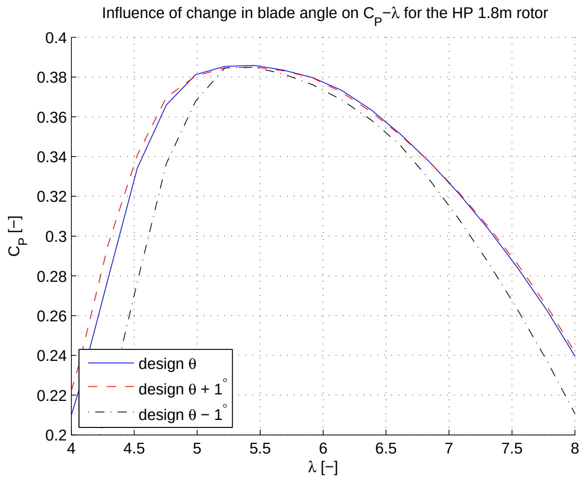

Figure 3.10: Effect of blade angle θ on rotor performance, calculated on designed blade geometry and Re=110000

The effects of change in the airfoil shape are described in Appendix B. The real airfoils do not perfectly resemble the Naca airfoils, partially because of the fact that they have a sharper nose. To investigate the influence of this, an XFOIL analysis is done. The shape of the Naca airfoils is adapted such that it resembles the real airfoils better. With XFOIL the lift and drag polars of the adapted and original airfoils can be calculated. With the BEM code the effect on the power can be calculated. As expected, the imperfections in airfoil shape lead to a decrease in power, as shown in Appendix B.
The effect of a sharp leading edge is measured during experiment 2, described in Chapter 8.

Chapter 4

Wind tunnel experiment 1 - Total performance identification of the HP 1.8m turbine

To identify the performance of the Hugh Piggott (HP) 1.8m test wind turbine, the wind turbine has been tested in the Open Jet Facility (OJF) wind tunnel at the TU Delft. The goal of the first experiment was to get more insight in the following three aspects of the HP 1.8m turbine:

- Aerodynamic performance
- Generator performance
- Furling behaviour

In Section 4.1 the test matrix of the experiment is given. The experimental set-up of the test is described in Section 4.2 and the measurement techniques and devices required are described in Section 4.3. Section 4.4 discusses the data reduction that is required to process the results, consisting out of wind velocity corrections and the effect of measurement accuracy on the determined power. Finally the results of the tests are given in Section 4.5.

4.1 Test matrix

In Table 4.1 the test matrix of the experiment is given. In this table the measurement goals and the configuration in which they are tested are given. Only the main measurements that are discussed in this chapter are shown here. Next to these main measurements also the influence of changing the measurement set-up is measured. These results are given in Appendix D. All changes in measurement set-up (dismounting the tail, attaching prony brake pipes) do not have a significant influence on the power output of the turbine. In Appendix E the remaining results of the tests that are not described in this chapter are given.

Table 4.1: Test matrix of experiment 1

Measurement	Load	Tail	Prony brake pipes	Yawing
Rotor performance	prony brake	removed	attached	$\gamma = 0°$
	prony brake	removed	attached	$\gamma = 20°, 40°, 60°$
Generator performance	dummy load	removed	attached	$\gamma = 0°$
Furling behaviour	dummy load	attached	removed	free yawing

4.2 Experimental set-up

The wind tunnel tests are conducted in the Open Jet Facility (OJF) wind tunnel at the TU Delft. The OJF is a low speed wind tunnel with a cross section of 2.85 m. The 1.8 m diameter wind turbine can be placed full scale in the wind tunnel. Because of the open jet characteristic of the OJF wind tunnel the blockage effects, discussed in Section 4.4.1, are small. The characteristics of the OJF can be found in Table 4.2. In Figure 4.1 a drawing of the OJF wind tunnel is shown.

In Figure 4.2 a picture of the set-up of the wind tunnel in the test section of the OJF wind tunnel is shown. In Figure 7.4 a schematic drawing of the set-up is shown. The tower of the turbine is placed in the center of the test section at 1 rotor diameter (1.8 m) from the exit of the

Table 4.2: Open Jet Facility wind tunnel characteristics

OJF characteristics	
Type	Closed circuit
Tunnel exit (w x h)	285 x 285 cm
Cross section	Octagonal
Maximum wind speed	35 m/s
Turbulence level	0.23%

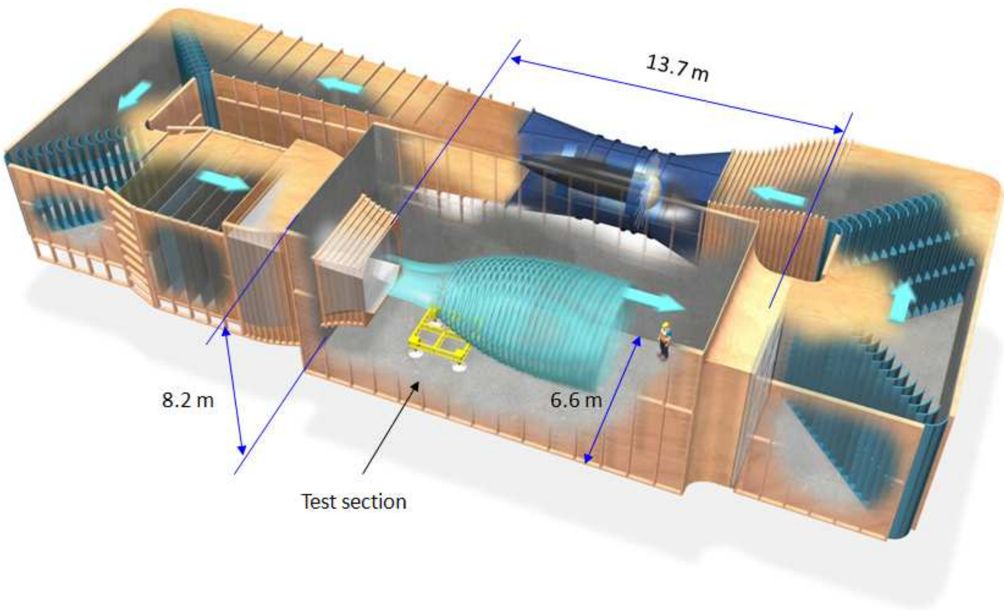

Figure 4.1: Drawing of the OJF wind tunnel

nozzle. Because of the offset of the rotor axis with the tower, the rotor is not centered. This is done to make sure that when the tail is mounted on the turbine, the tail is still located within a reasonable distance from the center of the nozzle, in all tail positions.

The wind turbine that is used for the tests is described in Chapter 2. The tower is held in place by means of three guy wires, which in this case are threaded rods that are brought under tension.

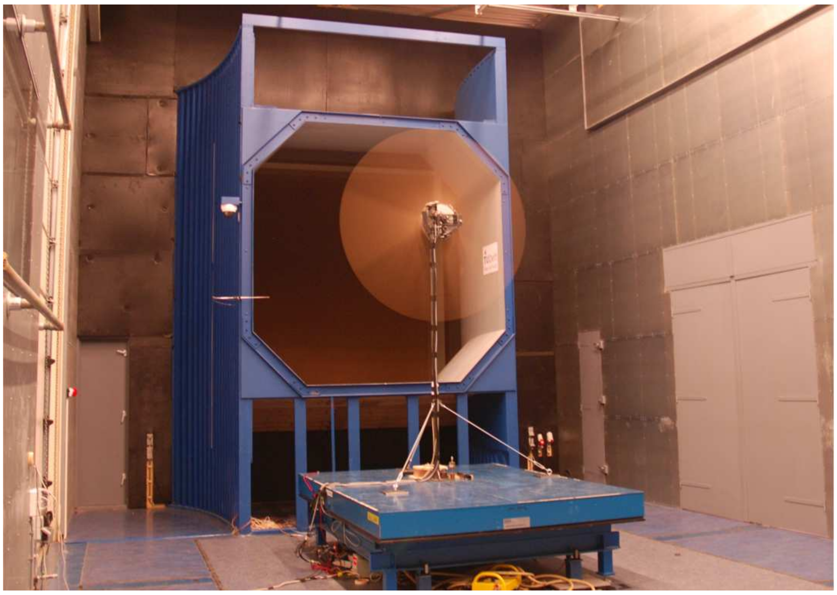

Figure 4.2: Picture of the experimental set-up in the OJF wind tunnel during operation of the wind turbine

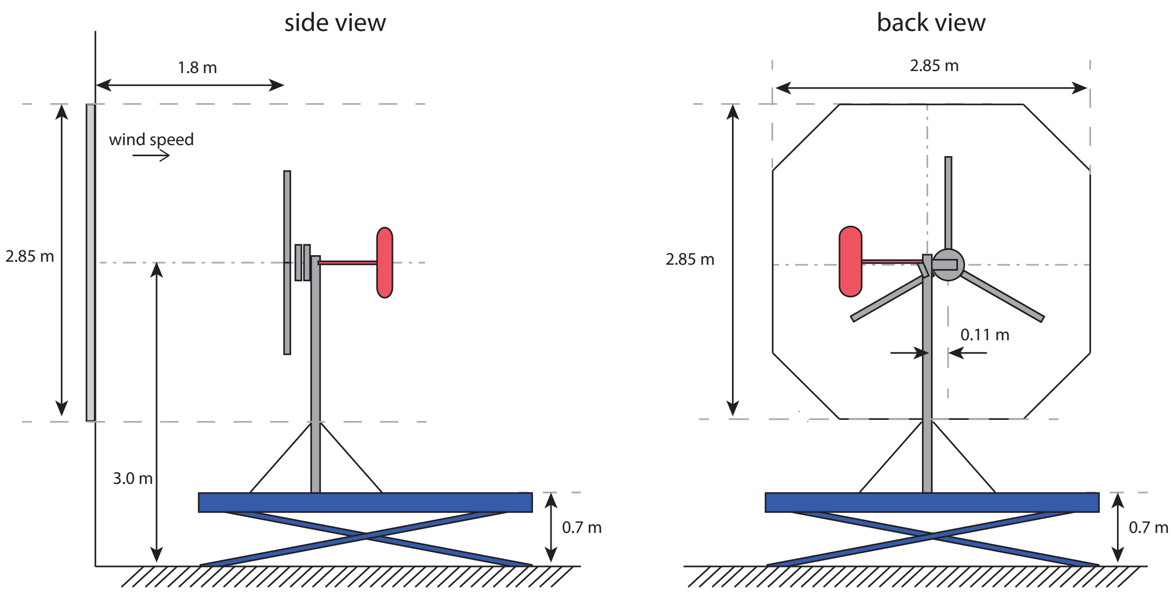

Figure 4.3: Schematic drawing of the experimental set-up in OJF wind tunnel, the tail is shown in red and is only mounted on the turbine for the tests of the furling behaviour

4.3 Measurement techniques and devices

In this section the measurement techniques that are used for the tests are discussed. First the principles of the techniques will be discussed, after that the measurement devices required for the tests and corresponding accuracies are given.

4.3.1 Prony brake

A prony brake is a simple way to measure the power produced by a rotor. The principle described here is taken from the PhD thesis of Mertens [Mertens, 2006].

The power P produced by the rotor can be calculated from the torque Q that is produced by the rotor and its rotational speed ω.

$$P = Q \cdot \omega \tag{4.1}$$

For the measurement of the torque Q a prony brake was used. A prony brake consists of a pulley that is mounted on the shaft of the wind turbine, such that it is rotating with rotational speed ω. There is a rope around the pulley that brakes the rotor. On one side of the pulley a weight is attached, causing a tension F_w in the rope. On the other side of the pulley the tension in the rope F_l is measured by a load cell. Because the rope is slipping over the pulley a friction force F_f is created. In Figure 4.4 the forces that act on the prony brake are shown. From this figure, the equilibrium of forces in the prony brake can be derived:

$$F_w(R_p + \frac{1}{2}d_p) + F_f \cdot R_p - F_l(R_p + \frac{1}{2}d_p) = 0 \tag{4.2}$$

where R_p is the radius of the prony brake pulley and d_p is the rope thickness. Since the power that is produced in the rotor is converted to the friction force between the rope and the pulley, the torque Q can be calculated from the friction force F_f in the following way:

$$Q = F_f \cdot R_p \tag{4.3}$$

By combining Equations 4.1, 4.2 and 4.3 the power P of the rotor can be calculated:

$$P = (F_l - F_w)(R_p + \frac{1}{2}d_p)\omega \tag{4.4}$$

The power coefficient C_P can be calculated from this in the following way:

$$C_P = \frac{(F_l - F_w)(R_p + \frac{1}{2}d_p)\omega}{0.5\rho U^3 \pi R_t^2} \tag{4.5}$$

where R_t is the rotor tip radius. The wind velocity U and air density ρ are the tunnel variables that are determined in the wind tunnel.

Because the power that is produced in the rotor is transferred to friction forces between the pulley and rope, the materials that are used should be heat and wear resistant. The rope that was used is a 3 mm diameter sisal rope. The prony brake pulley is a 300 mm diameter disc made of aluminum.

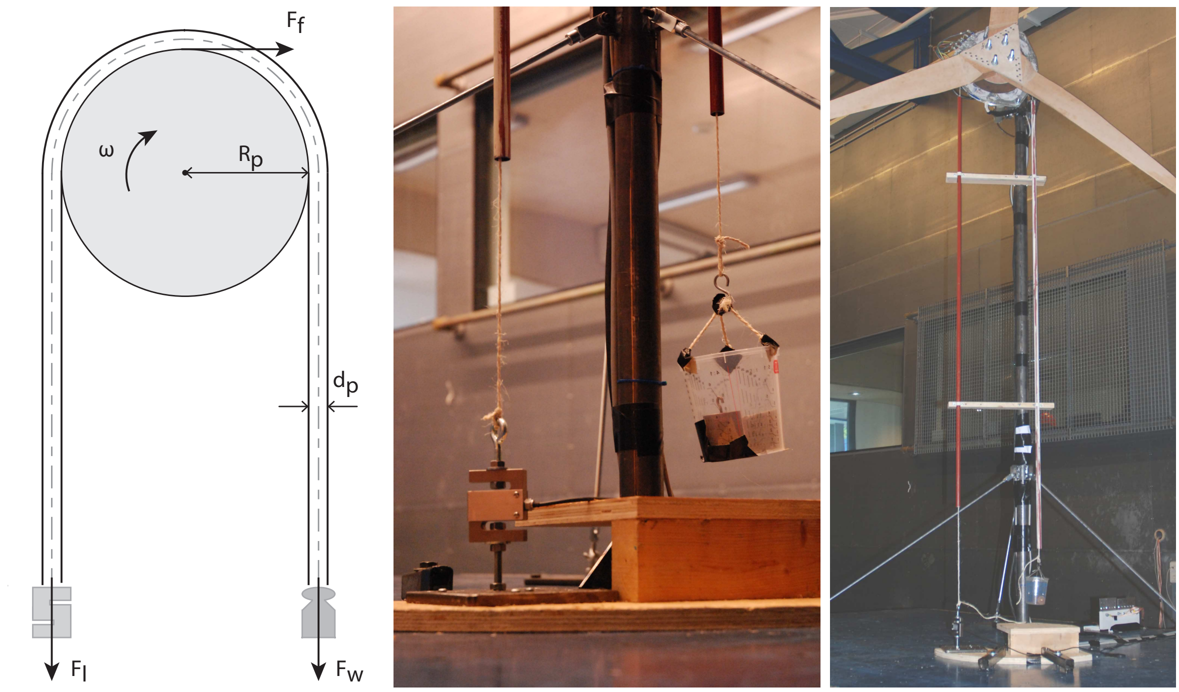

Figure 4.4: Prony brake principle

The prony brake ropes should be protected from the wind, to prevent that the wind exerts a force on the rope that would disturb the equilibrium in Equation 4.2. For this two pipes are attached to the wind turbine tower, as shown in Figure 4.4. The effect of the wind speed blockage because of the presence of these pipes on the power production of the rotor is negligible, as addressed in Appendix D.

Since the goal of this experiment is to measure only the power of the rotor, during the prony brake measurements the alternator is not connected to an electronic load. This means that the switches in Figure 4.5 are open and there is an open circuit.

Measurement procedure

The measurement procedure for the prony brake measurement is as follows. For each wind speed U and yaw angle γ a series of measurements is performed, starting at high rotational speed ω and tip speed ratio λ. For each measurement an extra weight is added, which will increase the rope force F_w and therefore the load on the turbine. Therefore ω and λ will decrease. The measurement can start after a new equilibrium is reached. A minimum measurement time of 5 seconds is used to make sure that unsteady effects are leveled. For the lowest measured rotational speed this means a minimum of 40 rotations. For the results shown in this thesis an average value of this measurement is used. After each measurement a weight is added for a new measurement until the load has become so high that the turbine brakes and stops rotating. This occurs just after the peak performance $C_{P,max}$ is reached. At this point, when more weight is added the friction torque increases, whereas the rotor torque decreases. This means that there can be no longer an equilibrium, which causes the rotor to brake.

4.3.2 Dummy load

To be able to test the performance of the combination of the rotor and generator (total performance) and the generator efficiency, an electrical load should be connected to the wind turbine. The generator is designed to be connected to a battery. However, testing with a battery is not recommended, because measurement conditions are not fixed: a half fully charged battery will impose a different load on the turbine than an empty battery and in this way it is difficult to reproduce the measurement.

Another option for an electrical load on the wind turbine is to use a dummy load. The most simple variant of this is a large variable resistance. For a given current I that is produced by the wind turbine, the total dummy load resistance R_{dump} should be varied in order to keep a constant voltage of 12 V. This is an approximation of the real battery situation, since the battery voltage of 12 V will slightly increase for increasing current. However, for this thesis we will approximate the situation by assuming a constant battery voltage of 12 V, and the dummy load resistance will be adapted to this.

For this experiment two large variable resistances of 5 Ω and maximum 20 A each are connected in parallel to the circuit, forming a total resistance R_{dump}. The electrical circuit for the generator and total performance tests is given in Figure 4.5. The electrical characteristics and resistances of the wind turbine itself are given in Section 2.2. The total resistance of the connecting cables on the ground R_c, as defined in the figure, is $R_c = 0.125\ \Omega$.

In Figure 4.5 the variables that were measured during the test are shown. These are the dump load voltage V_{dump}, the wind turbine voltage V_{wt} and the current I.

Since the dump load power P_{dump} is the power that would normally be transferred to the battery, this is the power that will be considered in this chapter. The dump load power P_{dump} and nondimensional $C_{P,dump}$ can calculated in the following way:

$$P_{dump} = V_{dump} I \tag{4.6}$$

$$C_{P,dump} = \frac{V_{dump} I}{0.5 \rho U^3 \pi R_t^2} \tag{4.7}$$

Measurement procedure

During normal operation the wind turbine will be connected to a battery. In this situation the wind turbine will not experience a load until $V_{wt} > V_{bat}$ and therefore the turbine is free to start-up. For this experiment the turbine is connected to a resistance, which will also pose a load on the turbine when $V_{wt} < V_{bat}$ and therefore the start-up speed will be higher. Therefore the turbine is started up at a higher wind speed, about 5 m/s. After that the wind speed is adjusted to the measurement speed, and the measurement can start. Depending on the measurement, either the resistance of the dummy load or the wind speed will then be adjusted. When a new equilibrium situation is reached, a new measurement can start. Similar to the prony brake measurements a minimum measurement time of 5 seconds is used, from which an average value is obtained.

4.3.3 Measurement devices

In Table 8.2 the measurement devices that are used for the tests are shown. For the angular velocity measurements two sensors were mounted on the wind turbine. The optical sensor is only used as a calibration tool and as a back-up sensor for the tachometer.

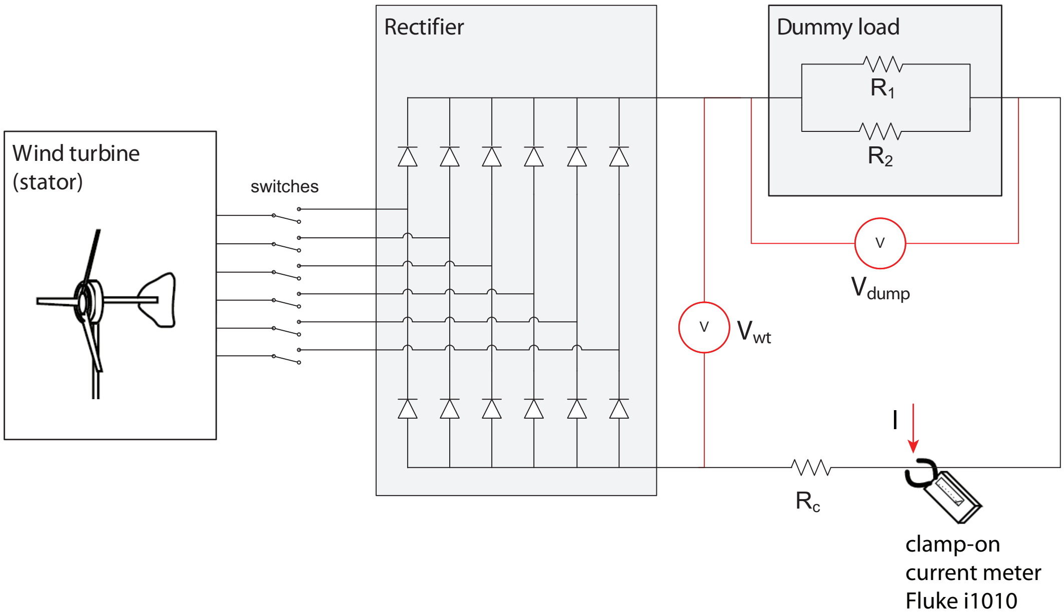

Figure 4.5: Electrical circuit for generator and total performance testing

Table 4.3: Measurement devices

Quantity	Measurement device	Device type	Accuracy
angular velocity ω	Digital hand tachometer	Ono Sokki HT-5100	0.5%
angular velocity ω	Transmissive optical sensor	Vishay TCST2000	$< 0.01\%$
F_l	Loadcell	Scaime ZFA 25kg	0.075 N
yaw angle γ	Potentiometer	Sakae CP30	lin 0.5%
tail angle ψ	Potentiometer	Sakae LNB22	lin 0.5%
current I	AC/DC Current Clamp	Fluke i1010	0.5%
weight W	Digital scale	Wedo Accurat 2000	1 g

4.4 Data reduction

4.4.1 Wind tunnel velocity corrections

Because of the open jet characteristic of the OJF wind tunnel, the flow can move easily around a tested object. This makes the wind tunnel less sensitive to blockage than closed test section wind tunnels. However, blockage effects will still be present, and corrections should be applied for that. On the wind velocity that is determined from tunnel measurements (air density and dynamic pressure) two corrections will be applied for this experiment:

- blockage correction: due to blockage effects of the rotor the actual wind velocity is higher than the determined velocity
- non-uniformity correction: the wind velocity at the location of the blade tips is higher than the determined velocity in the center of the tunnel jet

The blockage correction is calculated with a correction sheet from the TU Delft Wind Energy group, using the nozzle method for open test sections from AGARD-AG-336. The correction factor is mainly dependent on the thrust coefficient C_T of the rotor, the model frontal area, and the distance to the nozzle exit.

For C_T a value of 0.8 will be taken, based on the calculations done in Chapter 3. This is the C_T that is calculated at the peak λ, in which we are most interested. The error on the wind velocity that is introduced by this assumption is maximum 0.5% at high λ.

The distance of the rotor axis to the tunnel exit is assumed to be constant for every test. The dependency on the frontal area of the rotor makes it necessary to apply a different correction for each yaw angle, according to the relation in Table 4.4.

Next to blockage effects, an extra correction is applied for the difference in velocity at different locations in the tunnel jet. The wind tunnel velocity U_m is determined in the center of the tunnel jet. However, the outer part of the blades are responsible for most of the power production. At this location the wind velocity is slightly higher than at the jet center. During calibration of the Open Jet Facility windtunnel this was measured. At 1.8 m from the tunnel exit, where the rotor is located, the average increase in velocity 0.7 m out of the center of the tunnel jet was determined to be 0.84%.

The maximum total error on the wind velocity measurement, after applying corrections, is estimated to be around 0.5%.

Table 4.4: OJF windtunnel wind speed corrections for experiment 1

	Wind speed corrections U/U_m [-]		
γ [deg]	Blockage	Off-center	Total
0	1.032	1.0084	1.041
20	1.029	1.0084	1.038
40	1.022	1.0084	1.031
60	1.011	1.0084	1.019

4.4.2 Error in power coefficient determined from measurements

The limited accuracy of the measurement devices causes an error in the final results. In order to determine whether differences between results are significant, it is important to know what the measurement error is. The measurement devices and corresponding accuracies were already shown in Table 8.2.

In this section the effect of the measurement accuracy on the power coefficient C_P that is calculated from these measurements is discussed. In Equations 4.5 and 4.7 the calculation of C_P from the measurements were shown. In Table 4.5 all measurement influences on calculated power coefficient are given.

For the prony brake tests, a digital scale was used to measure the mass of the weights. The effect of the accuracy of the scale on the calculated power coefficient is different for different loadings of the wind turbine. At low wind speed and low rpm (smaller weights are used) the error is larger than at high wind speed and high rpm (larger weights are used). It is assumed that each measurement will have an accuracy of 1 g, regardless the amount of weights that are used. The effect on power is shown in Table 4.5.

The same holds for the measurement of the force in the load cell: accuracy is lower at lower wind speeds.

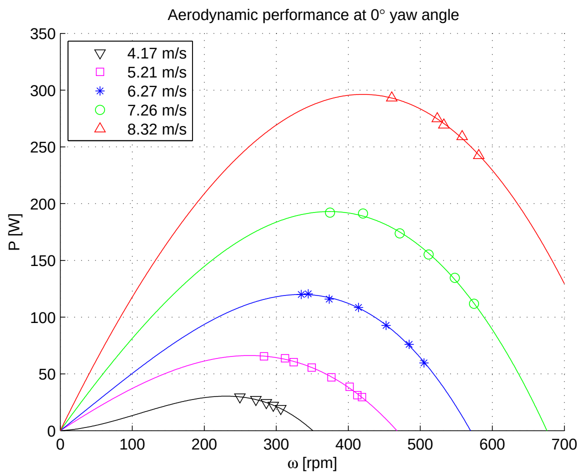

Figure 4.6: $P-\omega$ curve of current rotor performance at yaw angle $\gamma = 0°$

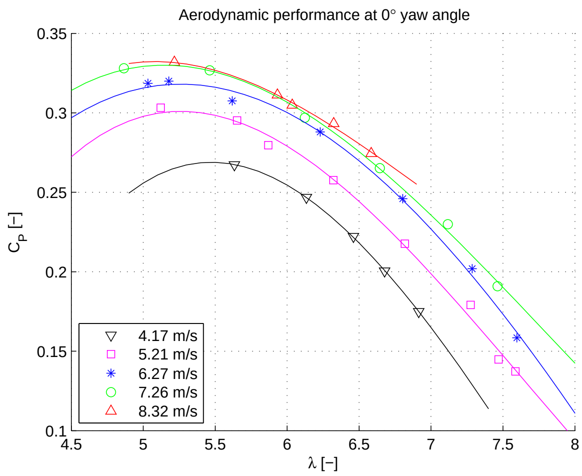

Figure 4.7: $C_P - \lambda$ curve of current rotor performance at yaw angle $\gamma = 0°$

The total accuracy for C_P determined from the prony brake measurement is 2.2% at high wind speed (8 m/s) and 3.6% at low wind speed (4 m/s).

For the generator measurements the total accuracy of C_P adds up to 2%.

Table 4.5: Effect of measurement accuracy on C_P

Quantity	Measurement accuracy	Effect on C_P
ω	0.5%	0.5%
F_l	0.075 N	0.2-1.4%
F_w	0.01 N	0.02-0.2%
U	0.5%	1.5%
I	0.5%	0.5%

4.5 Results

In this section the results of experiment 1 are presented and briefly described. A comparison of the results with calculations and a more detailed evaluation of the results is presented in Chapter 5.

4.5.1 Rotor performance

In Figures 4.6 and 4.7 the $P-\omega$ and its nondimensional form $C_P - \lambda$ for the current rotor are given, measured at a yaw angle of $\gamma = 0°$. It can be observed that the $C_P - \lambda$ curve shifts up for higher wind velocities. The wind turbine thus operates more efficient at high wind velocities. This is not surprising, since Reynolds numbers are larger here and from Section 3.1 it is known that this causes higher lift and lower drag coefficients. A comparison of the results with the BEM calculations is given in Section 5.1.1.

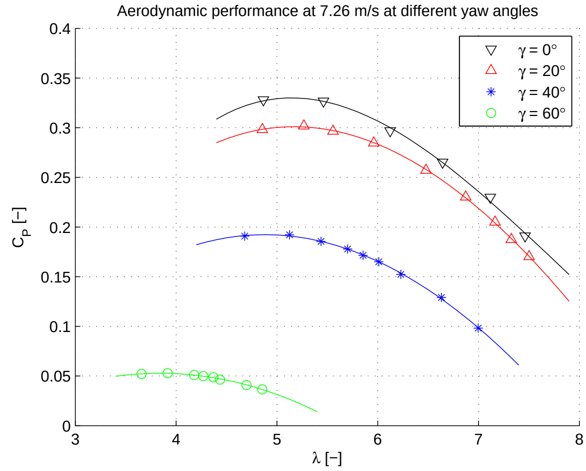

Figure 4.8: $C_P - \lambda$ for different yaw angles, at U =7.26 m/s

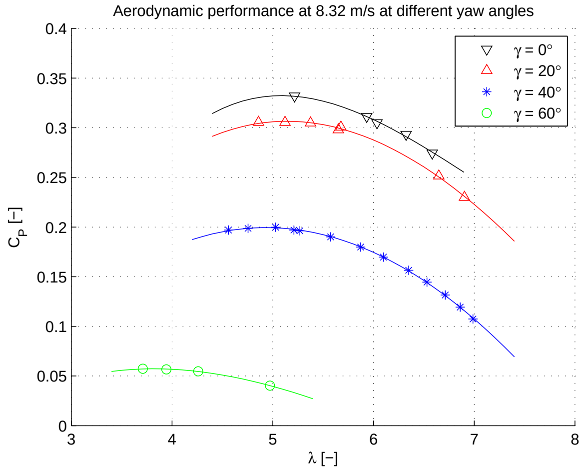

Figure 4.9: $C_P - \lambda$ for different yaw angles, at U =8.32 m/s

The $C_P - \lambda$ curves from Figures 4.6 and 4.7 are also measured at yaw angles of 20°, 40° and 60°. For a wind velocity of 7.26 m/s and 8.32 m/s the $C_P - \lambda$ curves at different yaw angles are shown in Figures 4.8 and 4.9. What can be observed from the figures is that the performance only slightly decreases when the yaw angle is increased from 0 to 20°. However, the yaw angles of 40° and 60° create a significant power drop.
The power drop for an increasing yaw angle is expected, since the velocity component normal to the rotor plane has decreased for a yawed flow. Also the tip speed ratio λ decreases for an increasing yaw angle. This is caused by the fact that a higher wind speed U is required to reach the same rotational speed ω of the turbine, due the fact that the normal component of the wind velocity has decreased for yawed flow. In Section 5.1.2 a comparison of the results with the calculations for yawed flow with the BEM model is given.

4.5.2 Generator performance

The generator efficiency can be determined when both the rotor performance and total performance at the same yaw angle are known. With total performance the turbine output power when the turbine is connected to the dummy load is meant. Total performance was tested in two ways, depending on the dummy load resistances:

- fixed dummy load resistance, variable V_{dump}.
- variable dummy load resistance, to maintain $V_{dump} \approx 12$ V

In this section only the $V_{dump} \approx 12$ V tests are presented, since this resembles the normal (battery) operation mode of the wind turbine. The results of the fixed dummy load resistance tests are presented in Appendix E.

The results for a situation resembling a 12 V battery are presented in Figures 4.10, 4.11 and 4.12. Also the maximum aerodynamic power at each wind speed is shown in these figures, to show the losses caused by the generator. From Figure 4.11 it can be observed that there is a significant power loss caused by the generator.

In Figure 4.12 the power P versus rotational speed ω of maximum aerodynamic and total power are shown. In this figure each wind speed is presented as a different symbol. It can be seen that for low wind speeds the rotational speed at which the total system operates is not the same rotational speed at which the maximum aerodynamic power was measured. This is one of the reasons for power loss in the total system. However, at higher wind velocities the turbine does operate at its optimum rotational speed, and losses are even higher here. This indicates that a mismatch between the rotor and generator is not the main cause of power losses. A more detailed discussion on the power losses and their causes is given in Chapter 5.

In Figure 4.13 an important generator characteristic is given, which is the open circuit $V-\omega$ graph. This characteristic is measured in open circuit condition, when the dummy load is not connected to the circuit. As expected, the voltage increases linearly with the rotational speed. At

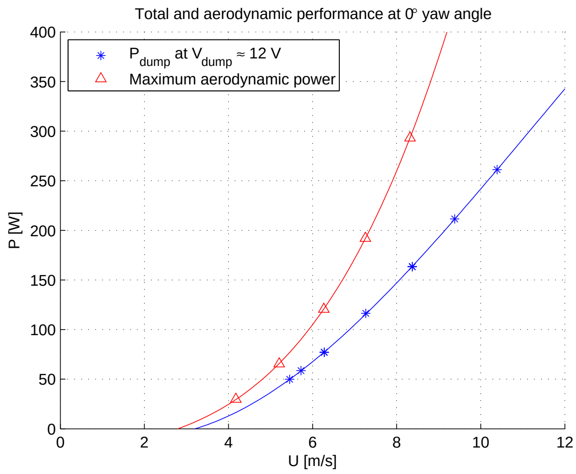

Figure 4.10: Total and aerodynamic power curve $P-U$ at $0°$ yaw angle

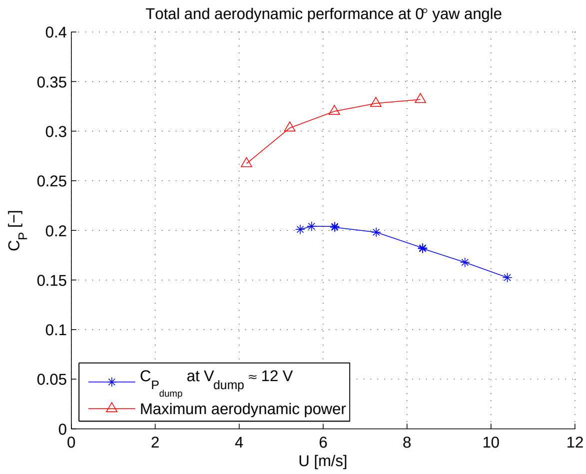

Figure 4.11: Total and aerodynamic C_P-U curve at $0°$ yaw angle

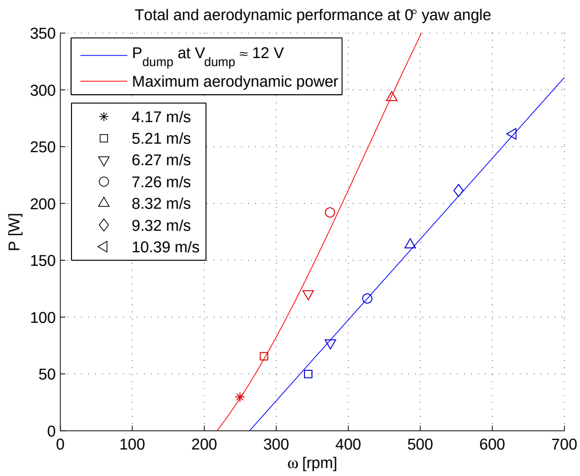

Figure 4.12: Total and aerodynamic $P-\omega$ curve at $0°$ yaw angle

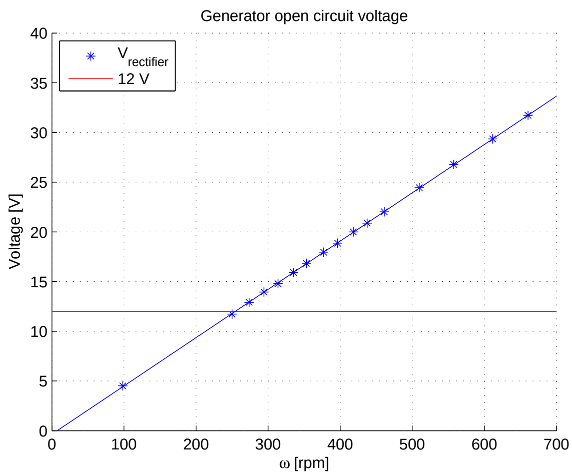

Figure 4.13: Open circuit $V-\omega$ of the generator

about 250 rpm the voltage reaches the 12 V level. This is the cut-in wind speed of the turbine, which is $U_{cut-in} = 3.2$ m/s. If a battery would be connected to the system, the difference in voltage between the generator and the battery would cause a current to flow, as soon as $V_{wt} > V_{bat}$. Therefore, the cut-in wind speed of the generator will be just above 3.2 m/s. Unfortunately the total performance of this low wind speed with the dummy load connected could not be measured because of the limited range of resistance of the dummy load.

4.5.3 Furling behaviour

To determine the total power curve of the wind turbine in normal operation, the tail should be attached to the wind turbine and the wind turbine should be free to yaw. This introduces extra losses, since the wind turbine will be no longer at $\gamma = 0°$, as was the case in the previous subsection.

In Figures 4.14 and 4.15 the losses due to furling, both in dimensional and nondimensional form, are clearly visible. In Figure 4.16 the corresponding yaw and tail angles are given, according to the angle definitions given in Figure 2.6. An interesting result is that wind turbine immediately turns to 20° at the starting wind speed. However, here the losses are still limited. At about 11 m/s the power P_{dump} reaches its peak. The yaw angle at that moment is about 40°. From that moment the losses due to furling are so high that the power starts to decrease with increasing wind speed. Figures 4.8 and 4.9 confirm the low losses up till 20° and the high losses above 40°.

The furling losses at low wind speeds are undesired, because overload of the wind turbine is not yet a danger there. This indicates that a resizing of the furling tail would be required to improve the performance. In Section 5.3 the percentage of losses caused by furling are discussed in more detail.

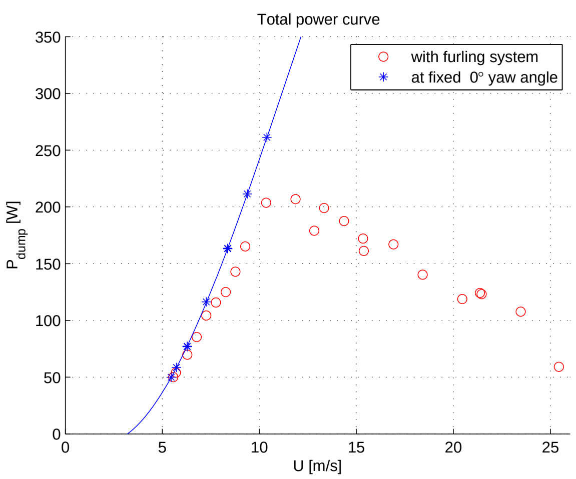

Figure 4.14: $P-U$ for total performance at fixed wind turbine ($\gamma = 0°$) and furling wind turbine (varying γ)

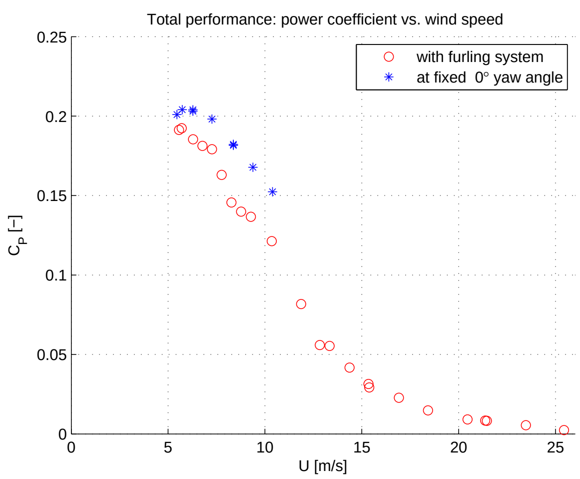

Figure 4.15: C_P-U for total performance at fixed wind turbine ($\gamma = 0°$) and furling wind turbine (varying γ)

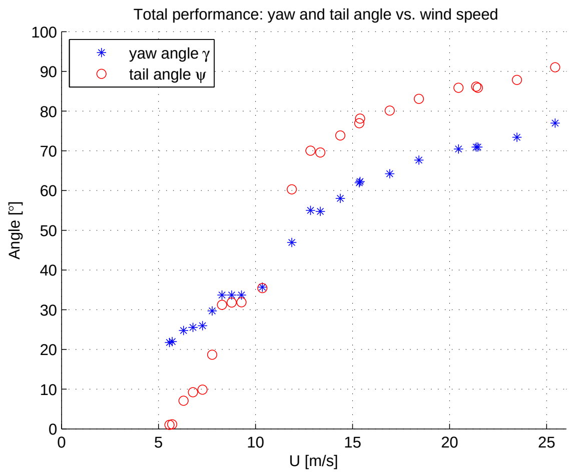

Figure 4.16: Yaw angle γ and tail angle ψ versus wind speed U for the furling wind turbine

Chapter 5

Evaluation of the HP 1.8m turbine

In this chapter the different aspects of the Hugh Piggott 1.8m wind turbine are evaluated based on the manufacturability of the turbine that was discussed in Chapter 2, the performance calculations and experiment 1. The evaluation of the different aspects is based on the criteria that were set in Section 2.8, which are performance, production, availability of materials, and material costs. The focus is on the parts that were tested during experiment 1, which are the rotor, generator and furling system. Other aspects like the support structure were briefly discussed in Chapter 2.

The rotor, generator and furling system are discussed in respectively Section 5.1, Section 5.2 and Section 5.3. A conclusion on which of these turbine parts will be investigated further in the remaining of this thesis is given in Section 5.4.

5.1 Rotor evaluation

In this section an evaluation of the rotor is given. First the performance evaluation is described, both at zero yaw and yawed flow, by comparing the experiments from Chapter 4 with the calculations of Chapter 3. After that the manufacturability of the rotor, discussed in Chapter 2 is recapitulated.

5.1.1 Performance evaluation at zero yaw

In Figure 5.1 the calculated and measured $C_P - \lambda$ at $\gamma = 0°$ are given. For the low wind velocity measurements, a lower maximum C_P is found. This is due to the fact that Reynolds numbers are higher at higher wind velocities, which increases the lift and decreases the drag of the blade. The difference between 4 and 5 m/s is much larger than the difference between 7 and 8 m/s. This shows that for wind speeds even larger than 8 m/s the performance will not increase much further. It would be beneficial to have a larger rotor diameter than 1.8 m, since Reynolds numbers would be higher and therefore C_P at low wind speed would be higher.

In Figure 5.1 also the calculated $C_P - \lambda$ is given. Recall from Section 3.1 that $Re = 1.1 \cdot 10^5$ represents a wind velocity of approximately 5 m/s and $Re = 2.1 \cdot 10^5$ represents a wind velocity

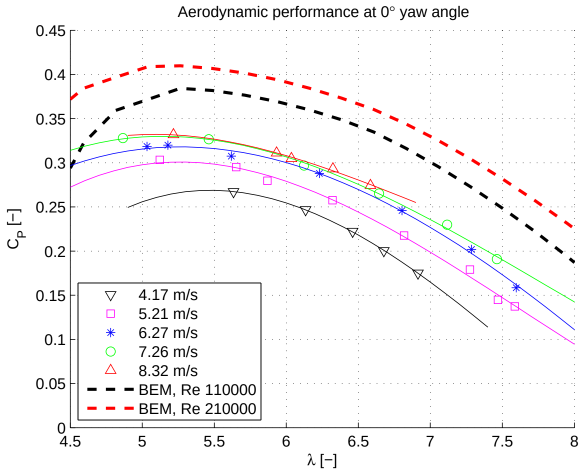

Figure 5.1: Measured and calculated C_P at 0 deg yaw

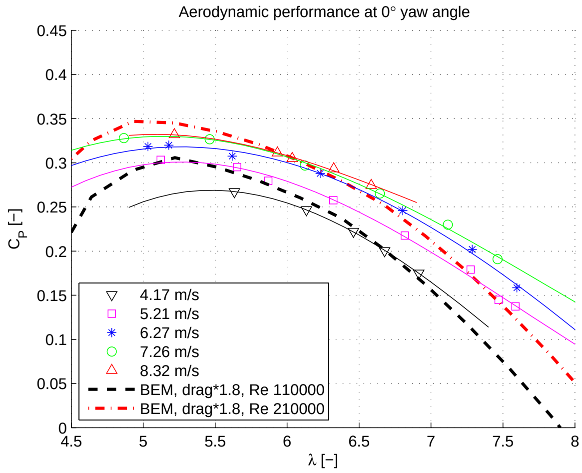

Figure 5.2: Measured and calculated C_P at 0 deg yaw, the BEM model is adapted with a 80% increased drag

of approximately 10 m/s. Therefore the measurements at wind velocities between 5 and 8 m/s are expected to lie within this region. From Figure 5.1 it can be observed that the performance that was predicted with BEM is higher than the measured performance. This difference between theory and practice can have multiple reasons:

- Deviation of the real geometry of the rotor from the geometry and airfoil shapes that are used as in input for the BEM model
- Limited accuracy of the BEM model
- Limited measurement accuracy

The imperfections in the blade shape are likely to cause an extra drag on the turbine, reducing performance (Appendix B). Also the BEM model does not include the very inner part of the blade near the root, where the blade is very thick. This will also cause an increase in drag. Another important source of drag that can not be included in the BEM model is the friction in the hub, which will also lower performance. On the other hand, 3D effects on the blade that are included in the BEM model can increase the measured performance compared to calculations [Burton et al., 2001]. Looking at the differences between experiment and calculations, the extra drag is likely to have a larger influence and therefore performance has decreased.

To validate that the extra drag is indeed the reason for the differences between calculations and measurements, a drag measurement is performed on the rotor. For this the rotor is rotated by hand until it reaches a rotational speed of about 150-200 rpm, and then the rotor is released and free to rotate. Because there is no driving force anymore, the rotor will decelerate. From the deceleration of the rotor the total drag of the rotor can be derived. This measured drag can be compared with the drag that was calculated using BEM.

Between experiment 1 and 2 a first (rough) drag measurement was performed, to be able to judge whether the BEM model is accurate enough to be used as a design tool for this project.

During experiment 2 the equipment of the experiment could be used for the drag measurement, which resulted in a more accurate measurement.

A description of both drag measurements is given in Appendix C. After the first drag measurement it was decided that the BEM model can be used as a design tool. This is confirmed by the more accurate second measurement. The measured drag from the experiment is determined to be 1.8 times the calculated drag. When this correction factor is applied to the drag calculated with BEM, the new $C_P - \lambda$ curves in Figure 5.2 are obtained. The maximum C_P results are now more consistent to the calculations. The C_P at high λ gives a result that is slightly lower for the corrected measurements. This could be due to the fact that the drag correction is applied as a multiplication of the original drag, which is not totally correct.

It should be noted here that the drag correction described above is an approximation of the real situation. The imperfections in airfoil shape are likely to cause not only an increase in drag, but also a decrease in lift. This is not included in the result in Figure 5.2. The decrease in lift would decrease the calculated C_P even further. However, also 3D effects on the blades are not included in the model. This will slightly increase the calculated C_P. Since there is a large uncertainty in the input for the BEM model for this rotor, the calculation should be considered as an estimation only.

5.1.2 Performance evaluation at yawed flow

In Figure 5.3 and 5.4 the calculated and measured $C_P - \lambda$ at different yaw angles are given, for wind speeds of 7.26 and 8.32 m/s and $Re = 2.1 \cdot 10^5$. Recall that the calculation is based on the $\cos^3 \gamma$ rule (Appendix A) and an increased drag of 80%, as explained in the previous section. Up to 40° the difference between the calculated and measured optimum λ is only small. However, the measured C_P decreases less with increasing yaw angle than was calculated. The approximation of C_P at a yaw angle of 60° is more consistent with the results again. At very large angles (60°) the BEM model does not give a good approximation of the λ anymore.

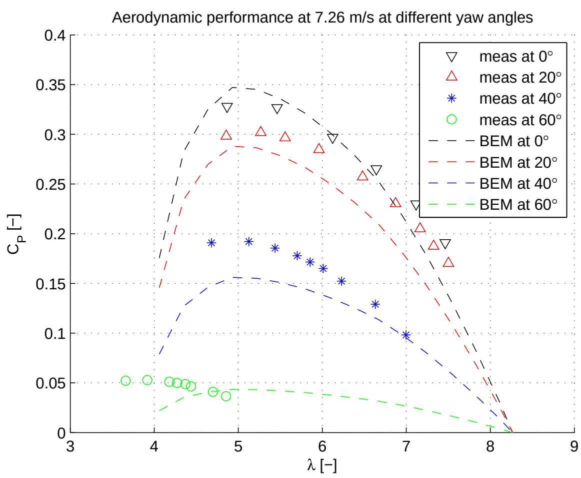

Figure 5.3: Measured C_P at 7.26 m/s (meas) and calculated C_P for $Re = 2.1 \cdot 10^5$ (BEM). The BEM result is corrected for an increased drag of 80%

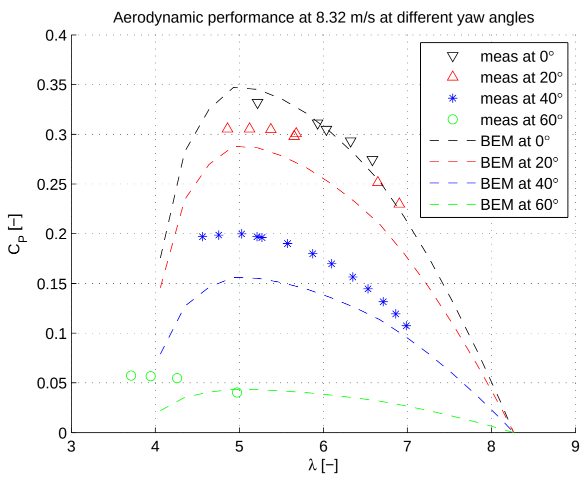

Figure 5.4: Measured C_P at 8.32 m/s (meas) and calculated C_P for $Re = 2.1 \cdot 10^5$ (BEM). The BEM result is corrected for an increased drag of 80%

The $\cos^3 \gamma$ approximation gives a lower output power than measured. This is expected, because the $\cos^3 \gamma$ rule neglects the component of the wind velocity parallel to the rotor plane. This component cannot be completely neglected, because it will also have a (small) contribution to the total power.

To judge the use of the $\cos^3 \gamma$ rule for the yaw calculations and to predict if other methods would give a better approximation of the calculated power, a comparison is made in Figure 5.5. In this figure the fraction of available wind power is shown as a function of yaw angle for the measurements of experiment 1, the $\cos^3 \gamma$ and $\cos^2 \gamma$ approximations and Glauert correction method for yawed flow. The Glauert curve is obtained from 'Wind Energy Handbook' [Burton et al., 2001]. For yaw angles up to 20° the Glauert correction gives a good approximation of the measurement, but for larger yaw angles the measured power is much lower than calculated with the Glauert method. At yaw angles above 30° the $\cos^3 \gamma$ rule gives a better approximation than the Glauert method. In Figure 5.5 also the $\cos^2 \gamma$ approximation is shown. This approximation shows a better overall agreement with the measurement results, because here the wind velocity component parallel to the rotor plane is not completely neglected.

To compare the results of this experiment with results of other experiments, in Figure 5.5 the fraction of available rotor torque is shown as a function of yaw angle. In this figure the measurements from experiment 1 and measurements from the unsteady aerodynamics experiment of NREL [Tongchitpakdee et al., 2005] are shown. The experimental data from NREL is obtained from the NREL Phase VI rotor, which is a 10m diameter two-bladed stall regulated turbine. The result at a wind speed of 7 m/s, where the flow is attached, is shown. The NREL measurements results show a fraction of available torque that is even lower than the measurements from experiment 1. This confirms that the Glauert method cannot be used for large yaw angles, and the $\cos^3 \gamma$ rule or $\cos^2 \gamma$ rule give a better approximation.

These results show that to calculate the power output at yaw angles up to 60° the Glauert

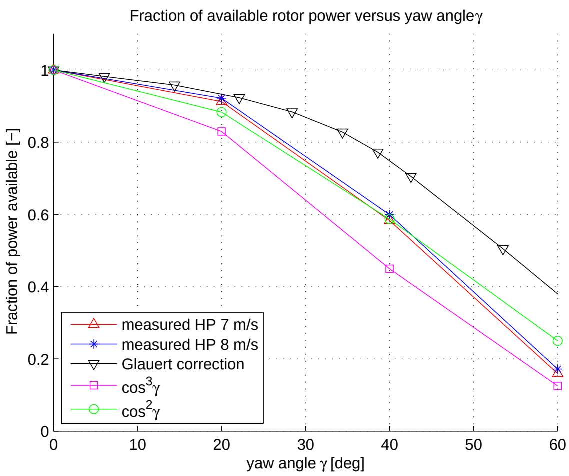

Figure 5.5: Fraction of available rotor power versus yaw angle γ, for the measured HP rotor at 7 and 8 m/s, the $\cos^3 \gamma$ approximation, the $\cos^2 \gamma$ approximation, and the Glauert method [Burton et al., 2001]

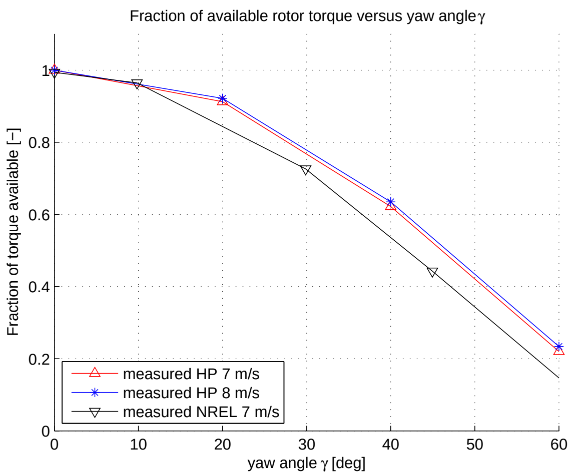

Figure 5.6: Fraction of available rotor torque versus yaw angle γ, for the measured HP rotor at 7 and 8 m/s and measured data from NREL [Tongchitpakdee et al., 2005] at 7 m/s

method is not a good approximation. For the measurements of experiment 1 the $\cos^2\gamma$ rule gives the best overall approximation. For a very accurate power calculation a more complex method should be used, for example one of the calculation methods described by Tongchitpakdee [Tongchitpakdee et al., 2005].

5.1.3 Evaluation of the manufacturability of the rotor

According to the wind turbine evaluation criteria set in Chapter 2, there are several other aspects that need to be evaluated to give a complete overview of the Hugh Piggott 1.8m rotor. Most of these aspects were already discussed in Section 2.1 and are only recapitulated here.

The production process is a very important aspect for a hand-made rotor. Because of the twisted and tapered shape of the rotor blades, the production process is time demanding and errors in blade geometry can be made. The sensitivity analysis in Appendix B shows that a small error in the blade angle of 1° (which is easily made near the blade tips) can cause a significant decrease in rotor performance. In Chapter 3 the deviation in design and measured geometry of this particular rotor and the corresponding performance differences were shown. These deviations show that for a perfectly constructed rotor higher performance can be expected. The difficulty in the production process determines the tolerance in the production process. A higher uniformity could be reached by simplifying or standardizing the production process.

In Section 2.1 it was also mentioned that good quality wood can be difficult to obtain for wind turbines larger than 3.0 m. For a tapered and twisted blade the dimensions (thickness and width) of the required wood are relatively large, which decreases availability.

The costs of the blades only have a small contribution to the total wind turbine costs and are therefore acceptable.

5.2 Generator evaluation

The generator performance can be evaluated by comparing the total power at 12 V (battery simulating situation) with the aerodynamic power, both at 0° yaw. In Figure 5.7 the losses of the system are shown. From aerodynamic power P_{aero} to power that is generated in the stator P_{gen} there are losses due to the fact that not all energy is captured by the coils. Also, due to the resistance of the coils there are power losses in the coil wiring. The generator power P_{gen} is defined here as the power of the generator when all losses other than coil losses are subtracted. The wind turbine system power P_{wt} is the generator power P_{gen} plus the power losses in the rectifier $P_{loss,rect}$. The final battery or dump load power P_{dump} is the wind turbine power P_{wt} plus the cable losses on the ground $P_{loss,Rc}$, due to the cable resistance R_c in Figure 4.5.

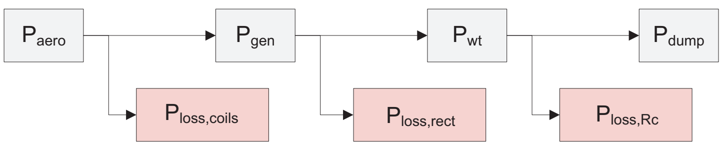

Figure 5.7: Power losses in the wind turbine system

In this analysis the efficiency of the generator-rotor matching η_{match}, the generator efficiency η_{gen}, the wind turbine efficiency η_{wt}, and the battery or dump load efficiency η_{dump} are considered, which are defined in the following way:

$$\eta_{match} = \frac{P_{aero}}{P_{aero,max}} \tag{5.1}$$

$$\eta_{gen} = \frac{P_{dump} + P_{loss,Rc} + P_{loss,rect}}{P_{aero}} \tag{5.2}$$

$$\eta_{wt} = \frac{P_{dump} + P_{loss,Rc}}{P_{aero}} \tag{5.3}$$

$$\eta_{dump} = \frac{P_{dump}}{P_{aero}} \tag{5.4}$$

In Table 5.1 and Figures 5.8 to 5.11 the power of the different subsystems and corresponding efficiencies are given. The power loss due to operation at a non-optimum λ (mismatch of rotor-generator) is 7% for a wind speed of 5.2 m/s, and decreases for higher wind velocities. This is because the operating λ decreases with increasing wind speed. This means that the rotor-generator matching for this system is quite good at high wind speeds. However, for low windspeeds a better matching can cause significant improvements.

The wind turbine efficiency η_{wt} at 5.2 m/s is 71% and decreases for higher wind speeds. This efficiency includes losses in the generator and rectifier, but no cable losses from wind turbine to dump load on the ground. Due to these extra cable losses the dump load efficiency η_{dump} is lower. However, these losses can be eliminated by placing the dump load (or battery in normal operation) closer to the wind turbine or using a thicker cable, and will therefore be different for each wind turbine. Therefore the η_{wt} will be considered as the total wind turbine efficiency in the rest of this thesis.

In the manual [Piggott, 2008] Piggott gives a rated power for this turbine of $P_{wt} = 350$ W at a wind speed of $U = 11$ m/s. In this thesis a power of $P_{wt} = 367$ W at $U = 11$ m/s is obtained when the measurements are extrapolated, which is very similar. This means a total C_P of 0.18 at $U = 11$ m/s. However, this is measured at a zero yaw angle and can therefore not be considered as the final power that is produced during normal operation. Extra losses due to the furling system are considered in the next section.

At the mean Malian wind speed of 4 m/s the power production is 15 W, based on an extrapolation of the results. The estimated power output at this wind speed according to Piggott, as described in Section 2.7, is 42 W. One of the reasons for the lower power output is that the Reynolds numbers for this turbine are very low at this wind speed, decreasing the maximum aerodynamic power that can be produced by the rotor. At 7 m/s the measured power output is 114 W and the Piggott estimated power output is 128 W, which is a much better approximation. Of course one should keep in mind that for the measurements only one turbine is tested. Therefore we can conclude that at high wind speeds the estimated power by Piggott is a good estimation for

Table 5.1: Power and losses during battery operation at zero yaw angle

Operational conditions				Power [W]				Efficiency [%]
U [m/s]	ω [rpm]	I [A]	V_{dump} [V]	P_{aero}	P_{dump}	$P_{loss,Rc}$	$P_{loss,rect}$	η_{wt}
5.2	322	2.9	12.2	61.4	42.2	1.1	4.1	71
6.3	375	6.5	11.9	117.0	77.3	5.2	9.1	71
7.3	426	9.6	12.1	188.0	116.3	11.6	13.4	68
8.3	488	13.0	12.0	287.1	160.4	22.0	18.2	64

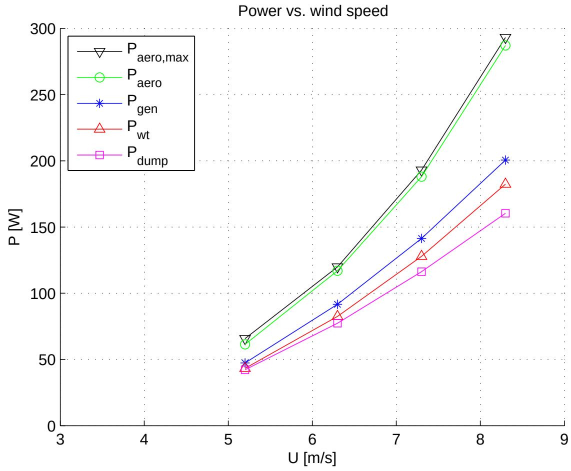

Figure 5.8: Power in the wind turbine system P vs. wind speed U

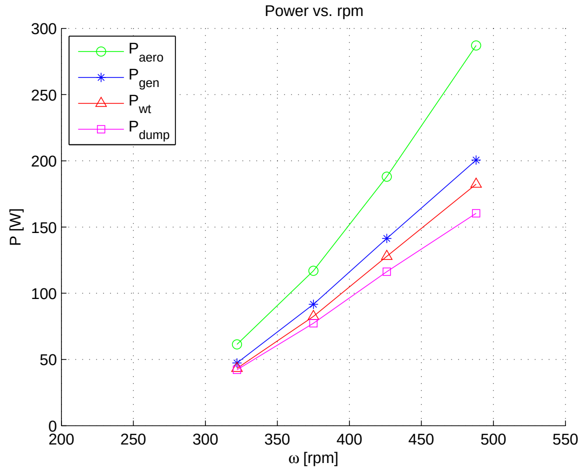

Figure 5.9: Power in the wind turbine system P vs. rotational speed ω

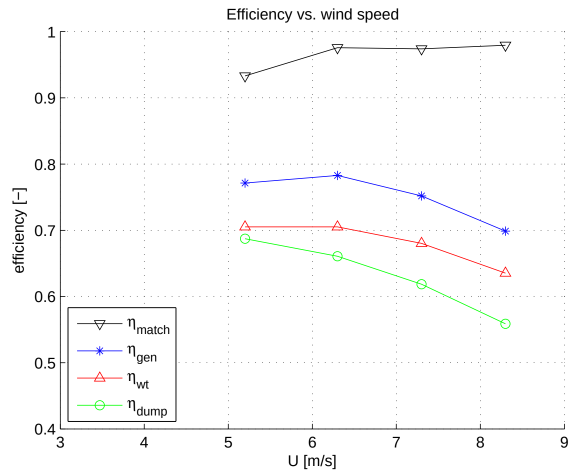

Figure 5.10: Turbine efficiencies vs. wind speed for a non-furling turbine ($\gamma = 0°$)

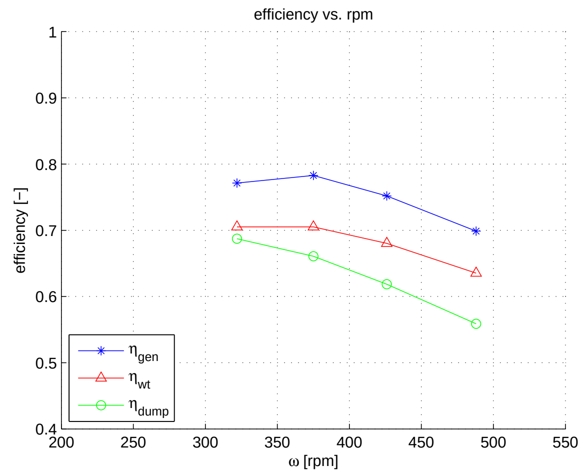

Figure 5.11: Turbine efficiencies vs. rotational speed for a non-furling turbine ($\gamma = 0°$)

this particular turbine, but at the Malian wind speed of 4 m/s a much lower power output is obtained.

Comparing the power of $P_{wt} = 367$ W at a wind speed of $U = 11$ m/s with other small wind turbines [Christensen, 2011], the performance is only slightly lower. Considering that this is a home build wind turbine, performance for non-yawed flow at high wind speeds is reasonable for this turbine.

To give a complete overview of the generator, also other aspects than the performance of the alternator should be considered. These aspects were discussed in Chapter 2. A good placement of the coils in the stator and magnets on the steel disks is essential for good generator performance. If the coils would have been aligned more optimal, the efficiency of the generator could have been higher. Therefore it would be interesting to investigate options to standardize the process more and thereby increasing product uniformity. Furthermore it would be interesting to investigate opportunities to lower generator cost and at the same time improve efficiency.

5.3 Furling system evaluation

The furling system is designed to protect the wind turbine from overspeed by means of turning the wind turbine out of the wind at high wind speeds. When the furling system is not sized correctly, this can cause unneccesary power losses at wind speeds where overloading is not a danger yet.

The power losses caused by the furling system can be evaluated by comparing the power at 0° yaw and the power when the turbine is furling to other yaw angles. The power curves from Figure 4.15 are shown again in Figure 5.12, but now expressed in wind turbine power P_{wt}. In this case power losses in the ground cables are excluded, as described in the previous section. From this figure the losses at high wind speeds (above 10 m/s) are clearly visible. However, at these high wind speeds the turbine was not tested at 0° so the absolute losses are not known. In Table 5.2 the losses for the lower wind velocities are shown. For wind speeds up to 6 m/s the losses remain below 10%.

In Figure 5.13 the efficiency of the furling system is shown. Due to friction forces in the yaw bearing the furling of the wind turbine is not very smooth and occurs in steps. The resulting efficiency curve therefore is not a smooth line. In Figure 5.14 the efficiency is shown as a function

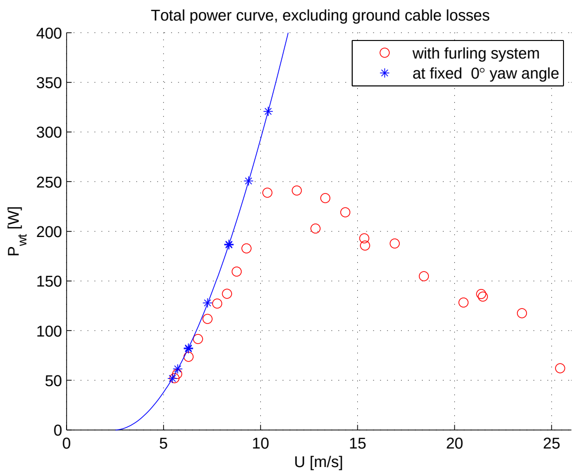

Figure 5.12: Powercurve $P_{wt} - U$ for total performance of a non-furling wind turbine ($\gamma = 0°$) and furling wind turbine (varying γ)

Table 5.2: Power losses caused by furling

U [m/s]	P_{wt} at $\gamma = 0°$ [W]	γ [°]	P_{wt} at γ [W]	η_{furl} [%]
5.7	60.2	22.0	56.4	94
6.3	83.3	24.8	73.7	88
7.3	127.9	26.0	111.8	87
8.3	187.0	33.7	137.1	73
9.3	250.6	33.7	182.8	73
10.4	320.8	35.4	238.9	74

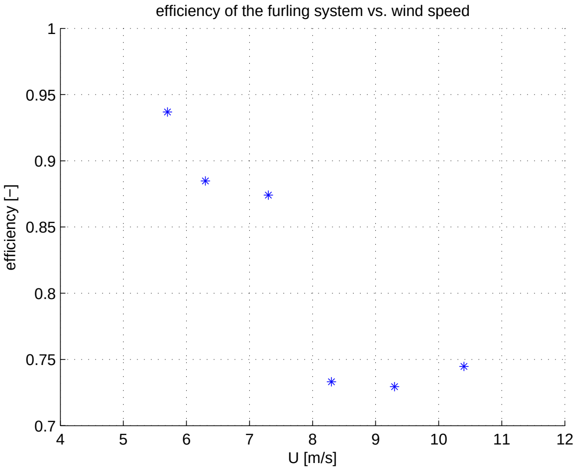

Figure 5.13: Turbine efficiency vs. wind speed due to losses caused by furling

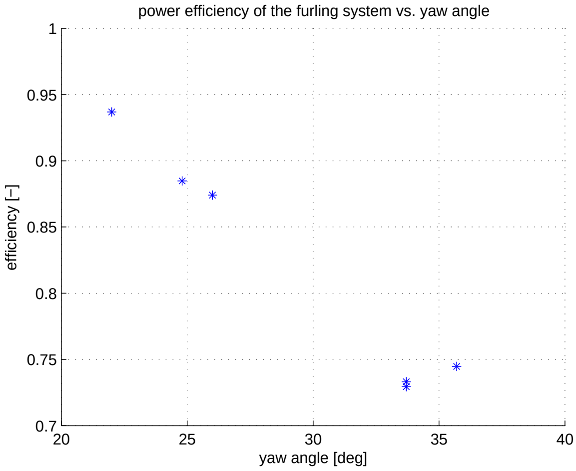

Figure 5.14: Turbine efficiency vs. yaw angle due to losses caused by furling

of yaw angle, and for this curve a more smooth line would be expected. The fact that at 36° the power loss is less than at 34° is likely to be a consequence of the measurement accuracy of the experiment.

It can be concluded that although the wind turbine starts furling directly at $U = 5$ m/s to $\gamma = 20°$, the losses at low wind speeds are limited. This can also be observed from Figure 5.5, which shows that losses up to $\gamma = 20°$ are low. However, for low wind speeds all losses that are caused by furling are in fact unnecessary. The wind tunnel tests have proven that (at least) up to 8.3 m/s there is no risk of overloading for an un-furled turbine. Therefore for this particular turbine a resizing of the furling tail is recommended. According to the Piggott manual [Piggott, 2008] this can be done by increasing the weight of the tail or increasing the area of the tail. If the effect of resizing is not sufficient a redesign of the furling system could be interesting. Several other furling concepts are known from literature, for example the concepts in KD 485 designed by Adriaan Kragten [Kragten, 2012].

5.4 Conclusion on the HP 1.8m turbine performance

From the evaluation of the different wind turbine aspects in this chapter the following interesting possibilities for improvements of the turbine follow:

- The rotor
  - Design a rotor with a higher tip speed ratio, to ensure better matching between generator and rotor at low wind speeds
  - Design a rotor that is easier and faster to produce, resulting in a better product uniformity
  - Design a rotor using materials with better availability in developing countries

- The alternator
  - Design a new generator that has an improved efficiency
  - Design a new generator that is easier to manufacture
  - Design a new generator that does not require the use of expensive permanent magnets
- The furling system
  - Optimize the current furling system such that yaw motion is postponed to higher wind velocities
  - Design a new furling system

From this it can be concluded that all three aspects would be interesting for improvement. Since we are focussing on the low wind speed regime that is characteristic for Mali, it is mainly important that the new product will have an improvement in this region. Also the ease of the production process is very important, since this determines the uniformity of the product and increases the change of success in developing countries.

This thesis study is conducted at an aerodynamic research department and to make optimal use of this knowledge it is for this study more evident to focus either on the improvement of the furling system or the rotor. Although it would be interesting to investigate opportunities to improve the alternator design, this is left for other studies.

Since at low wind speeds the furling losses are still very low, the rotor would be the more interesting part to improve. Since the performance of the rotor was already quite good, the focus will be on designing a rotor that is more easy to produce. A side goal is that the new rotor should be designed for higher tip speed ratio, to ensure better generator matching and increase efficiency at low wind speeds.

Chapter 6

Conceptual rotor design

In Section 5.4 it was concluded that for this thesis the rotor design is the most interesting part of the wind turbine to improve further. The main goal will be to design a rotor that is more easy to produce, resulting in a higher product uniformity. At the same time the overall performance of the new wind turbine should be similar or better. The new rotor should be designed for higher tip speed ratio, to ensure better generator matching at low wind speeds. The evaluation aspects for a wind turbine for developing countries that were set in Section 2.8 can be rewritten into requirements for the new rotor in the following way:

- **Similar or better Performance**
  - Similar or better maximum performance, expressed in $C_{P,max}$ of the rotor
  - A design tip speed ratio of 6, to lower generator losses at the Malian wind climate where $U_{mean} = 4$ m/s
  - The start-up speed should be below the cut-in speed of the turbine, which is $U_{cut-in} = 3.2$ m/s
- **Easier production process**
  - A production process that is less prone to manufacturing errors, causes a larger product uniformity
  - Lower production time
  - The production should only require the use of basic tools
- **Good availability of good quality materials in Mali**
  - Good quality materials, meaning that the durability and strength of the rotor should not be worse than for the current rotor
  - Usage of local materials as much as possible
- **Material costs**
  - Material costs of the new rotor should be similar or lower

Based on these requirements several concepts for a new rotor are composed and presented in the following sections:

- Designing more simple wooden rotor blades
- Designing rotor blades made from curved plates

At the end of the chapter, in Section 6.3 a choice is made on which concept will be worked out in detail.

6.1 Design of a simple wooden rotor

In Section 2.1 the use of wood as a wind turbine blade material has been discussed. Overall wood can be regarded as a suitable material for small scale usage in developing countries, since it requires little tools to work with and it has good strength. Disadvantages do exist, but since wood is the material that is currently used in Mali for the blades, this is a proven material. In this section an alternative design for a wooden rotor, that is more simple to produce than the current rotor, is presented.

6.1.1 Concept 1: Untapered and untwisted rotor blades

The Hugh Piggott wind turbine rotor blades are optimized twisted and tapered blades. It is particularly this shape change along the blade that makes manufacturing complex. A much more simple option would be to design wooden blades that do not have the twist and taper, and therefore have constant geometry over the complete blade length. This will speed up the production process, and since there are less dimensions that have to be marked out on the blades, less mistakes can be made.
On the other hand, for a non twisted blade the angle of attack variation along the blade will be larger, which means that not every blade section can operate at the optimum angle. This can decrease the lift and increase drag of the blade, and therefore the rotor power would be lower.

In Figure 6.1 a first comparison of a straight and untwisted rotor with the theoretical Hugh Piggott rotor (designed geometry, see Section 2.1) is given. The airfoil that is used here is the Naca 4412 airfoil, the chord is 75 mm and the blade angle is $\theta = 5°$. This is the optimum geometry for a design tip speed ratio of $\lambda = 6$ and the Naca 4412 airfoil for a three bladed rotor, determined iteratively using the BEM model from Appendix A.

The maximum C_P of the simple wooden rotor is 0.32. This means that in the theoretical case there would be a significant decrease for the straight bladed rotor compared to the Hugh Piggott rotor. However, when the result is compared with the Hugh Piggott rotor measurements (Section 4.5.1), the results are much more consistent. One should keep in mind here that due to imperfections in the real Hugh Piggott rotor, measured performance was less. For a more simple straight bladed rotor the tolerance in the production process will be lower and therefore less imperfections in the real blade geometry can be expected. Also, since the new rotor will be designed for a higher tip speed ratio, the performance decrease at high tip speed ratio will be less.

Summarizing, although the theoretical performance of a straight bladed rotor is less, due to less imperfections the real performance could be similar.

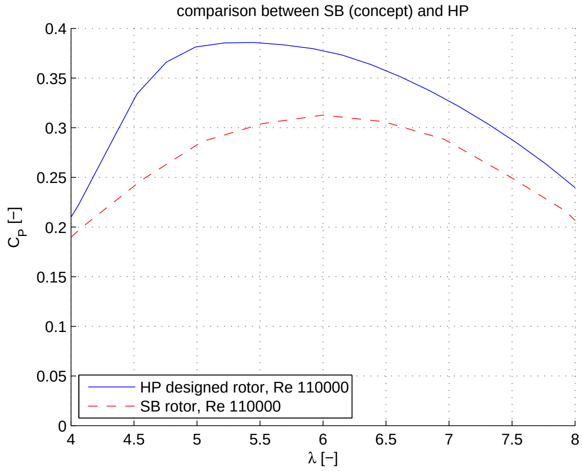

Figure 6.1: Calculated $C_P - \lambda$ of the Hugh Piggott (HP) rotor with design geometry and the straight bladed (SB) rotor concept

6.2 Curved plate rotor blade design

The Reynolds numbers at which the 1.8 m turbine operates are very low, in the range of 50000-200000 (Figure 3.1). The airfoil behaviour in this low range of Reynolds numbers is very different from higher Reynolds numbers of larger wind turbines. For small wind turbines therefore curved plate rotor blades become very interesting. In Figure 6.2 it is shown how a curved plate rotor can outperform a smooth airfoil for low Reynolds numbers.

In Figure 6.3 and 6.4 the lift and drag polar of the Naca 4412 airfoil and two curved plate airfoils with thicknesses of 10% and 12% are shown. Both are obtained from the Imperial Collega data

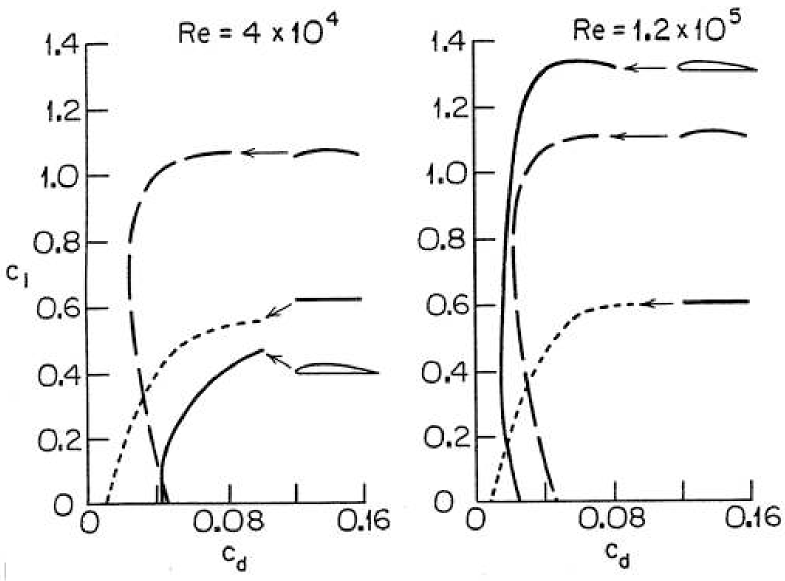

Figure 6.2: Comparison of lift-drag polars for smooth airfoils and flat and curved plates at $Re = 4 \cdot 10^4$ and $Re = 1.2 \cdot 10^5$, [Jones, 1990]

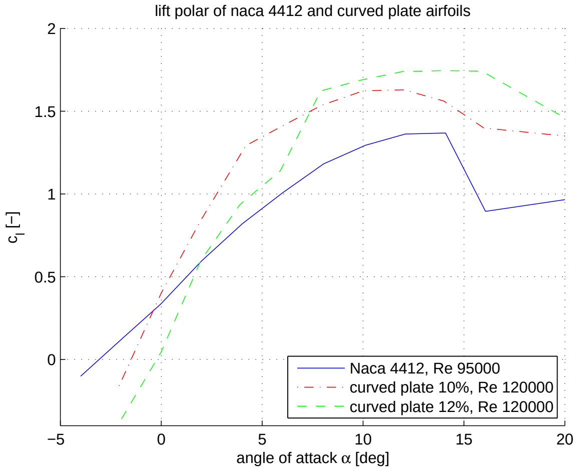

Figure 6.3: Lift polar of Naca 4412 and curved plate airfoils, from Imperial College [Hageman, 1980]

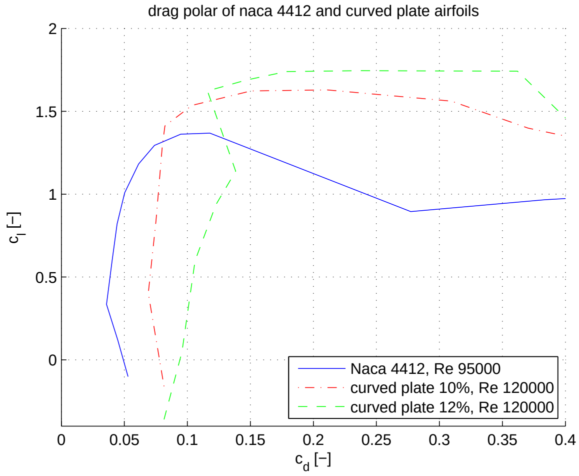

Figure 6.4: Drag polar of Naca 4412 and curved plate airfoils, from Imperial College [Hageman, 1980]

in the catalogue of Hageman [Hageman, 1980]. For comparison the Naca 4412 polars shown in these figures are also from Imperial College.

To investigate the possibilities of curved plate blades further, two concepts are composed in this section.

6.2.1 Concept 2: Metal curved plate rotor blades

One of the options of applying curved plate airfoils for rotor blades is by using metal plates. A lot of experience in this field is gained by Adriaan Kragten, who made several wind turbine designs based on this concept.

One attractive option is the VIRYA-3B2 that can be obtained from from KD 467 [Kragten, 2011]. This is a two bladed rotor with untwisted and untapered blades, made from steel sheets that are pressed into a curve. There is no twist an no taper, which make them easy to produce. Good performance is obtained, maximum C_P of 0.38 at $\lambda = 6.5$. Despite the fact that the blade are relatively easy and fast to produce, a large press is required to make the curved shape in the metal sheets. For small scale usage like in Mali this is very undesirable, because start up costs are expected to be high. For production in developing countries on a larger scale this could be an interesting option.

6.2.2 Concept 3: PVC curved plate rotor blades

Another interesting concept that has been used a lot by home wind turbine builders is to make rotor blades from PVC pipes. The idea is to cut a blade out of a PVC pipe in such a way that a change in blade angle and chord is created along the span of the blade. The airfoil profile will be a curved plate.

Production of this PVC rotor blade is very easy. Because the curved plate shape is already existing by the curvature of the pipe, the blade should just be cut out of the pipe and the edges should be shaved.

The main problem arising when using PVC is the strength of the blade. By increasing the wall thickness of the PVC pipe the strength of the blade can be increased. However, the curved plate airfoils in Figures 6.3 and 6.4 have a small wall thickness ($0.02c$) and it is likely that increasing the thickness will also increase drag. Also thick walled PVC pipes in good quality have a much lower availability.
Another option is to increase the stiffness by using stiffeners. Bruining investigated that stiffeners at the pressure side of the airfoil do not decrease performance [Hageman, 1980], so this could be a very interesting option.

For blades that do not have enough torsional stiffness, flutter can occur. This is an oscillating movement of the blades that mainly occurs for slim blades at high rotational speed. To prevent flutter it would be beneficial to have a larger blade chord. However, for a tip speed ratio of 6 a three-bladed rotor should have relatively slim blades. For this reason a two-bladed rotor would be a better option. The chord of these blades should be much larger to obtain the same optimum tip speed ratio.

Another problem for PVC pipes is the deterioration of the blades from sunlight. This will make the PVC material more brittle and decrease strength even more. It is important that a protective coating is applied to prevent this. Even when this coating is applied, PVC is expected to be less durable than wood. However, replacement of the blades would be very easy because of the fast production of a new set of blades.

To ensure strength of the blade, it is important that good quality PVC with enough wall thickness is used. In Mali this material is difficult to obtain.

In Figure 6.5 the $C_P - \lambda$ of a twisted and tapered curved plate two-bladed rotor is given, calculated with the BEM model. The airfoil used in this calculation is the 10% thick curved plate airfoil, described at the beginning of this section. This is an approximation of the real airfoils, because near the root the relative airfoil thickness will be different than near the tips. The pitch angle and chord distribution for this rotor is given in Table 6.1. The performance of this blade is slightly lower than the performance of the straight blade wooden rotor that was described in Section 6.1. The optimum C_P of this rotor is 0.3, which is significantly lower than the (theoretical) Hugh Piggott rotor.

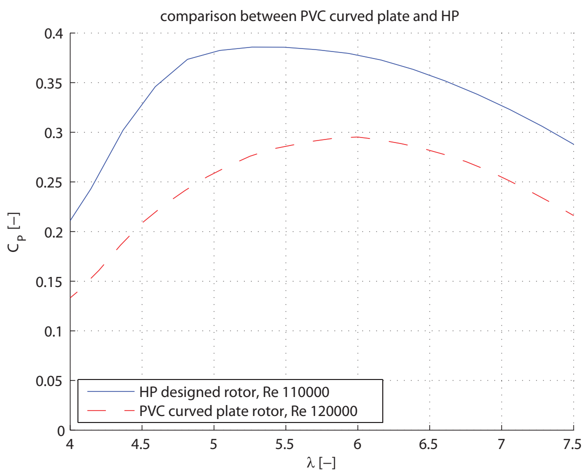

Figure 6.5: Calculated $C_P - \lambda$ of the Hugh Piggott (HP) rotor with design geometry and the curved plate PVC rotor concept

Table 6.1: Twist and chord distribution for a PVC curved plate two-bladed rotor

r [m]	0.8625	0.7875	0.7125	0.6375	0.5625	0.4875	0.4125	0.3375	0.2625
c [mm]	32	37	43	50	59	71	88	112	150
θ [deg]	3.62	4.25	5.02	5.96	7.16	8.73	10.87	13.96	18.80

6.3 Selection of concept for further research

In this chapter three new rotor concepts have been discussed. In this section the main advantages and disadvantages of these concepts will be summarized, after which one concept can be selected for further design.

The biggest disadvantage of using curved metal plate blades is that a press is needed to curve the blades. For local and small scale usage in Mali this is not wanted, since start-up costs will be high. However, for other usage where the production will be done by more central production on a larger scale, this could be an interesting concept to investigate.

Curved plate PVC is another promising concept. However, flutter of the blades is an expected problem. More extensive research on strength should be done to validate the feasibility of this concept. The availability of good PVC in Mali is another downside of this concept.

The remaining concept is a simple, untwisted and untapered wooden rotor, having a constant airfoil over the complete span. For this concept only the shape of the blades has to be changed compared to the original rotor. So the least adaptations are required regarding production tools and material. According to the calculations presented in this chapter the performance of a simple wooden rotor is also slightly better than the PVC rotor. Furthermore, there is already experience in making wooden blades in Mali. This makes a simple wooden rotor the most attractive option. In Chapter 7 this concept will be worked out in more detail.

Chapter 7

Detailed rotor design and manufacturing

In this chapter the best design concept that was chosen in Section 6.3, which is an untwisted and untapered wooden rotor, is worked out in more detail. The chapter starts with an explanation on the choice of number of blades in Section 7.1. After this the optimum geometry of the rotor is determined in Section 7.2 and the corresponding power curve is given. This is followed by a calculation of the strength, presented in Section 7.3. Finally the production process and upscaling of the rotor is described in Section 7.4.

7.1 Choice of number of blades

Most modern wind turbines nowadays have three blades. However, it would be interesting to investigate if this indeed would be the most effective option for this particular rotor design.

For a design tip speed ratio of 6, a three-, two- or single bladed rotor would be the best option [Burton et al., 2001]. The key is to find an optimum between structural design complexity, manufacturing time and costs, and performance efficiency.

For a single bladed rotor there is the problem of a large imbalance in the turbine, which causes structural problems. A two bladed rotor will eliminate most of this imbalance and would be a much better option. However, a two-bladed rotor poses a significant disadvantage over a three bladed rotor, caused by the gyroscopic force imbalance.

Spinning rotors act like gyroscopes in their plane of rotation. When a yawing motion causes the blades to rotate out of their plane, large forces are created. Particularly for a free yawing rotor like the turbine considered for this thesis gyroscopic forces can be large, because of large yaw rates. For a three bladed rotor the gyroscopic forces cancel out mostly. This effect is described in several wind turbine design books, of which one of those is the book *'Small Wind Turbines'* by Wood [Wood, 2011].

To achieve optimum performance, the chord length of a two-bladed rotor has to be larger than for a three-bladed rotor. This follows from the Blade Element Momentum (BEM) model described in Appendix A. Due to larger chord the blades have a higher Reynolds number, which would cause a small increase in performance. However, also tip losses will be larger because of a larger chord at the tip. These effects together are assumed to have minimal influence on performance.

The main advantages of a two-bladed rotor are considered to be the following:

- increased stiffness due to larger chord and less sensitive to flutter
- lower production time
- lower material costs

The main disadvantage is:

- large forces on the blades and structure due to the gyroscopic effect

To eliminate the disadvantage of the gyroscopic effect a teetered hinge between the rotor and the shaft would be a good option [Burton et al., 2001]. The advantage of a teeter hinge is that it decouples the gyroscopic force from the turbine. A more simple method would be to use a flexible connection of the blades to the hub, which is also done by Adriaan Kragten in his two-bladed wind turbine design [Kragten, 2011].

For this rotor a three-bladed design will be chosen. This is structurally the most simple option. When this rotor design appears to be successful, the next step could be to further improve the system and design a two-bladed straight rotor.

7.2 Optimum rotor geometry and performance calculation

In this section the geometry of the rotor, including an airfoil selection and determination of the optimum blade angle and chord distribution, will be discussed. After that the Reynolds number distribution for different wind speeds is given and the performance calculation using the BEM method of Appendix A is described.

7.2.1 Airfoil selection

The airfoil that will be used for the new rotor is the Naca 4412 airfoil. This is a simple airfoil with a nearly straight pressure side, that was also used for the Hugh Piggott rotor. The airfoil has gradual stall characteristics, meaning that lift drops only gradually after stall. This is very important for an untwisted blade, because the local angle of attack will vary much more than for a twisted blade.

In Figure 3.4 and 3.5 the characteristics of the Naca 4412 airfoil for different Reynolds numbers were given.

7.2.2 Blade angle and chord distribution

The blade will be a straight blade, which means that it has a constant chord c along the complete blade length. Furthermore the blade is untwisted, so it has a constant blade angle θ_m. Recall from Section 3.1 that θ_m is the blade angle measured from the straight pressure side of the airfoil and θ for a Naca 4412 airfoil is $\theta = \theta_m - 1.8°$.

To determine the optimum blade shape, the Blade Element Momentum (BEM) model described in Chapter 3 is used. The optimum geometry is found through an iterative process. With a chord length c of 80 mm the optimum tip speed ratio λ is around 6. If the chord would be even smaller the blade would become very thin, which will make it more vulnerable to flutter. The pitch angle that gives optimum performance at this geometry is $\theta_m = 7°$.

7.2.3 Reynolds number distribution

The distribution of Reynolds number along the blade is given in Figure 7.1. Because of a larger chord length c at the blade tip, the Reynolds numbers are higher than for the Hugh Piggott rotor. This will be beneficial for the performance.

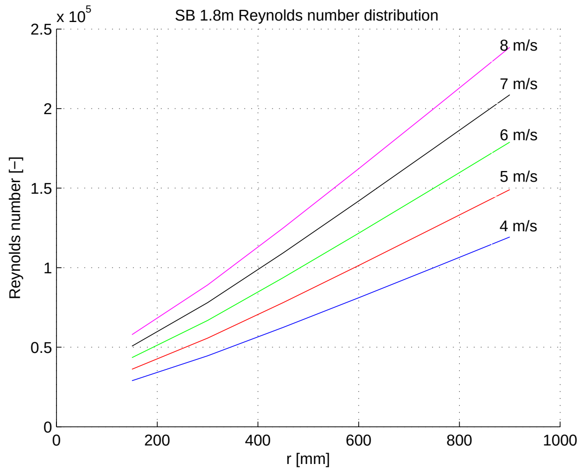

Figure 7.1: Reynolds number distribution for the straight bladed rotor for different wind velocities, at $\lambda = 5.5$

7.2.4 Performance calculation

The performance of the new rotor can be calculated with the BEM model. The performance of the optimum pitch angle of 7° is shown in Figure 7.2, as well as the performances at 6° and 8°. It can be observed that differences are only very small, but the 7° gives the overall best performance. The maximum power coefficient C_P that is achieved for 7° is 0.32 at a tip speed ratio λ of 5.9.

7.2.5 Start-up wind speed calculation

The start-up wind speed can be calculated by comparing the start up torque, caused by friction in the bearings, with the lift that the blade produces when the rotor is not rotating. From Appendix C the starting torque of the wind turbine is known to be $Q_{start-up} = 0.05$ Nm. The start-up torque produced by the lift should be larger than this value to get the rotor rotating.

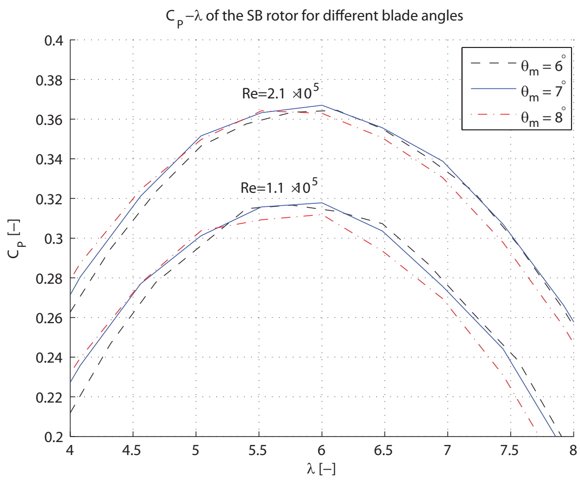

Figure 7.2: Calculated $C_P - \lambda$ of the straight bladed design rotor

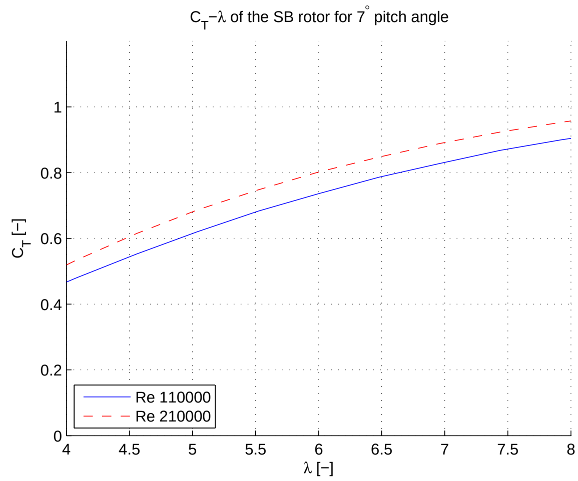

Figure 7.3: Calculated $C_T - \lambda$ of the straight bladed design rotor

For a non-rotating rotor the start-up torque can be calculated in the following way:

$$Q_{start-up} = B \cdot \sum_{r=R_r}^{R_t} f_{tan}(r) \cdot r \tag{7.1}$$

where B is the number of blades, R_t is the blade tip radius, R_r is the blade root radius and r is the radius of a blade element. The tangential force f_{tan} of a blade element produced by the lift of that element is calculated by:

$$f_{tan}(r) = \frac{1}{2} \cdot C_l(r) \cdot \rho \cdot U_{eff}^2 \cdot c(r) \cdot dr \tag{7.2}$$

where ρ is the air density, c is the constant blade chord of 80 mm and dr is the span of the blade element. Because $\omega = 0$ rpm, the following holds for the effective velocity U_{eff} in a start-up situation and the angle of attack α:

$$U_{eff}(r) = U_{start-up} \tag{7.3}$$

$$\alpha = 90^\circ - \theta = 90^\circ - (7^\circ - 1.8^\circ) = 84.8^\circ \tag{7.4}$$

The lift coefficient C_l corresponding to this high angle of attack for the Naca 4412 airfoil can be obtained from Hageman [Hageman, 1980] and amounts $C_l = 0.25$.

With these equations the theoretical start-up wind speed $U_{start-up}$ can be calculated and is $U_{start-up} = 1.9$ m/s. This means that start-up of the turbine will occur well before the cut-in wind speed of $U_{cut-in} = 3.2$ m/s.

7.3 Strength calculation

In this section a brief strength calculation will be presented for the new rotor design. In this calculation only the bending stress will be considered, which is caused by the axial force on the

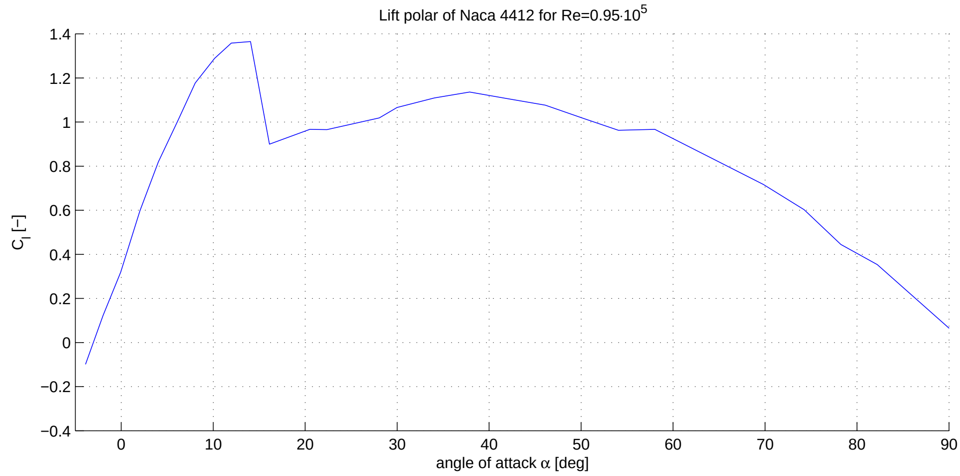

Figure 7.4: Lift polar of Naca 4412 airfoils for $Re = 0.95{\cdot}10^5$, from Imperial college [Hageman, 1980]

rotor blades. Also in tangential direction forces act on the blade, but the stresses caused by these loads will be neglected here. Unsteady flow effects or yawed flow will not be taken into account either.

For manufacturing of the blades Oregon pine wood will be used, which is a very good quality wood. From various online sources ([Centrum Hout, 2011] and [Boogaerdt Hout, 2011]) the characteristics of Oregon pine wood are known. The characteristics that will be used here are the ultimate bending stress $\sigma_{max} = 89$ N/mm^2 and the elasticity modulus E=13500 MPa.

With the flexure formula [Hibbeler, 2005] the bending stress σ in a beam caused by a bending moment M can be calculated:

$$\sigma = \frac{M \cdot y}{I_x} \tag{7.5}$$

where y is the perpendicular distance to the neutral axis and I_x is the second moment of inertia about the neutral axis. The bending moment for a single blade for a certain operational condition can be calculated using the BEM model. For $U = 9$ m/s and $\omega = 700$ rpm the bending moment of a single blade is 24 Nm. The second moment of inertia can be calculated by the following equation:

$$I_x = \frac{1}{12} b h^3 \tag{7.6}$$

A rectangular shape of $b * h = 8 * 60$ mm is used as an approximation of the cross section of the airfoil. For the distance to the neutral axis y =4 mm is chosen. With Equation 7.6 the second moment of inertia I_x can then be calculated and amounts $I_x = 2560$ mm^4.

Using Equation 7.5, the maximum bending stress σ amounts 37 N/mm^2. Since the ultimate bending stress σ_{max} of Oregon pine wood is 89 N/mm^2, this can be considered to be a safe situation. To validation this strength calculation, a small test is performed. The deflection of the blade δ is tested by hanging a weight at the tip of the blade. The deflection of the blade in this situation can also be calculated by Equation 7.7 [Hibbeler, 2005].

$$\delta = \frac{2ML^2}{2EI_x} \tag{7.7}$$

Where L is the length of the (free) beam, which is 750 mm, and E is the elasticity modulus, which is 13500 MPa for Oregon pine wood. For a weight of 1.2 kg the calculated deflection δ is 72 mm. The measured deflection is much less, 40 mm. This indicates that the actual strength is much larger than calculated in this section (e.g. due to the estimation of I_x and different wood properties) and therefore the bending strength will be well below the ultimate strength.

7.4 Manufacturing process and upscaling

One of the main goals of the new rotor design was that it could be easily produced using simple tools, decreasing the chance of production errors. In Appendix G the production manual for the new blades is given. Only the production of the blades is shown here, the assembly of the complete rotor and the production of the rest of the turbine is unchanged and can be found in the Hugh Piggott wind turbine manual [Piggott, 2008].

Because a smaller wood size is needed for the blades, the costs of the new blades are lower. The cost of the new rotor is approximately 60 euros, compared to 80 euros for the original Hugh Piggott rotor. This is a decrease of blade costs of 25%.

Also the production time of the new rotor is less than for the original rotor. The new production time amounts approximately 40 man hours. Comparing this to the original production time of 50 man hours (Section 2.1), a decrease of 20% is obtained. These percentages should be regarded as an estimation of the improvement.

To make the Naca 4412 airfoil profile shape in the blade, a template was used. The straight bladed rotor has the advantage that it has a constant chord and airfoil shape over the complete blade length, so only one template has to be used. Using this template and sandpaper it was relatively easy to obtain a good approximation of the airfoil shape. A picture of this is shown in Figure 7.5. The trailing edge of the airfoil is left a little thicker than the Naca 4412 airfoil, to prevent breaking of the wood during production. Due to the use of a template production errors are minimized and a good approximation of the Naca 4412 airfoil shape can be obtained. This increases the uniformity of the product. For the twisted and tapered Hugh Piggott blades the use of a single template is not possible, and a whole range of templates would be required.

After production of the blades the blade angles θ_m were measured using a digital angle gauge. For the 1.8 m rotor the chord is very small and therefore a small deviation from the design blade angle is inevitable. The blade angles that were measured amount 6°, 7° and 8° for the three different blades. Since the blade angles are constant over the entire length of the blades, the error in blade angle can be easily corrected. This is done by using a small wedge of +1° for the 6° blade and -1° for the 8° blade. A picture of these wedges is shown in Figure 7.6. Wedges can also be used to adjust the pitch angle during the measurements, which will be explained in Chapter 8.

A picture of the rotor after assembly of the three blades is shown in Figure 7.7.

Upscaling the rotor

For this thesis a rotor with a diameter of 1.8 m was chosen, since this is the maximum size that could still be tested in the Open Jet Facility wind tunnel. For real usage, a larger diameter would be more interesting from an economic point of view. The increase in material costs will be compensated by the extra power production that a larger rotor will give. Also the increase in

Reynolds number gives an important improvement at low wind velocities. For this reason, the optimum dimensions for a 3.0 m diameter rotor are also calculated.

The generator for the 3.0 m turbine is designed for a tip speed ratio of 7 [Piggott, 2008]. Since this is different from the tip speed ratio of 6 for the 1.8 m rotor, a new geometry should be designed for this rotor. For a three-bladed rotor this means that the blade chord c would have to be only 90 mm to achieve optimum performance (calculated with BEM). For a 3.0 m rotor this would be very small from a structural point of view and therefore a blade chord c of 110 mm is chosen. With this chord and a blade angle θ_m of 6° the optimum C_P would be 0.37 at $\lambda = 6.5$. This result is calculated for a Reynolds number of 210000. Due to the larger dimensions of the turbine the Reynolds numbers are higher and a Reynolds number of 210000 is already achieved at 4 m/s.

The dimensions of the 3.0 m turbine are also given in Appendix G.

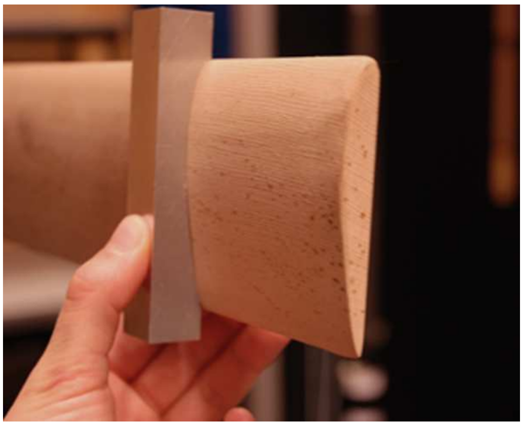

Figure 7.5: Airfoil shape in the blade, which is made using the template shown in the picture

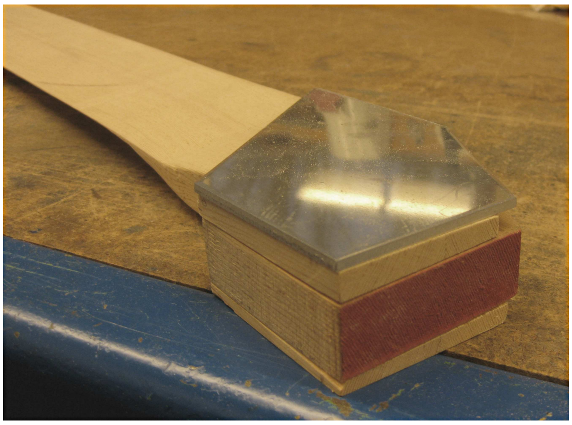

Figure 7.6: Wedges at the root of the blade, to adapt the blade angle

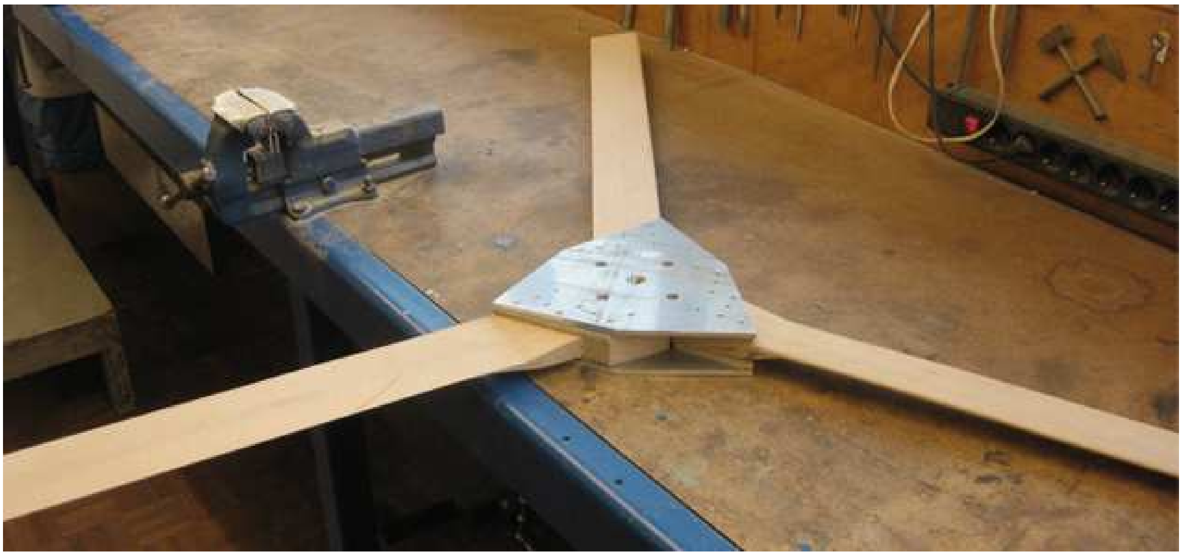

Figure 7.7: Straight bladed rotor after assembly

Chapter 8

Wind tunnel experiment 2 - Testing the new straight bladed rotor

The main goal of the second measurement campaign was to assess the performance of the new rotor that was described in Chapter 7 in order to compare it with the performance of the original rotor described in Chapter 2. To judge the validity of the comparison, the repeatability of the experiment has been tested as well. Next to these main goals the sound produced by both rotors was tested. The measurements goals are summarized as follows:

- Performance testing of the current rotor
- Performance testing of the new straight bladed rotor
- Test of measurement repeatability
- Sound measurements

In Section 8.1 a test matrix of all tests that are conducted during this experiment is discussed. The experimental set-up of the experiment is discussed in Section 8.2 and the measurement techniques and devices for this are described in Section 8.3. Data reduction of the measured results is discussed in Section 8.4. Finally the results are reported in Section 8.5.

8.1 Test matrix

In Table 8.1 the test matrix for experiment 2 is given. First the performance of the original Hugh Piggott (HP) rotor was tested again. This was first done in the original rotor configuration of experiment 1, with a relatively sharp blade nose. After this the nose of the blades was rounded off using sandpaper. This test is done because the rotor from experiment 1 is too sharp according to the manual, as discussed in Section 2.1. After this test the HP rotor was dismounted and the new straight bladed (SB) rotor was installed on the turbine. This rotor was tested for three different pitch angles. The procedure to change the pitch angles is described in Section 8.2.

To test the measurement repeatability of the experiment the new rotor is tested multiple times in the same configuration.

Apart from these main tests, additional tests are performed to test the difference between different experimental set-ups. These tests include testing the influence of heating up the bearings caused by operation of the wind turbine, influence of repositioning the table (this is described in Section 8.2), and the usage of different prony brake pulleys (Section 8.3). The results of these tests are presented in Appendix D. These results show that the small changes in experimental set-up do not cause a significant effect on the measured power.

To test the difference in noise production between the two rotors, sound measurements are performed. Since this is a side goal of the experiment, these tests are described in Appendix F. The most important results from these tests are shown at the end of this chapter.

Table 8.1: Test matrix of experiment 2

	Rotor	Blade shape	Pitch angle
Hugh Piggott rotor performance	HP-sharp	sharp nose	fixed
	HP-round	round nose	fixed
straight bladed rotor performance	SB-8	fixed	8°
	SB-6	fixed	6°
	SB-7	fixed	7°
Repeatability	SB-7	fixed	7°

8.2 Experimental set-up

Similar to experiment 1, experiment 2 will be conducted at the Open Jet Facility (OJF) wind-tunnel at the TU Delft. The same measurement set-up will be used as for experiment 1, except for the following modification:

- The rotor will now be placed in the center of the tunnel jet. During this experiment the wind turbine will only be tested without a tail, so there is no need to place the rotor off-center. By placing the rotor centered in the tunnel jet, the tower is placed 11 cm off center. The influence of this difference in position is presented in Appendix D and as expected this is not significant. The distance to the tunnel exit remains the same (1.8 m).

The wind turbine that is used for the tests is described in Chapter 2. However, since a new rotor will be tested, there are a few modifications to the original wind turbine. The modifications on the wind turbine are:

- for the second part of this experiment the original rotor is replaced by the new rotor
- an extra prony brake pulley of 14 cm diameter is mounted on the turbine, to be used at low wind speeds, see Figure 8.1 and Section 8.3.
- due to the extra prony brake pulley, the rotor is placed 11 cm further from the tower
- the pitch angle of the new rotor is changed throughout the experiment

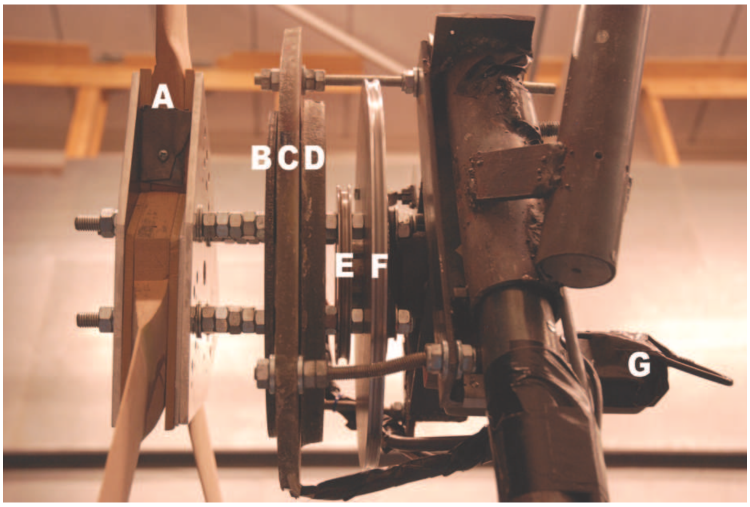

Figure 8.1: side view of the rotor hub, from left to right the following components can be distinguished: rotor (A), steel disk (B), stator (C), steel disk with magnets (D), small prony pulley (E), large prony pulley (F), frame and tachometer (G)

The pitch angle of the new rotor blades can be changed by changing the wedges, shown in Figure 7.6. For this the rotor had to be dismounted from the hub and the blades had to be disassembled. Only one blade was disassembled at a time to make sure that the blades could be assembled back in exactly the same position. After this the new rotor was mounted back on the turbine hub.

During the complete experiment the stator wires (the switches in the electrical circuit of Figure 4.5) were open circuit. In this way the generator is decoupled from the rotor.

8.3 Measurement techniques and devices

For this experiment only the rotor performance was tested, so only prony brake measurements were performed. The technique and devices required for this are discussed in this section. The set-up and apparatus for the sound measurements are discussed in Appendix F.

8.3.1 Prony brake

For the prony brake measurements the same principle as described in Section 4.3.1 is used. For experiment 1 a prony brake pulley of 300 mm diameter was used. Because of the large diameter, the forces in the cable are relatively small at low wind speeds. The consequence of this was that very small weights had to be used, which caused a low measurement accuracy of the forces in the prony cable F_w and F_l, see Section 4.3.1. The use of very small weights also made the measurements more difficult. To increase measurement accuracy at low wind speeds, for experiment 2 an additional smaller prony brake pulley is installed of 140 mm diameter. The large pulley is not removed and can be used at high wind speeds. The effect of using different prony brake pulleys is measured and the result is given in Appendix D. As expected no significant changes can be observed between the results obtained with both pulleys.

The measurement procedure is similar to the prony brake measurements of experiment 1. When a weight F_w is added on one side of the pulley rope a new equilibrium situation will be reached. Only after this equilibrium is reached, the measurement can start. The results that are presented are an average of a measurement of at least 5 seconds, to make sure that unsteady behaviour is levelled out.

8.3.2 Measurement devices

In Table 8.2 the measurement devices that are used for the tests are shown. These measurement devices are the same as used in experiment 1.

Table 8.2: Measurement devices for experiment 2

Quantity	Measurement device	Device type	Accuracy
ω	Digital hand tachometer	Ono Sokki HT-5100	0.5%
ω	Transmissive optical sensor	Vishay TCST2000	$< 0.01\%$
F_l	Loadcell	Scaime ZFA 25kg	0.075 N
W	Digital scale	Wedo Accurat 2000	1 g

8.4 Data reduction

In this section the wind velocity corrections that are applied to the results are presented first. After that the effect of limited measurement accuracy on the determined power coefficient is presented.

8.4.1 Wind tunnel velocity corrections

In between experiment 1 and 2 the wind tunnel was subjected to a new calibration. The consequence of this is that there is a new relation between the velocity in the center of the tunnel jet and the velocity at the 0.7 m off-center position, which is the position of the most effective part of the blades. The blockage correction for the velocity remains the same as described in Section 4.4.

The new wind velocity corrections can be found in Table 8.3. In this table U_m is the uncorrected wind speed determined in the tunnel and U is the wind speed after correction.

Table 8.3: OJF windtunnel wind speed corrections for experiment 2

	Wind speed corrections U/U_m		
γ (deg)	Blockage	Off-center	Total ($-$)
0	1.032	1.0028	1.035

8.4.2 Error in power coefficient determined from measurements

At low wind speeds better accuracy is achieved than for experiment 1, because of the usage of a smaller prony pulley. This results in larger weights and larger force in the loadcell. The new accuracies relevant for the prony brake measurements and their effect on the power coefficient C_P are presented in Table 8.4. The total C_P measurement accuracy for experiment 2 amounts minimum 2.2% (high wind speed) and maximum 3.0% (low windspeed). The accuracy for low windspeeds for experiment 1 was 3.6%, so accuracy has slightly improved.

Table 8.4: Effect of measurement accuracy on C_P for prony brake measurements for experiment 2

Quantity	Measurement accuracy	Effect on C_P
ω	0.5%	0.5%
F_l	0.075 N	0.2-0.9%
F_w	0.01 N	0.02-0.1%
U	0.5%	1.5%

8.5 Results

In this section the results of measuring the aerodynamic performance of the original rotor and the new rotor are presented. First the results for the original rotor are presented, both with a sharp and round blade nose. After that the results for the new rotor are presented, for the three tested pitch angles. Finally the main results of the sound measurement are presented.

8.5.1 The Hugh Piggott rotor

During wind tunnel experiment 1, the aerodynamic performance of the Hugh Piggott wind turbine was already assessed. The rotor blades had a relatively sharp leading edge. In this second wind tunnel experiment the influence of rounding the leading edge will be tested. To be able to make a good comparison between the two situations, both cases should be tested in the same measurement set-up. This will also validate the reliability of the first experiment.

The experiment started by testing the sharp nose blades from experiment 1 again. This rotor is called HP-sharp. After that the nose was rounded, while the rotor was not removed from the hub. This configuration is called HP-round.

In Table 8.5 the start-up wind speed of both configurations of the HP rotor are shown. This is the wind speed at which the blades just start rotating. It should be noted here that this is measured for an open circuit generator. The measurement spread for this measurement is quite large. This is mainly due to the fact that static friction in the bearings is not perfectly constant. Also the starting position of the blades can have an influence on start-up wind speed. As expected, the average values of start-up wind speed are in close agreement, since the rotor shape changes are very small.

In Figure 8.2 the aerodynamic $C_p - \lambda$ curves at several wind speeds for both the sharp and round Hugh Piggott blades are shown. A comparison of these results is easier using Figure 8.3. In this

Table 8.5: Start-up speed measurements of the HP rotor

	U_{start}[m/s]					mean U_{start}[m/s]
HP-sharp	3.0	2.8	3.1	2.9	2.8	2.9
HP-round	3.3	2.5	2.3	3.2	3.5	3.0

figure for each velocity three measurements are shown: the sharp blades from experiment 1 and the sharp and rounded blades from experiment 2.

From these figures it can be observed that although the sharp nose rotor of experiment 1 and 2 is exactly the same, the results are slightly different. This can be explained by the fact that there is a certain measurement accuracy in the results. From the results of measurement repeatability in Section 8.5.3 it is known that the confidence interval of C_P around the $C_{P,max}$ value (up to $\lambda = 6$) is 3.9%. The differences between the two HP-sharp rotors lie within this confidence interval. This validates the reliability of the prony brake results of the first experiment and shows that the measurement set-up has not changed significantly. This makes a comparison between the results of experiment 1 and 2 possible.

When looking at the HP-sharp and HP-round results of experiment 2 it can be observed that, as expected, the round nose rotor performs slightly better than the sharp nose rotor. In Table 8.6 the changes in $C_{P,max}$ between the two results are shown. The improvement is in the order of $1.2 - 5\%$, which means that not all of the measurements show a significant improvement. However, the fact that for all five wind velocities the performance has improved and for three measurements the improvement is significant indicates that there is indeed an improvement.

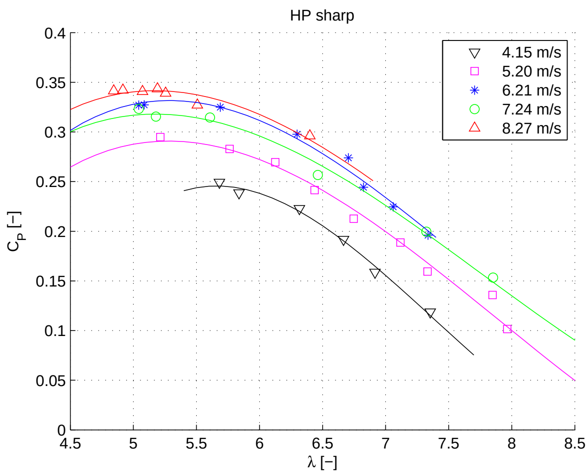

(a) HP-sharp (exp2)

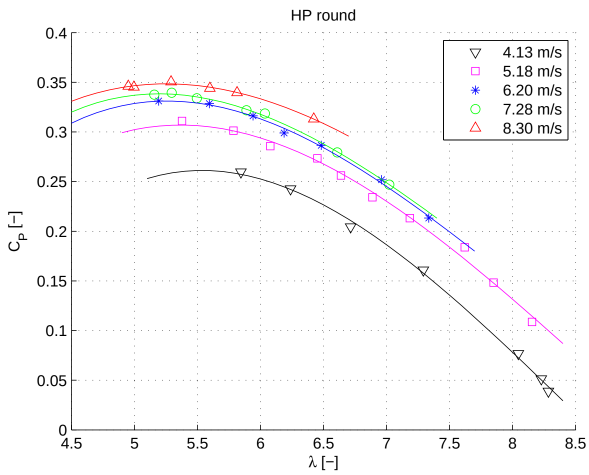

(b) HP-round

Figure 8.2: $C_P - \lambda$ for the HP rotor tested in experiment 2

Table 8.6: Comparison of peak $C_{P,max}$ values for the HP sharp and round rotor from experiment 2

U [m/s]	$C_{P,max}$[-]		improvement [%]
	HP-sharp	HP-round	
4.14	0.249	0.260	4.4
5.19	0.295	0.311	5.4
6.21	0.327	0.331	1.2
7.25	0.323	0.340	5.3
8.28	0.343	0.351	2.3

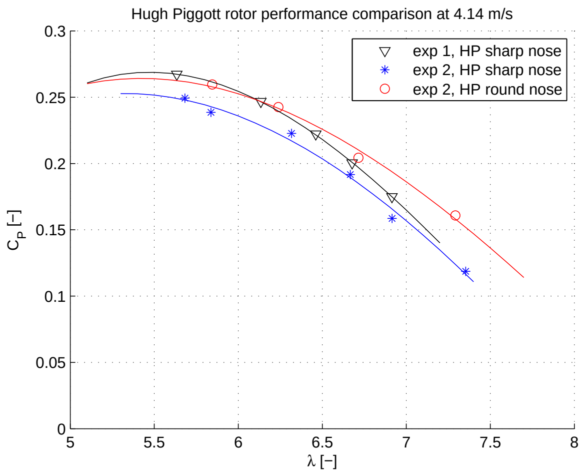

(a) 4.14 m/s

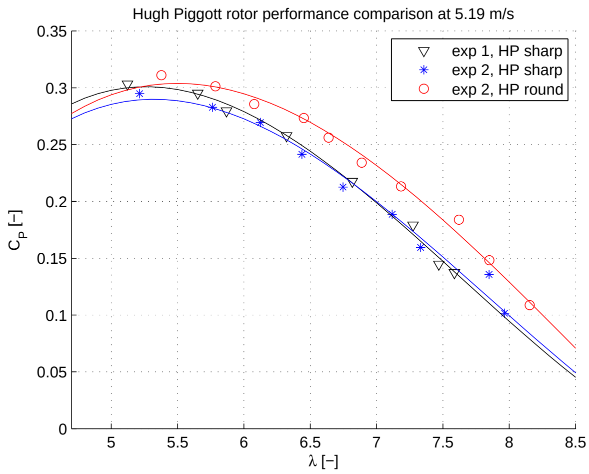

(b) 5.19 m/s

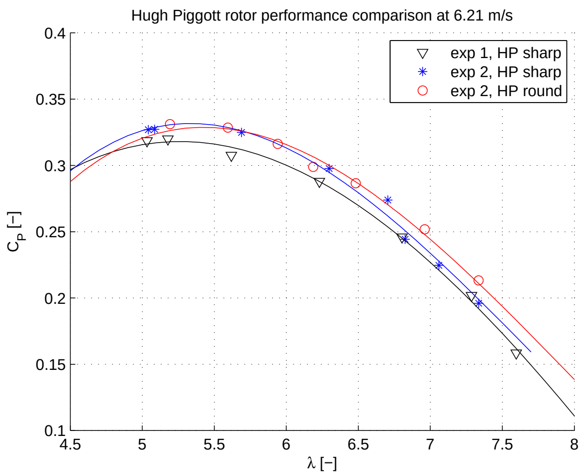

(c) 6.21 m/s

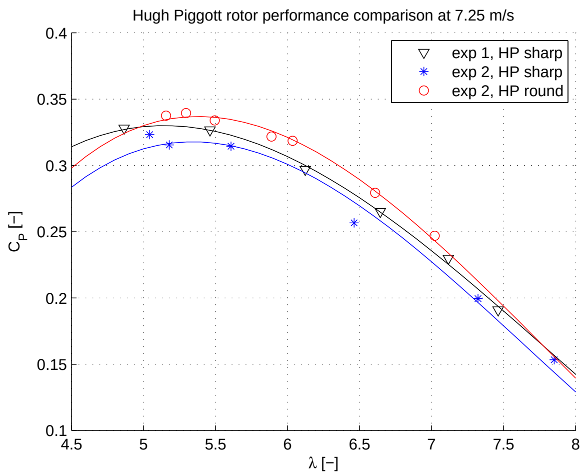

(d) 7.25 m/s

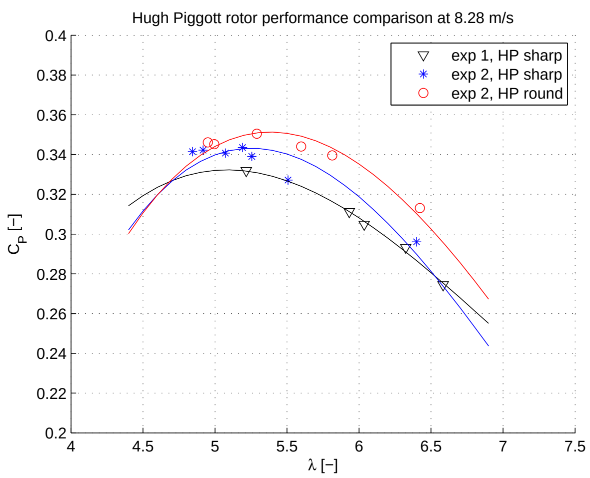

(e) 8.28 m/s

Figure 8.3: $C_P - \lambda$ comparison of results from experiment 1 and 2 for the HP rotor at different wind speeds

8.5.2 The straight bladed rotor

The straight bladed (SB) rotor is tested for three different blade pitch angles. For all configurations the start-up wind speed and the $C_P - \lambda$ curves are measured and presented in this section.

The start-up speed measurements for the different configurations of the tested SB rotor and the HP-round rotor are shown in Table 8.7. Similar to the HP start-up speed (as described in Section 8.5.1) the measurement spread is quite large. In general the start-up speed for the SB rotor is slightly higher than for the HP-round rotor. The SB-7 rotor shows the lowest start-up wind speed of the three configurations.

Table 8.7: Start-up speed measurements of the HP rotor

	measurements U_{start}[m/s]					mean U_{start}[m/s]
HP-round	3.3	2.5	2.3	3.2	3.5	3.0
SB-6	3.6	3.5	3.3	3.4	3.5	3.5
SB-7	3.0	3.0	3.7	3.2	3.1	3.2
SB-8	3.1	3.9	3.6	3.7	3.3	3.5

The $C_P - \lambda$ curves of the three configurations of the SB rotor are shown in Figure 8.4. The difference between these configurations at each wind speed becomes more clear from Figure 8.5. For comparison also the HP-round result from experiment 2 is shown.

The performance of all three SB configurations are very similar to the HP-round performance. The SB-7 rotor seems to be the most optimum configuration for the SB rotor. However, the differences are only small. When the differences are compared with the confidence interval from Section 8.5.3 they can not be considered significant. However, at all wind speeds a slightly higher performance is measured for SB-7. Next to that, in Chapter 7 it was calculated that this would theoretically be the most optimum configuration. Therefore the SB-7 rotor will be considered as the most optimum configuration here. The fact that the other pitch angles show very similar behaviour is a positive thing, because this indicates that a small error in blade angle made during the production process does not decrease the performance considerably.

From Figure 8.5 also the HP-round rotor tested in experiment 2 and the SB-7 rotor can be compared. The SB-7 has a slightly improved performance $C_{P,max}$ compared to this rotor. However, more important is the change in tip speed ratio λ, which causes the C_P to be higher at increased λ. In Chapter 9 the SB-7 rotor will be compared with the HP rotor in more detail. In that chapter it will also be determined whether the change in C_P is significant and what the consequence of a higher tip speed ratio is on total wind turbine performance.

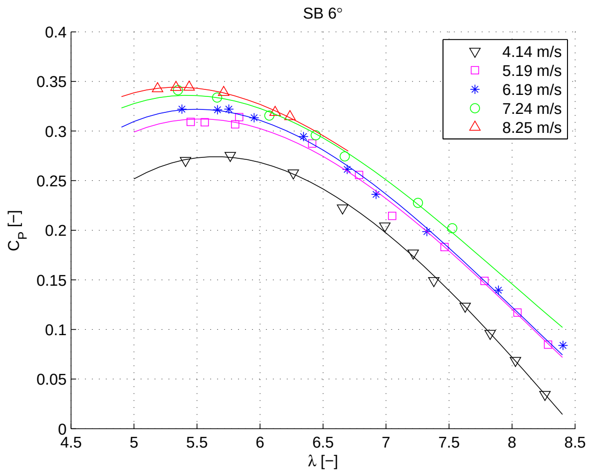

(a) $\theta = 6°$

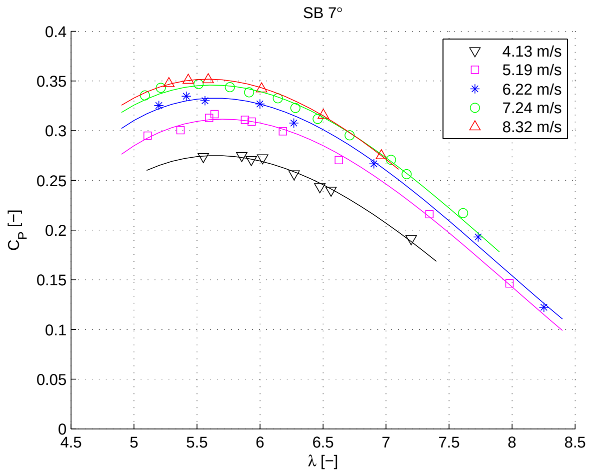

(b) $\theta = 7°$

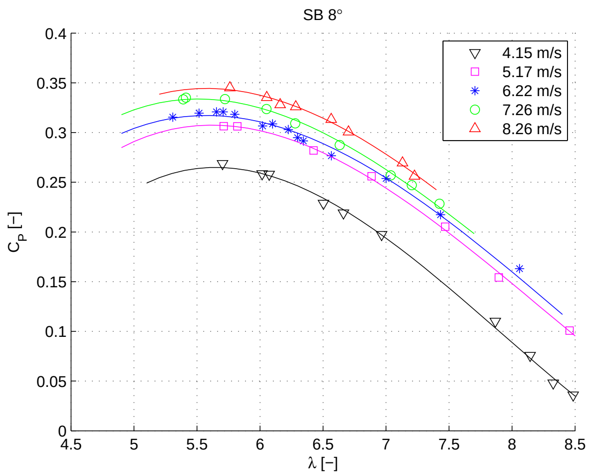

(c) $\theta = 8°$

Figure 8.4: $C_P - \lambda$ for the SB rotor at different configurations

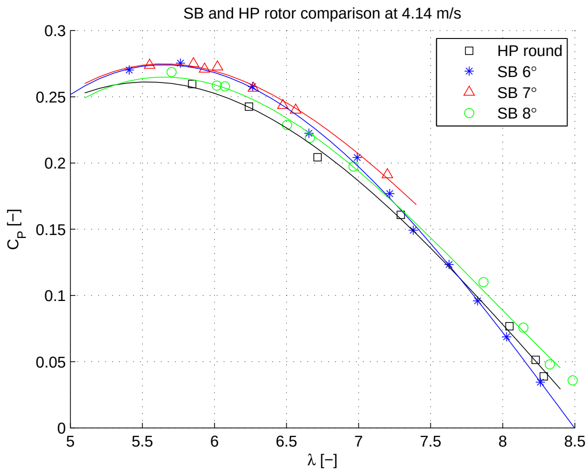

(a) 4.14 m/s

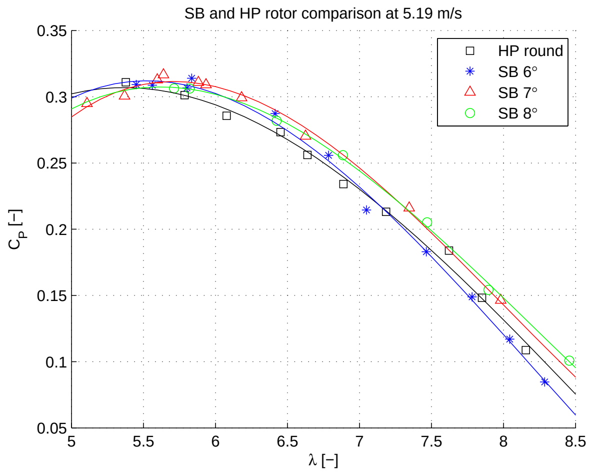

(b) 5.19 m/s

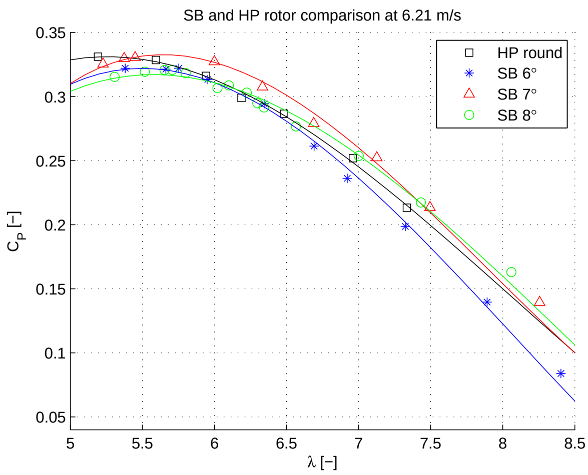

(c) 6.21 m/s

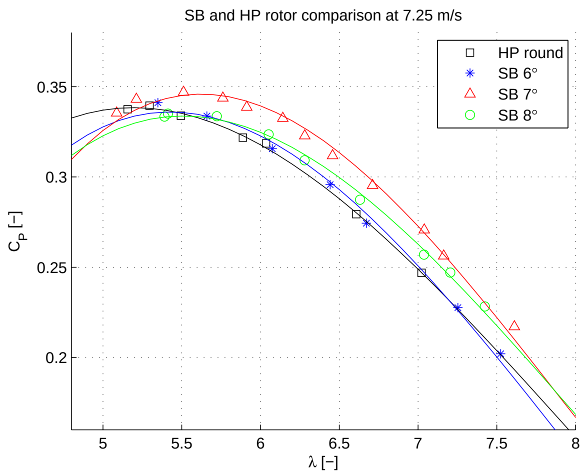

(d) 7.25 m/s

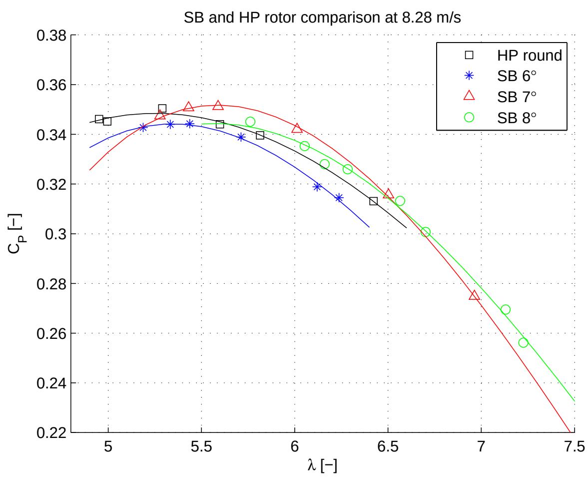

(e) 8.28 m/s

Figure 8.5: $C_P - \lambda$ comparison for the SB rotor at different wind speeds

8.5.3 Measurement repeatability

In Figures 8.6 and 8.6 seven different measurement sets for wind speeds of respectively 6.21 m/s and 7.25 m/s are shown. The measurements are all performed on the SB-7 rotor. The dataset that is used in the previous section for the comparison with other rotors and rotor configurations is data set 7, for both wind velocities. This data set was the most average data set, as can be seen in the figures.

To show the measurement spread in the results, in Figures 8.8 and 8.9 the confidence intervals of the measurements are shown. Assuming a normal distribution of the measurement spread, about 95% of the scores lie within two standard deviations of the mean. The mean and standard deviations are determined with the Matlab standard functions *polyfit* and *polyval*. The 95% interval indicates that you have a 95% chance that a new observation will fall within the bounds. A seperate spread for high and low tip speed ratio λ is shown because the spread at the optimum λ is much lower than at higher λ. A reason for this could be that the measurement accuracy of the devices is worse at low output power (Section 8.4.2), because of the lower forces in the prony brake rope.

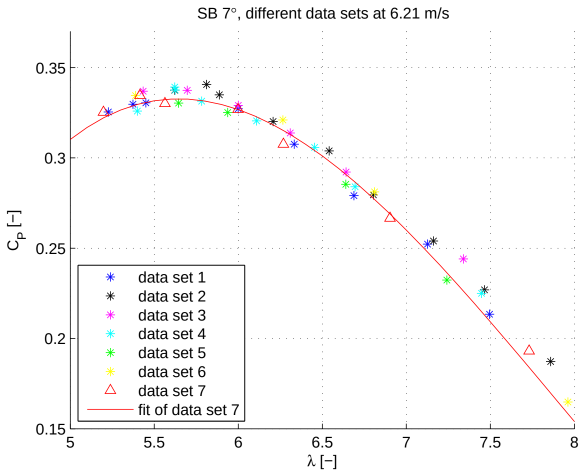

Figure 8.6: Datasets of SB-7 at 6.21 m/s

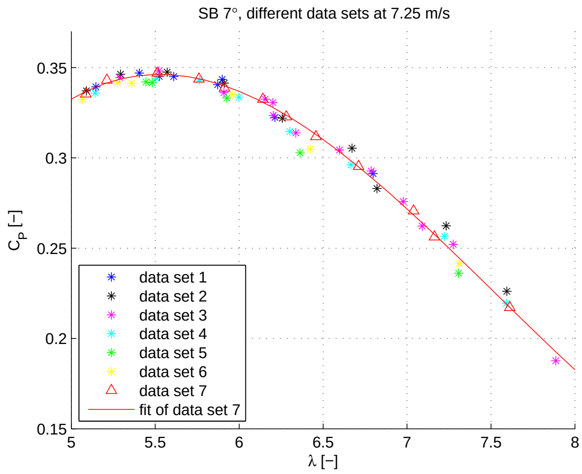

Figure 8.7: Datasets of SB-7 at 7.25 m/s

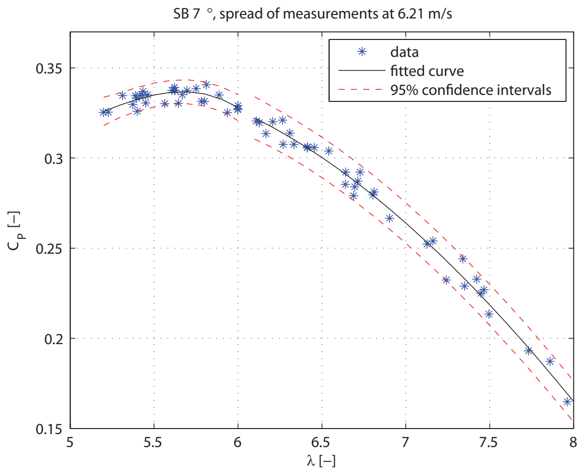

Figure 8.8: Measurement spread at 6.21 m/s

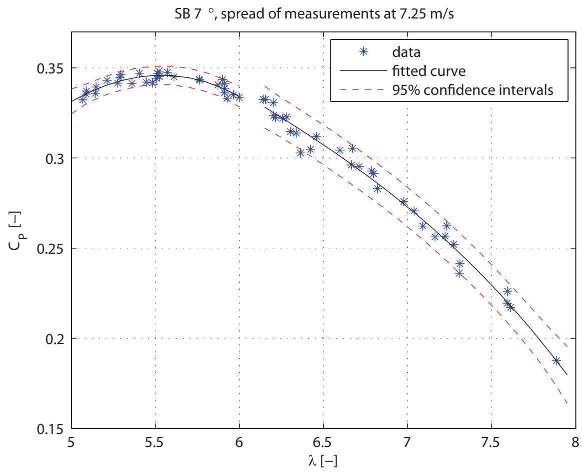

Figure 8.9: Measurement spread at 7.25 m/s

The C_P measurement spread for 6 m/s is 0.013 at the peak and 0.023 at higher λ. For 7 m/s the measurement spread is 0.010 at the peak and 0.022 at higher λ.
The measurement spread in percentage of $C_{P,max}$ is 3.9% for 6 m/s and 2.9% for 7 m/s. The spread of 3.9% will be used in the the rest of this report to compare the different rotors, because this is the largest spread. From Figures 8.8 and 8.9 we know that it is valid to use this spread for tip speed ratios up to 6.

8.5.4 Sound measurements

In this section the results of the sound measurements of both the Hugh Piggott (HP) and straight bladed (SB) wind turbine are shown. The sound pressure levels are measured with a Bruel and Kjaer (type 2231) sound level meter. All measurements are corrected for background noise. Only the measurements at locations in the center of the tunnel jet at different distances upwind and downwind of the rotor are shown. More information of the measurement set-up and measurement results at other locations than shown in this section can be found in Appendix F

In Figure 8.10 the corrected dBA levels of different testing cases for both wind turbine rotors are shown. The sound measurements for the Hugh Piggott rotor are performed on the HP-round rotor. For the SB rotor the sound measurements are performed on different pitch angle configurations (SB-6, SB-7 and SB-8). However, regarding the very small differences in performance that were shown in Figure 8.5, the differences in sound production between these configurations are assumed to be negligible.

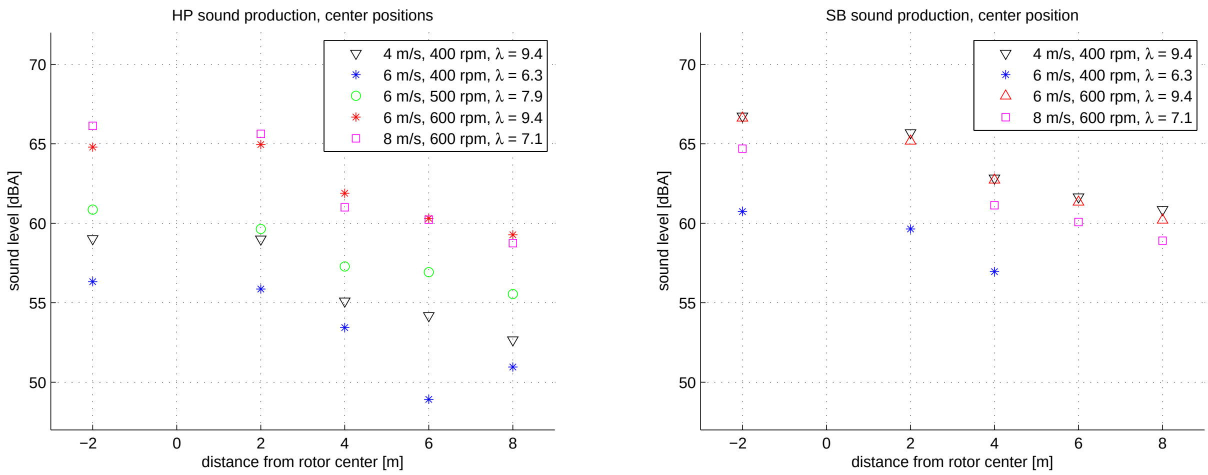

(a) Hugh Piggott rotor (b) Straight bladed rotor

Figure 8.10: Sound level measurements at locations in the center of the tunnel jet at different distances upwind and downwind of the rotor, corrected for background noise

HP sound production

For the sound produced by the HP rotor, there is a clear relation between sound production, wind speed and rotational speed. When looking at the three measurements performed at 6 m/s, it can be seen that higher rotational speed causes a higher sound production. However, it is not just rotational speed that is important. When the measurements of 400 rpm at 4 and 6 m/s are compared, the 6 m/s measurement gives a higher sound production. This can be explained by the fact that the resultant wind speed on the blade is higher for the higher wind speed. When two results of equal tip speed ratio are compared, as expected the measurement at the highest wind speed gives the highest sound production. Summarizing we can conclude that both tip speed ratio and wind speed determine the sound production of this wind turbine.

SB sound production
For the SB rotor the relation between sound production, tip speed ratio and wind speed is slightly different than for the HP rotor. In Figure 8.10b equal tip speed ratio measurements at 4 and 6 m/s show similar results. The lower tip speed ratio measurements shown in this figure give a lower sound production. This would indicate that for this rotor the tip speed ratio is the most important factor that determines noise. The fact that the SB blades have a larger chord length at the tips could be one of the reasons for extra sound production. The blade tips are responsible for most of the noise production because the relative velocity here is highest.

Relation between sound production and distance from source
Looking at the variation of sound production with distance from the rotor center, as expected the sound production is decreasing with increasing distance. However, for a point source, the sound pressure level is expected to fall by 6 dB when the distance to the source is doubled [Rogers et al., 2006], which is not the case for these measurements. A reason for this could be that the walls of the wind tunnel are reflecting part of the sound. The tests should be performed in the open field to cancel this effect out completely. Hence, the sound measurement tests presented in this thesis should only be regarded as a comparison tool for both rotors and an indication of what the real sound level is.

Comparison of the sound production of the two rotors
Comparing the source production (sound at 2 m distance from rotor) of both rotors, the SB rotor produces more sound at low wind speeds than the HP rotor. To be able to judge whether the sound that is produced is still acceptable, not the source power but the power at ground level is important. Assuming a minimum distance of 16 m to the turbine rotor (doubling the distance of 2 m three times) the decrease in sound pressure level amounts 18 dBA ($3 \cdot 6$ dBA). This would mean a sound level of maximum 49 dBA for the SB rotor. This can be compared to the sound level of a living room or quiet conversational speech [Rogers et al., 2006]. Normally the wind turbine would be placed much further away from human activity, so noise of this wind turbine is not expected to give much problems.

Chapter 9

Evaluation of the new straight bladed rotor

In this chapter the differences between the new straight bladed (SB) rotor and the tested Hugh Piggott (HP) rotor are discussed. The comparison is done based on the following aspects:

- Performance
- Strength
- Manufacturability, availability of materials and material cost
- Noise production

In the following sections the above aspects are discussed one by one. After that an overview of all improvements of the new wind turbine rotor compared to the original one is given.

9.1 Performance evaluation

In this section the performance of the new rotor is compared to the original rotor. The following questions are addressed:

- What is the difference between the calculated and measured performance of the new rotor?
- How does the rotor performance of the new rotor compare to the original rotor?
- What effect does the differences in rotor performance have on total performance?
- What effect does the differences in rotor performance have on the furling wind turbine?

9.1.1 Comparison of the calculated and measured SB rotor performance

For the HP rotor in Section 5.1.1 a comparison was made between the performance calculated with the BEM model and the measurements. Large differences between these results were found, which could be explained by the fact that there is an uncertainty in the input of the BEM model. This uncertainty is partly caused by the extra profile drag due to deviations in the actual airfoil shape from the Naca 4412 and 4415 that were used for the calculations.

For the SB rotor a template was used to produce the rotor blades and therefore a better approximation of the Naca 4412 airfoil could be obtained. In Figure 9.1 the calculated and measured $C_P - \lambda$ curve for the straight bladed rotor with a 7° pitch angle (SB-7) are shown. The maximum C_P that was measured at 5.19 m/s is in good agreement with the maximum C_P at a Reynolds number of $Re = 1.1 \cdot 10^5$. Recall from Figure 7.1 that this Reynolds number is the average Reynolds number at 5.19 m/s for this rotor.

Although there are small differences between the optimum λ and C_P at higher λ, it can be concluded that overall the calculations are in reasonable agreement with the measurements. This shows that for the new rotor a better approximation of the design geometry can be obtained, resulting in smaller differences between calculations and measurements. The uniformity of the product has therefore improved.

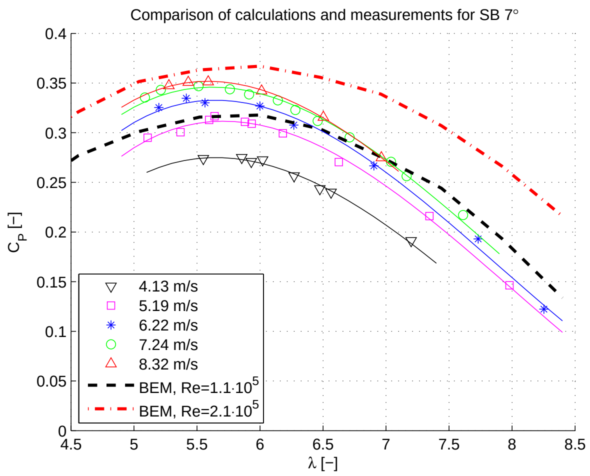

Figure 9.1: $C_P - \lambda$ for the SB-7 rotor, measured and calculated with BEM

9.1.2 Comparison of the SB and HP rotor performance

To address the differences in aerodynamic performance of the two rotor types, the $C_P - \lambda$ curves that result from experiment 2 are compared. For both rotor types the best configurations, determined in Section 8.5, is used for comparison. For the Hugh Piggott rotor this is the rotor with a rounded nose (HP-round). For the straight bladed rotor this is the rotor with a 7° pitch angle (SB-7).

In Table 9.1 the maximum power coefficient $C_{P,max}$ and corresponding tip speed ratio $\lambda_{C_{P,max}}$ for both rotors are given. In this table the values of the fitted curves, obtained from Figure 8.5, are given. This is necessary because the exact peak values were not always measured. The improvement that is given in the table is the improvement of the $C_{P,max}$ of SB-7 with respect to the $C_{P,max}$ of HP-round. From the results of measurement repeatability in Section 8.5.3 it is known that the confidence interval of the C_P around the $C_{P,max}$ value (up to $\lambda = 6$) is 3.9%. Therefore, the small improvement in $C_{P,max}$ of the SB-rotor can not be regarded as a significant result.

In Table 9.1 also the optimum tip speed ratios $\lambda_{C_{P,max}}$ of the two rotors are presented. The tip speed ratio of the SB-7 rotor is larger than the HP rotor. The consequence of this is that at low wind speeds the turbine will operate closer to its optimum tip speed ratio, which increases performance. This can be observed in Figure 8.5 as well. The consequence of the change in optimum tip speed ratio is discussed in the next section.

Table 9.1: Comparison of peak $C_{P,max}$ values for the HP round and SB-7 rotor measured in experiment 2

U [m/s]	$C_{P,max}$ [-]		$\lambda_{C_{P,max}}$ [-]		$C_{P,max}$ improvement [%]
	HP-round	SB-7	HP-round	SB-7	
4.14	0.261	0.275	5.6	5.7	5.4
5.19	0.307	0.312	5.4	5.7	1.6
6.21	0.331	0.333	5.3	5.7	0.6
7.25	0.338	0.346	5.2	5.6	2.4
8.28	0.348	0.352	5.3	5.6	1.1

Looking at the start-up wind speed of both rotors in Table 8.7 the average start-up wind speed for the SB-7 is $U_{start-up} = 3.2$ m/s and for the HP-round rotor $U_{start-up} = 3.0$ m/s. These start-up wind speeds are measured in open circuit. The cut-in wind speed of the wind turbine, where the turbine starts producing power, was determined at $U_{cut-in} = 3.2$ m/s in experiment 1 and is therefore equal to the start-up wind speed of the new rotor. When the start-up wind speed would be higher than the cut-in wind speed, power will be lost at that low wind speed, since the rotor would not start up. However, since the difference between the HP and SB windspeed is only very small it is not expected that this change will have a considerable negative effect on the performance.

9.1.3 Effect of rotor improvement on total performance

During normal operation the wind turbine will be connected to a battery. This battery operation causes the wind turbine to operate at variable rotational speed and tip speed ratio (see results of total performance in Section 4.5.2). The tip speed ratio of operation at low wind speeds is high and decreases with increasing wind speed. Therefore, not only $C_{P,max}$ is important to compare two rotors but the difference in C_P should be evaluated at each wind speed and corresponding operating tip speed ratio.

If the new wind turbine rotor would be connected to the same electrical circuit (12 V battery operation) as for experiment 1, the loading of the wind turbine would be the same. It is therefore assumed that at a certain wind speed U the rotational speed ω at which the new rotor will rotate is the same as for the original rotor. In Table 9.2 the wind speed U and corresponding rotational speed ω and tip speed ratio λ for the battery operating HP wind turbine at $\gamma = 0°$ are shown. The aerodynamic C_P values at λ for both the HP rotor from experiment 1 (HP-exp1) and the SB-7 rotor are given. The improvement given in the table is the improvement of C_P for SB-7, with respect to HP-exp1.

From Table 9.2 a clear improvement in C_P at the operating λ for the SB-7 rotor is visible for low wind speeds. For U =4 m/s the increase in C_P is determined to be even 11%. At higher wind speeds the improvement is not significant anymore, because of the lower operating tip speed ratio.

This result shows that the new rotor will give a better matching between generator and rotor at low wind speeds. The power loss at low wind speed that was caused by rotor-generator mismatching presented in Figure 5.13 will be mostly eliminated. Recalling from Section 2.6 that the average wind speed in Mali is 4 m/s, this is an important improvement.

Table 9.2: Comparison of peak C_P values for the HP round and SB-7 rotor measured in experiment 2

U [m/s]	ω [rpm]	λ [-]	C_P (HP-exp1) [-]	C_P (SB-7) [-]	C_P improvement [%]
4.19	307	7.0	0.186	0.207	11.3
5.19	337	6.1	0.290	0.305	5.2
6.21	376	5.7	0.325	0.333	2.5
7.25	425	5.5	0.336	0.345	2.7
8.28	483	5.5	0.347	0.351	1.2

9.1.4 Effect of rotor improvement on furling system

In Section 2.3 the principle of the furling system of the wind turbine was described. Since the rotor is mounted at a certain distance off-center of the tower, the thrust force of the rotor causes a yawing moment. The equilibrium of the thrust moment and tail moment determine when the turbine will start furling. The purpose of this yawing system is to protect the wind turbine from overspeed.

For a different rotor design a different thrust force can be expected, which will have an effect on furling behaviour. The effect of this is not measured during the experiments in this thesis and can therefore only be estimated using calculations. The calculated thrust coefficient C_T as a function of tip speed ratio λ is shown in Figure 9.2 for both the SB-7 and HP rotor. The C_T of the SB-7 rotor is smaller than for the HP rotor, which means that the yawing moment caused by the thrust will be smaller for the new rotor. The consequence of this will be that the new rotor will start yawing out of the wind at higher wind speeds than the current rotor.

In Section 5.3 it was concluded that the wind turbine started furling at very low wind speeds, where overspeed is not yet a danger. This caused a loss in power output. The fact that the new wind turbine is expected to start furling at higher wind speeds can therefore be regarded as an improvement. However, the danger exists that the turbine will not start furling at wind speeds where overloading does become a danger. If this would be the case the tail should be resized, according to the description in Section 2.3.

It can be concluded that the lower thrust coefficient of the new rotor is likely to postpone furling to higher wind speeds, which will lower the furling losses. Additional tests should be performed to determine if the overspeed protection at high wind speeds is still sufficient.

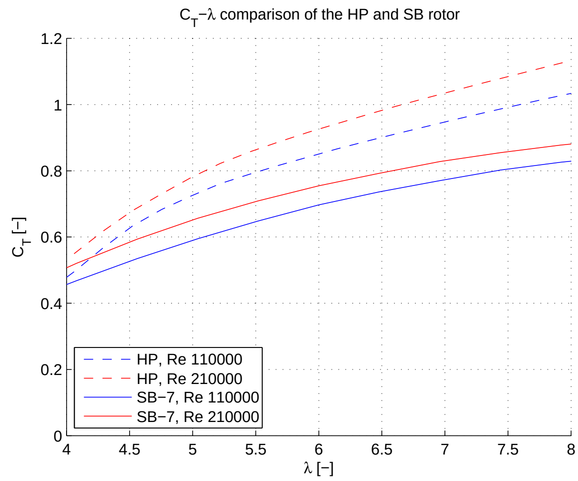

Figure 9.2: $C_T - \lambda$ calculation comparison for the HP and SB-7 rotor

9.2 Strength evaluation

The new rotor blades are thinner and more flexible than the HP blades and therefore it is important to consider the strength of the blades. During experiment 2 the new rotor was tested at a zero yaw angle at maximum wind speeds of 8.5 m/s and rotational speeds up to 800 rpm. During another experiment which was not part of this thesis the rotor is tested at even higher wind speeds, up to 11 m/s at zero yaw angle. Also, during the prony brake measurements, when too much weight was added to the prony brake rope the wind turbine suddenly braked, which poses quite some loads on the blades. The blades are proved to be strong enough for these situations.

During normal operation in the field, with a properly working furling system, the wind turbine will not be subjected to wind speeds of 11 m/s at zero yaw. However, yawing of the wind turbine will pose additional unsteady loads on the wind turbine.

Based on the fact that the wind turbine blades were strong enough to survive the 11 m/s wind speed at zero yaw angle it is expected that the strength of the wind turbine will be sufficient to resist the forces caused by furling. However, before the wind turbine can be operated in the field it is recommended that the turbine is first tested in yawing motion.

9.3 Manufacturing, availability of materials and material cost

In Section 7.4 the production process of the new rotor was discussed. Conclusions that can be drawn from this is that production is easier, which has the following consequences:

- lower production time (40 hours for the new rotor compared to 50 hours for the current rotor)
- higher uniformity of the product, which means that because of the simplicity of the design and the use of airfoil templates it is easier to resemble the design, which makes the final product less dependent on the skills of the producer

Next to this, because of the smaller chord and thickness of the blade a smaller and thinner piece of wood is required. This does not only reduce rotor costs by 25%, but more important it increases the availability of wood. Thick wood of good quality can be difficult to obtain in Mali, so this can be considered as an important improvement as well.

9.4 Noise production

In Section 8.5.4 the noise production for both wind turbines was discussed. The conclusion drawn from this is that the new rotor produces more noise in the low wind speed region ($U = 4$ m/s). However, since sound is decreasing by distance, the noise at ground level is still at an acceptable level.

9.5 Overview of improvements

In this chapter a comparison between the new straight bladed wind turbine and the Hugh Piggott wind turbine that was tested for this thesis is given. The improvements of the new wind turbine are summarized below:

- an increased total performance (when furling is not considered) of 11% at a wind speed of 4 m/s, caused by better generator matching and slightly higher optimum rotor performance
- easier manufacturing, which decreases production time of the rotor by 20%
- higher uniformity of the rotor
- higher availability of materials
- lower cost of blade materials of 25%

The negative effects of the new rotor are summarized as follows:

- more noise is produced at low wind speed, but the noise at ground level is still at an acceptable level

Considering the above, the new wind turbine rotor is a very promising rotor for small scale usage in developing countries like Mali, as an alternative for the Hugh Piggott rotor. However, in this thesis the following aspects have not been considered in enough detail and require additional testing:

- the effect of the difference in thrust force on the furling system
- the strength of the rotor during (unsteady) furling behaviour

As discussed in Section 9.1.4 it is expected that the difference in thrust force will cause the power losses due to furling to be lower. A resizing of the furling system could be done as well if this is necessary to ensure enough overspeed protection. Also the strength of the turbine is expected to be sufficient to survive the unsteady loads. Additional testing should be done to prove this.

Chapter 10

Conclusions and recommendations

The research objective of this thesis was stated in Section 1.2 and consisted of two tasks. The first was to identify the performance of the Hugh Piggott wind turbine, as it is used by the i-love-windpower movement in Mali. The second task was to design a new wind turbine that has improved compared to the current wind turbine in one or more aspects. In this chapter a conclusion on these research questions is drawn. Furthermore recommendations on further research of this topic are given.

10.1 Conclusions

Objective 1: Identify the performance of the Hugh Piggott wind turbine as it is used in Mali

For this thesis the performance of a 1.8 m diameter wind turbine, which is built according to the design of Hugh Piggott, was identified. The power production of the rotor was estimated by means of a Blade Element Momentum (BEM) model and tested by means of wind tunnel tests. Furthermore the total power production of the rotor and generator together and the furling behaviour have been measured during these wind tunnel tests.

Rotor performance
To identify the rotor performance, the rotor has been tested separately from the generator (in open circuit) in the wind tunnel. These tests showed a maximum power coefficient $C_{P,max}$ ranging from 0.27 for a wind speed of $U = 4.2$ m/s to 0.33 for $U = 8.3$ m/s at a tip speed ratio λ of around 5.3. At low wind speeds a small increase in wind velocity increases the performance considerably, because of the higher Reynolds numbers. For wind speeds of 7 m/s and higher the $C_{P,max}$ does not increase much further than 0.33. For a larger rotor diameter Reynolds numbers would be higher, which means that not only the power P will increase, but also the $C_{P,max}$ at low wind speeds.

The measured C_P is somewhat lower than calculated by the BEM model. This difference is caused by the limited accuracy of the BEM model and the uncertainty in the input of the BEM model. Imperfections in the actual blade compared to the Naca 4412 and 4415 profiles that were used as an input in BEM are likely to cause extra profile drag on the actual blade. A separate drag measurement was performed on the rotor to confirm this extra drag.

Total system performance
The complete wind turbine system, where the rotor is connected to the generator and a variable resistance dummy load, has also been tested. By varying the resistance a 12 V battery operation is resembled. Due to losses in the generator the total power that would be transferred to the battery is lower than the maximum aerodynamic power. These losses are partly caused by the resistance of the coil wires and losses in the rectifier, but also imperfect placement of the coils in the stator might have caused losses. The total wind turbine efficiency (battery power + ground cable losses), for a non-furling rotor is 71% at U = 5.2 m/s and decreases to 64% at U = 8.3 m/s. The losses due to not operating at the optimum tip speed ratio are 8% at U = 5.2 and decrease to 2% at U = 8.3. For the non-furling wind turbine the wind turbine power that was determined at a wind speed of U = 11 m/s amounts 367 W. The power at the average Malian wind speed of 4 m/s amounts 15 W.

Furling behaviour
The furling behaviour has been tested in the wind tunnel as well. At a low wind speed of 5 m/s the yaw angle has already increased to 20°, but the power losses are still only 5%. At 10 m/s the yaw angle has increased to 36°, which causes a power loss of 22%. At higher wind speeds the yaw angle and losses increase even further. From this it can be concluded that the furling system provides good overspeed protection, but causes unnecessary power losses at low wind speeds. The maximum power that was measured during total behaviour including furling is 239 W at a wind speed of 11.9 m/s. The losses due to furling at 4 m/s can be neglected and therefore the total power at this point amounts 15 W.

Manufacturability of the wind turbine
The manufacturability of the turbine has been addressed by means of experience from the field and estimated production times. The manufacturing of the rotor has with 39% the largest contribution to the total production. Due to a relatively complex production process of the rotor, there is a large tolerance in the production process which affects the uniformity of the turbine.

Final conclusion on performance identification
The power of the complete wind turbine system at 4 m/s amounts 15 W, and the rated power is measured at a wind speed of 11.9 m/s and amounts 239 W. For operation and local production in developing countries with a low average wind speed like Mali it is most interesting to improve the turbine efficiency at low wind speeds and simplify the production process such that a higher uniformity of the product can be obtained.

For a 1.8m turbine the Reynolds numbers at low wind speeds are very low. A larger diameter turbine would not only increase the power P, but also the aerodynamic power coefficient C_P at low wind speeds.

Objective 2: Design a new wind turbine that has improvements in one or more aspects

The goal of the second objective was to design a new wind turbine that has improved in one or more aspects, compared to the current wind turbine that was the subject of the first objective. Based on the conclusions from objective 1 it was decided to make a new rotor design, since this part is responsible for the largest production time, and its efficiency at low wind speeds can be improved. The goal was therefore to design a more simple to manufacture rotor, with similar or better performance and better generator matching at low wind speeds.

Performance comparison
From three design concepts the straight bladed (SB) wooden rotor was determined to be the most simple and efficient option. This rotor has no twist and has a constant chord length for the complete blade. The theoretical performance calculated with the BEM model was determined to be less than for the original rotor. However, the simplicity of the design and the use of airfoil templates decrease the tolerance in the production process. This decreases the chance of production errors and increases the uniformity of the product. For this rotor a detailed design was made and the rotor was manufactured. The new rotor and the original rotor were both tested in the wind tunnel to measure rotor performance.

First the original rotor (HP) rotor was tested in two configurations, with a relatively sharp leading edge and with a rounded leading edge. The rounded blade showed a slightly improved performance for all measurements. However, this increase in performance was below 4% and regarding measurement spread of the experiment this is not significant. Still, for a new design a rounded leading edge (resembling the Naca 4412 and Naca 4415 profiles) would be recommended.

The SB rotor was tested for three different pitch angles of 6°, 7° and 8°. The 7° pitch rotor (SB-7) appeared to be the best option, from both measurements and BEM calculations. However, changes are only small. When the new SB-7 rotor is compared with the HP rotor, the maximum power coefficient C_P of both rotors are very similar and in general the changes are not significant. However, the SB-7 has a larger tip speed ratio λ. This has a positive effect on the rotor-generator matching at low wind speeds, since the wind turbine can now operate more close to its optimum λ. This is expected to cause an increase in power of 11% for $U = 4$ m/s, which decreases to 0% at $U = 10$ m/s. This is an important improvement, since the average wind speed in Mali is $U = 4$ m/s.

With the BEM model the thrust force of both rotors has been calculated. The SB rotor has a lower thrust, which will have the consequence that furling will be postponed to higher wind speeds. This would lower the losses at low wind speeds. However, additional testing is required to prove that the overspeed protection at high wind speeds is still sufficient.

Comparison of other aspects
The fact that the new rotor has untapered and untwisted blades makes the production process easier. The estimated decrease in production time is 20%. Because of the untwisted and untapered shape of the blade and the use of an airfoil template the tolerance in the production process has decreased, resulting in a more uniform rotor. For a twisted and tapered blade it would be difficult to use templates, because each blade section would require a different template.

The smaller dimensions of the wood that is required for the blades decreases the blade costs by 25%. More importantly it increases the availability of wood in Mali. This is mainly an important improvement for larger turbine dimensions, above 3 m diameter.

During the tests the blades have proven to be strong enough to face wind conditions up to 11 m/s at zero yaw angle. During normal operation the furling system would prevent these situations to occur. The blades also proved to be strong enough to survive a sudden brake of the rotor. The blades have not been tested yet during yawing conditions, which can pose additional loads on the turbine. It is recommended that this test is done first, before the turbine can be operated.

Final conclusion on the new rotor design
The new rotor design has proven to lower the manufacturing time by making the process more simple. This increases the uniformity of the product, which ensures a more constant quality of the rotor. The total performance for a non-furling turbine has improved by 11% for the average Malian wind speed of 4 m/s. For higher wind speeds the performances of both rotors are very similar. Since the axial force produced by the new rotor is calculated to be lower, it is expected that furling will be postponed to higher wind velocities. More testing on this rotor is required to address both the performance and strength during yaw behaviour.

It should be noted here that due to the tolerance in the production process of the HP rotor other rotors could perform (slightly) worse or better than the turbine that was tested here. In this case the percentages of improvement that were given would change. However, for the new straight bladed rotor the tolerance in the production process has decreased and therefore other straight bladed rotors are expected to have a similar performance. This is an important improvement of the new rotor.

10.2 Recommendations

The first research objective of this thesis was to identify the complete performance of the current wind turbine. From this a list of possible improvements followed, but for this thesis only the rotor has been improved. The performance identification forms a good basis for further research on small wind turbine design for developing countries. Also the new rotor design gives possibilities for further improvement and testing. The following recommendations are composed:

1. **Strength tests of the new rotor blades**
   Before the new rotor design can be actually used in the open field, additional testing of several aspects is recommended. One of those tests is a strength test of the blades in yaw behaviour. Large yaw rates can cause high forces on the blades and support structure, and this has not been tested yet. Furthermore, it is recommended to test the ultimate strength that can occur during very high wind gusts.

2. **Testing and improving of the furling system**
   During the first experiment in which the total performance of the current wind turbine was identified, the furling system caused the wind turbine to furl at low wind speeds where overspeed is not yet a danger. The losses caused by this at a wind speed of 4 m/s are still low, but for higher wind speeds the losses increase considerably. A resizing of the tail could possibly solve part of this problem. However, the need for resizing is known to occur more often. It would be interesting to investigate the possibilities of using a template that would decrease the errors in the production process of the tail hinge.
   For the new rotor the furling behaviour has not been tested and this should be done as well to determine whether furling losses are a problem for this new turbine as well.

3. **Design of a two-bladed rotor**
   In this thesis a three-bladed rotor design was chosen, since this was the most simple option from a structural point of view. However, a two-bladed rotor would be interesting since it decreases the blade manufacturing time and costs even further. Because gyroscopic effects cause large forces during yaw movement of a two-bladed rotor, an adaptation to the attachment of the blades on the hub might be necessary. For larger wind turbines a

teetered hinge is normally used, but for a small simple turbine a flexible connection, as used by Kragten, could be an option.

4. **Improving the generator performance**
   It would be interesting to investigate how the losses in the generator system could be lowered and how efficiency of the generator can be improved. Also, since the permanent magnets are an expensive part of the turbine and need to be imported from outside Mali, it would be interesting to investigate how the costs could be lowered by using less strong magnets or a different type of generator.

5. **Design of a new rotor from a material other than wood**
   For a simple, cheap and easy to manufacture rotor wood is a suitable material, which can be shaped into a blade using just a saw, wood shaves and sand paper. However, the availability of good quality wood in large dimensions is poor in Mali and therefore it would be interesting to design a rotor that is made from a different material. The use of PVC pipes could be interesting for countries where good quality PVC is available, which is not the case in Mali. Since strength can be a problem the designer should take this into account. It would also be interesting to look at possibilities to make easy to manufacture and cheap composite blades, for example polyester or epoxy resin reinforced blades. Because a mould would be needed, this is mainly an interesting option for a larger production scale.

6. **Design of a new tower structure**
   Currently the tower is responsible for a large part of the total wind turbine costs. This is because a guyed tower is used, which requires large diameter pipes, which has a low availability in Mali and is therefore very expensive. Another disadvantage of a guyed tower is its reliability. Another option for a tower structure is a lattice tower, which is a tower structure made of multiple smaller pipes. This not only has the potential to decrease costs, but it also increases redundancy in the tower structure. Currently one lattice tower is built in Mali, but an optimization of this type of tower design is required to decrease the costs further.

Bibliography

[Bartmann and Fink, 2009] Bartmann, D. and Fink, D. (2009). *Homebrew Wind Power: A hands-on guide on harnessing the wind*. Buckville Publications LLC, first edition.

[Boogaerdt Hout, 2011] Boogaerdt Hout (2011). Technische info oregon pine (technical information oregon pine). Available on: http://www.oregon-online.nl/technische-info-oregon-pine.html.

[Burton et al., 2001] Burton, T., Sharpe, D., Jenkins, N., and Bossanyi, E. (2001). *Wind Energy Handbook*. Wiley, second edition.

[Centrum Hout, 2011] Centrum Hout (2011). Hout database (wood characteristics database). Available on: http://www.houtdatabase.nl/?q=hout/gww/64/mechanisch.

[Christensen, 2011] Christensen, K. (2011). *Catalogue of Small Windmills*. Nordic Folkecenter for Renewable Energy.

[Haans, 2011] Haans, W. (2011). *Wind turbine aerodynamics in yaw: unravelling the measured rotor wake*. PhD thesis, Delft University of Technology.

[Hageman, 1980] Hageman, A. (1980). *Catalogue of aerodynamic characteristics of airfoils in the reynolds number 104-106*. Laboratory of fluid dynamics and heat transfer, department of physics, university of Technology, Eindhoven.

[Hansen, 2008] Hansen, M. O. (2008). *Aerodynamics of Wind Turbines*. Earthscan, second edition.

[Hibbeler, 2005] Hibbeler, R. C. (2005). *Mechanics of Materials*. Prentice Hall, second edition.

[i-love-windpower, 2011] i-love-windpower (2011). Website of the i-love-windpower movement, part of the organization Stichting Energy Solutions for Humanity. Available on: http://www.i-love-windpower.com/.

[Johnson, 2004] Johnson, K. E. (2004). Adaptive torque control of variable speed wind turbines. *National Renewable Energy Laboratory*.

[Jones, 1990] Jones, R. (1990). *Wing Theory*. Princeton University Press.

[Kragten, 2011] Kragten, A. (2011). *KD 467: Calculations executed for the 2-bladed rotor of the VIRYA-3B2 windmill (λ_d = 6.5, steel blades).* Available on: www.bidnetwork.org/person-42169-en.html.

[Kragten, 2012] Kragten, A. (2012). *KD 485: Safety systems for small wind turbines which turn the rotor out of the wind at high wind speeds.* Available on: www.bidnetwork.org/person-42169-en.html.

[Manwell et al., 2009] Manwell, J., McGowan, J., and Rogers, A. (2009). *Wind Energy Explained.* Wiley, second edition.

[Mertens, 2006] Mertens, S. (2006). *Wind Energy in the Built Environment.* Phd thesis, Delft University of Technology.

[Nygaard et al., 2008] Nygaard, I., Rasmussen, K., Badger, J., et al. (2008). Using modeling, satellite images and existing global datasets for rapid preliminary assessments of renewable energy resources: The case of mali. *Elsevier.*

[Piggott, 2008] Piggott, H. (2008). *Wind Turbine Recipe Book.*

[REEEP, 2010] REEEP (2010). Policy database details mali (2010). Available on: http://www.reeep.org/index.php?id=9353&text=policy-database&special=viewitem&cid=126.

[RIWIK, 2011] RIWIK (2011). Website of the company riwik wind energy b.v. Available on: http://riwik.nl/.

[Rogers et al., 2006] Rogers, A. L., Manwell, J. F., and Wright, S. (2006). *Wind turbine acoustic noise: a white paper.* Amherst, MA: University of Massachusetts at Amherst, Department of Mechanical and Industrial Engineering, Renewable Energy Research Laboratory.

[Tongchitpakdee et al., 2005] Tongchitpakdee, C., Benjanirat, S., , and Sankar, L. N. (2005). *Numerical Simulation of the Aerodynamics of Horizontal Axis Wind Turbines under Yawed Flow Conditions.* Journal of Solar Energy Engineering, Vol. 127, Nov. 2005, pp. 464474.

[UNDP, 2011] UNDP (2011). Human development index (hdi) - 2011 rankings. Available on: http://hdr.undp.org/en/statistics/.

[Wilson and Lissaman, 1974] Wilson, R. and Lissaman, P. (1974). *Applied aerodynamics of wind power machines.* Oregon State University, Corvallis Oregon.

[Wood, 2011] Wood, D. (2011). *Small Wind Turbines: Analysis Design and Application.* Springer.

Appendix A

Blade Element Momentum theory

In literature many aerodynamic performance calculation codes can be found to analyze wind turbine rotor behavior. These models are used to calculate the loads and thus the thrust and power of a wind turbine rotor, for different settings of wind speed, rotational speed and rotor geometry.

In this study the Blade Element Momentum (BEM) theory will be used to model the rotor behavior. The BEM model is a simple model and fast to use, but has limited accuracy. However, as a design tool in an early stage of the design, BEM is a very useful method.

In this section the BEM method will be explained briefly. The analysis uses momentum theory and blade element theory. Momentum theory refers to a control volume analysis of the blades based on the conservation of linear and angular momentum. Blade element theory refers to an analysis of forces at a section of the blade. The results of these theories are combined into the blade element momentum (BEM) theory.

Only the most important resulting equations are given. A detailed description on how to derive these equations is available in the book 'Aerodynamics of Wind Turbines', [Hansen, 2008].

Momentum theory

The main principle of a wind turbine rotor is that energy can be extracted from the wind by slowing it down. This principle can be visualized by means of a stream tube, shown in Figure A.1. Because of the conservation of mass along the stream tube, the stream tube then must expand. The induction velocity is defined as the fractional decrease in wind velocity between the free stream and the rotor plane.

The expansion of the streamlines causes a pressure drop across the actuator disk. Because of conservation of axial momentum, a thrust force in the rotor must be created to compensate for this pressure change. This can be done for each annular element, giving the corresponding thrust dT. In a similar way the torque must equal the change in angular momentum and dQ can be calculated for each annular element as well.

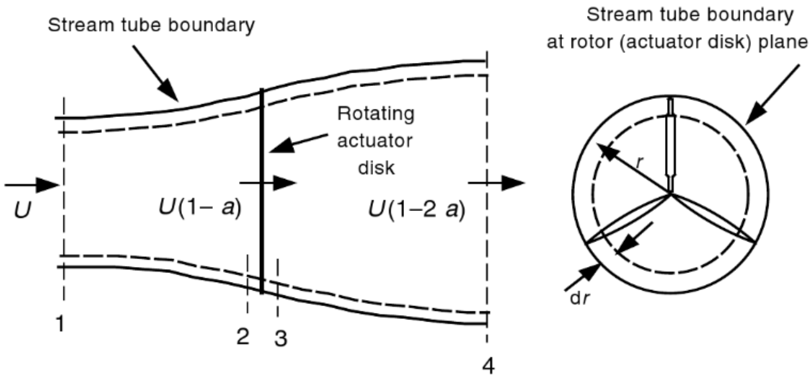

Figure A.1: The stream tube model used in BEM, [Manwell et al., 2009]

The resulting thrust and torque equations, given in Equations A.1 and A.2, can be used for each annular section of the blade.

$$dT = 4a(1-a)\rho U^2 \pi r dr \tag{A.1}$$

$$dQ = 4a'(1-a)\rho U \pi r^3 \omega dr \tag{A.2}$$

Blade element theory

The two key assumptions of the blade element theory are:

- There is no aerodynamic interaction between different blade elements
- The forces on the blade elements are solely determined by lift and drag coefficients

The definitions of the local conditions of each blade section are given in Figure 3.3. From these geometric relations the following equation can be derived:

$$\phi = \theta + \alpha \tag{A.3}$$

$$\tan\phi = \frac{U(1-a)}{\omega r(1+a')} \tag{A.4}$$

Using the equations above and the expressions for lift $L = \frac{1}{2}\rho U_{eff}^2 c C_l$ and drag $D = \frac{1}{2}\rho U_{eff}^2 c C_d$, the normal load coefficient C_n and tangential load coefficient C_t on the blade can be derived:

$$C_n = C_l \cos\phi + C_d \sin\phi \tag{A.5}$$

$$C_t = C_l \sin\phi - C_d \cos\phi \tag{A.6}$$

These equations can be used to calculate the axial force f_{ax} and tangential force f_{tan} per control volume for one blade:

$$f_{ax}(r) = \frac{1}{2}\rho U_{eff}^2(r) C_n c(r) dr \tag{A.7}$$

$$f_{tan}(r) = \frac{1}{2}\rho U_{eff}^2(r) C_t c(r) dr \tag{A.8}$$

Blade element momentum theory

By equalizing Equations A.1 and A.7 for dT, expressions for a and a' are obtained

$$a = \frac{1}{\frac{4\sin^2\phi}{\sigma C_n} + 1} \tag{A.9}$$

$$a' = \frac{1}{\frac{4\sin\phi\cos\phi}{\sigma C_t} - 1} \tag{A.10}$$

The induction factors a and a' can be obtained in an iterative way, using the following steps [Hansen, 2008]:

1. Guess values of a and a'
2. Calculate the flow angle ϕ
3. Calculate the local angle of attack α
4. Read off $C_l(\alpha)$ and $C_d(\alpha)$ from the airfoil polar plots
5. Calculate a and a'

This process is continued until the new induction factors are within a certain tolerance of the previous ones. The next step is then to calculate the local loads on the segments of the blades, according to equations A.7 and A.8. The power produced by the rotor is calculated by the sum of the tangential forces f_{tan} multiplied by the rotational speed of the rotor ω and the number of blades B.

$$P = B\int_{R_r}^{R_t} \omega f_{tan}(r) r \tag{A.11}$$

where r is the radius of the blade element, R_t is the blade tip radius and R_r is the blade root radius, where the hub ends and the actual blade starts. The power coefficient is calculated from the power:

$$C_P = \frac{P}{0.5\rho U^3 \pi R_t^2} \tag{A.12}$$

In order to obtain better results and to make the BEM model valid for a larger region, it is necessary to apply two corrections. The Prandtl tip correction is used to correct the assumption of an infinite number of blades. The Glauert correction is an empirical relation that is used to calculate the thrust for axial factors higher than $\frac{1}{3}$. This is necessary because BEM is no longer valid here. Both corrections are applied at step 5 and require an alternative calculation of the induction factors.

Momentum theory for a turbine rotor in steady yaw

When the wind turbine rotor has a non-zero yaw angle, the wind velocity component normal to the rotor disk is less and therefore less power can be extracted from the wind. The most simple method to assume that the loss in power would be a factor $\cos^3\gamma$ [Burton et al., 2001], where γ is the yaw angle as defined in Figure 2.6.

In reality the $\cos^3\gamma$ law is not perfectly accurate, because it neglect the wind component parallel to the rotor disk. The wind component causes the wake to skew sideways, which causes asymmetry in the axial induced velocity along the rotor disk. Therefore, in yawed flow, the blade forces will vary with azimuth position. To obtain an accurate calculation of the blade forces per blade and variations in time this variation in induction factor should be taken into account. Glauerts method is well known for this.

In Figure A.2 the fraction of available wind power as a function of yaw angle γ is shown [Burton et al., 2001]. In this figure the different calculation methods are compared. The axial momentum graph represents the $\cos^3\gamma$ rule described before. The figure shows significant changes between the different calculation methods. To assess which method gives the best approximation, a comparison with measurements is required. In Figure A.3 a comparison of measurements and the $\cos^3\gamma$ rule available from [Johnson, 2004] is given. Here the $\cos^3\gamma$ rule gives a reasonable approximation of the power.

Based on the results described above it was decided to use the $\cos^3\gamma$ rule as a first approximation to calculate the power in yaw.

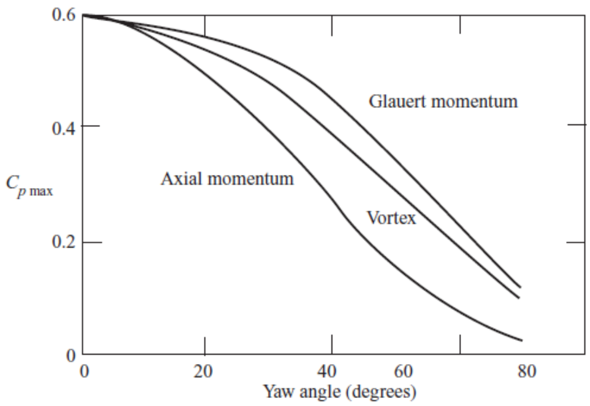

Figure A.2: Decrease in maximum available wind power vs. yaw angle, [Burton et al., 2001]. The axial momentum curve represents the $\cos^3\gamma$ approximation

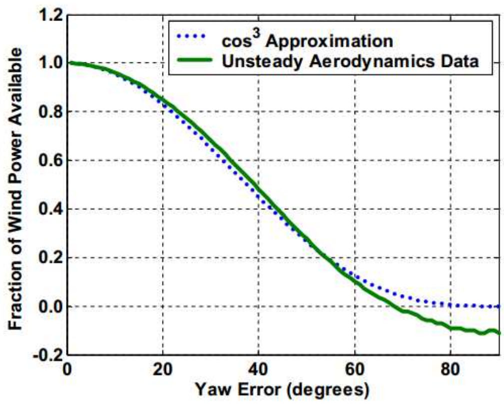

Figure A.3: Decrease in available wind power vs. yaw angle, [Johnson, 2004], the Unsteady Aerodynamics Data is obtained from NREL's Unsteady Aerodynamics experiment

Verification and validation of the model

To be able to use the model described in this appendix to predict the performance of the wind turbine for this thesis, both verification and validation of the model is required.

Verification

The BEM model used in this study is found in the book 'Aerodynamics of Wind Turbines' [Hansen, 2008] and is often used as a design tool is this form. To verify correct implementation of this model, the results of the BEM model described in this chapter are compared with results from the BEM code PROPSI. PROPSI is a modified version (developed by TU Delft) of the original PROP code developed by Oregon State University [Wilson and Lissaman, 1974]. Only the Glauert correction for highly loaded wind turbines and the tip correction of the PROPSI code are used, and 3D effects are not considered. For this comparison the designed Hugh Piggott wind turbine geometry (Section 3.1) is used.

In Figures A.4 to A.7 the $C_P - \lambda$ and $C_T - \lambda$ resulting from both BEM codes can be found. The results show small differences at higher tip speed ratio λ. A reason for this difference could be that the correction methods (Glauert and Prandtl tip) are slightly different for both methods. Overall the results of the BEM model are in reasonable agreement with the PROPSI model.

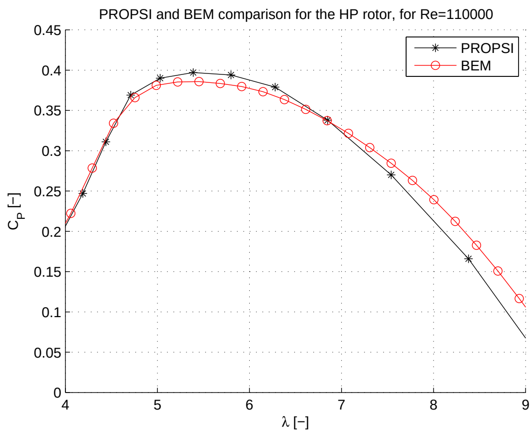

Figure A.4: $C_P - \lambda$ of HP1.8 (design geometry) for Re =110000, calculated with PROPSI and BEM

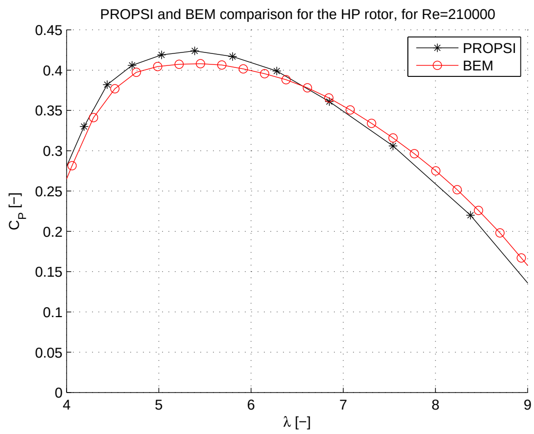

Figure A.5: $C_P - \lambda$ of HP1.8 (design geometry) for Re =210000, calculated with PROPSI and BEM

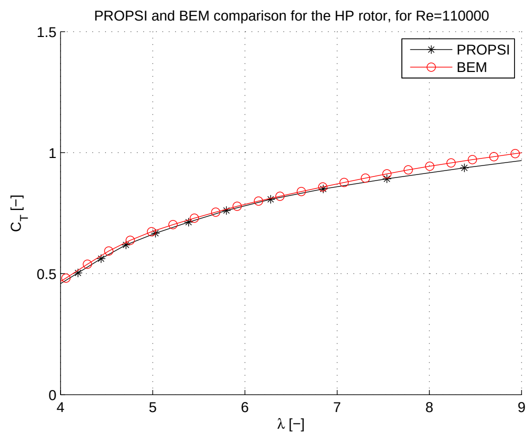

Figure A.6: $C_T - \lambda$ of HP1.8 (design geometry) for Re =110000, calculated with PROPSI and BEM

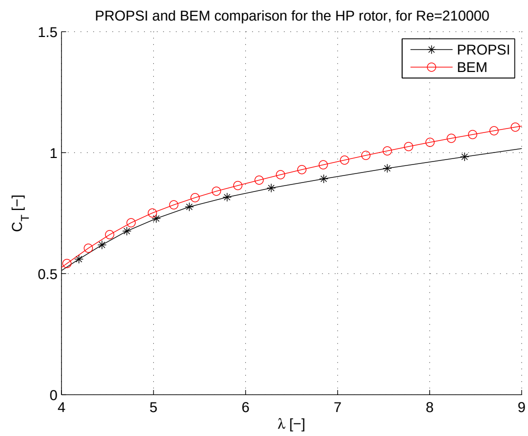

Figure A.7: $C_T - \lambda$ of HP1.8 (design geometry) for Re =210000, calculated with PROPSI and BEM

Validation

For validation of the model the BEM calculations have to be compared to measurements. From Haans the results of C_T measurements on a small (1.2 m diameter) two-bladed wind turbine are available [Haans, 2011]. These measurements are conducted in the same Open Jet Facility wind tunnel that was used for this thesis. With the BEM model described in this chapter, the C_T of this rotor can be calculated as well.

In Figure A.8 the $C_T - \lambda$ curve for the BEM code and the measurements are given. Considering the measurement accuracy in the measurements, the calculated results are in reasonable agreement with the measurements.

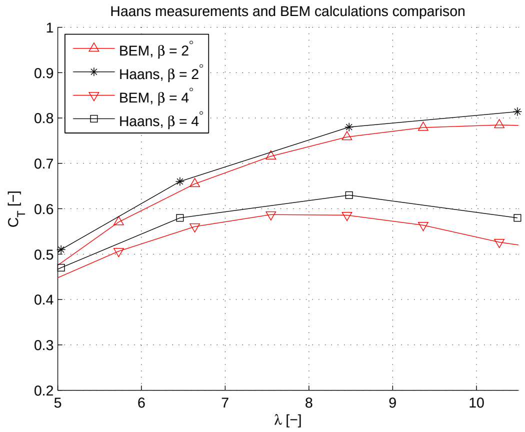

Figure A.8: $C_T - \lambda$ comparison of Haans measurements [Haans, 2011] and BEM calculations

Appendix B

BEM sensitivity analysis

To address the deviations in airfoil shape from a perfect Naca airfoil, a sensitivity analysis is done with XFOIL. XFOIL is an airfoil design code, that can be used to calculate lift and drag polars of airfoils.

The N_{crit} number used in the XFOIL code was calculated using Mack's correlation, using the OJF wind tunnel freestream turbulence level of $\tau = 0.23\%$.

$$N_{crit} = -8.43 - 2.4 * ln(\tau) = 6.3 \tag{B.1}$$

The calculations are done at a Reynolds number of 100000.

Since XFOIL in general gives a larger lift and lower drag compared to measurements, the analysis will only be used in a qualitative way. To keep the analysis simple, only one adaptation to each airfoil is made. The adapted shapes resemble the real rotor better than the perfect Naca airfoils. However, of course this is still an approximation of the real shape.

In Figures B.1 and B.2 the adaptations on the Naca 4412 and Naca 4415 airfoil are given. The differences in lift and drag polars that cause this effect are shown in Figures B.3 and B.4. The change in airfoil shape has a significant effect on C_P, as shown in Figure B.5.

This analysis indicates that changes in airfoil shape can cause significant changes in performance. Therefore, deviations between the performance calculated with the BEM model and performance measurements are very likely to occur.

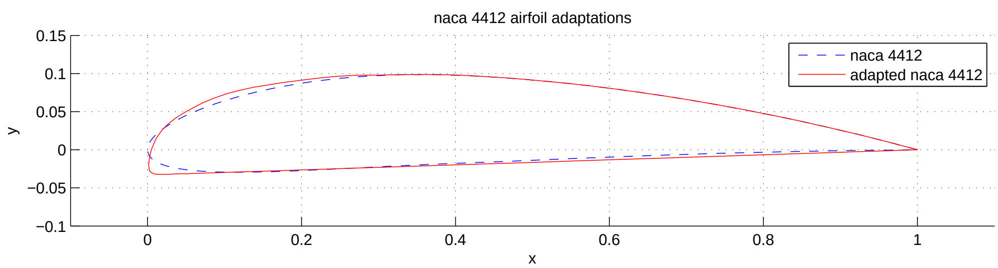

Figure B.1: Adaptation of Naca 4412 airfoil

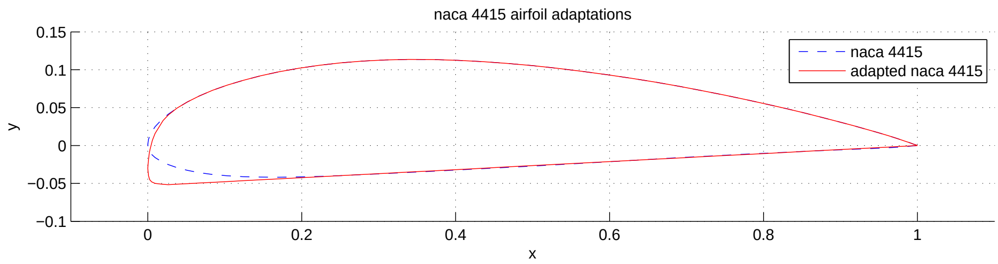

Figure B.2: Adaptation of Naca 4415 airfoil

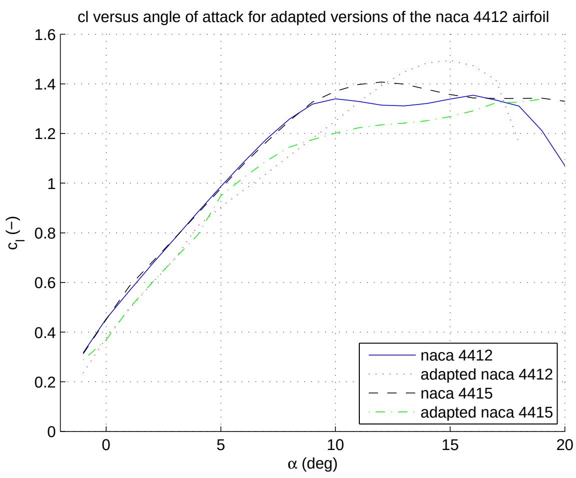

Figure B.3: Lift polar for adaptations of Naca 4412 airfoil

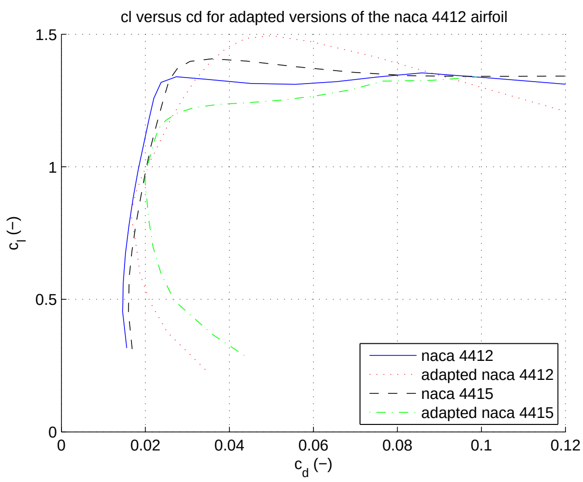

Figure B.4: Drag polar for adaptations of Naca 4412 airfoil

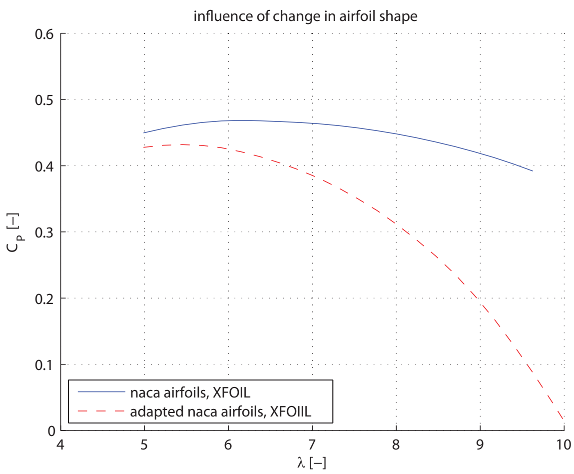

Figure B.5: Influence of change in airfoil shape on $C_P - \lambda$

Appendix C

Rotor drag measurements

To explain the differences between the BEM calculations and the wind tunnel experiments, a drag measurement is performed on the rotor. For this the rotor is rotated by hand until it reaches a rotational speed of about 150-200 rpm, and then the rotor is released and free to rotate. Because there is no driving force anymore, the rotor will slow down. From the deceleration of the rotor the total drag of the rotor can be derived. This measured drag can be compared with the drag that was calculated using BEM.

The calculation of the drag from the BEM model and airfoil properties is discussed first. This is followed by a description of the drag measurement. The difference between these two methods is used in chapter 5.

Drag calculation

The calculated drag of a single blade $D_{blade,c}$ can be calculated using the following equation:

$$D_{blade,c} = \sum_{r=R_r}^{R_t} \frac{1}{2} \cdot C_d(r) \cdot \rho \cdot U_{eff}(r)^2 \cdot c(r) \cdot dr \tag{C.1}$$

In which $C_d(r)$ is the drag coefficient at radius r, ρ is the air density, U_{eff} is the effective blade velocity, $c(n)$ is the chord at radius r and dr is the span of the blade element. The drag is calculated for the elements from the blade root radius R_r to the blade tip radius R_t.

The drag coefficient C_d can be read from the $\alpha - C_d$ graph of the Naca 4412 and Naca 4415 airfoils. Because $U = 0$ m/s, the following holds for the effective velocity U_{eff} and the angle of attack α:

$$U_{eff}(r) = \omega \cdot r \tag{C.2}$$

$$\alpha = -\theta \tag{C.3}$$

In Table C.1 the blade angle distribution for the actual blade geometry of the HP rotor is given. The drag characteristics are obtained from Hageman [Hageman, 1980] and can be found in Figure C.1. For an angle of attack smaller than -7° no C_d data was available, and therefore an extrapolation is made. This extrapolation is based on the shape of the drag polar from an airfoil series that has a very similar geometry as the Naca 44 series, which are the GOE 623 and GOE 624 airfoils [Hageman, 1980]. The extrapolation is shown in Figure C.1 as well. The extrapolated values are only used for the two blade sections closest to the root, as shown in Table C.1.

In Table C.1 the resulting drag distribution at a rotational speed of 300 rpm is shown. The total drag for one blade is 0.47 N.

The distance from the rotor axis at which the resultant of the drag force acts is r_{drag} and can be derived from the drag distribution and is:

$$r_{drag} = \frac{\sum_{r=R_r}^{R_t} d(r) \cdot r}{D_{blade,calc}} = 0.56 \tag{C.4}$$

Table C.1: Drag distribution calculated for the Hugh Piggott rotor with measured geometry, for $\omega = 300$ rpm

r [m]	c [m]	θ_m [°]	airfoil	θ [°]	C_d [-]	$d(r)$ [N]
0.8625	0.054	2.0	Naca 4412	0.2	0.032	0.057
0.7875	0.061	2.3	Naca 4412	0.5	0.033	0.056
0.7125	0.069	3.0	Naca 4415	1.2	0.034	0.053
0.6375	0.076	4.1	Naca 4415	2.3	0.035	0.048
0.5625	0.084	5.5	Naca 4415	3.0	0.037	0.044
0.4875	0.091	7.2	Naca 4415	4.7	0.044	0.042
0.4125	0.099	9.6	Naca 4415	7.1	0.054	0.040
0.3375	0.106	12.7	Naca 4415	10.2	0.12	0.065
0.2625	0.110	16.0	Naca 4415	13.5	0.18	0.061
					Total drag $D_{blade,calc}$ [N]	0.47

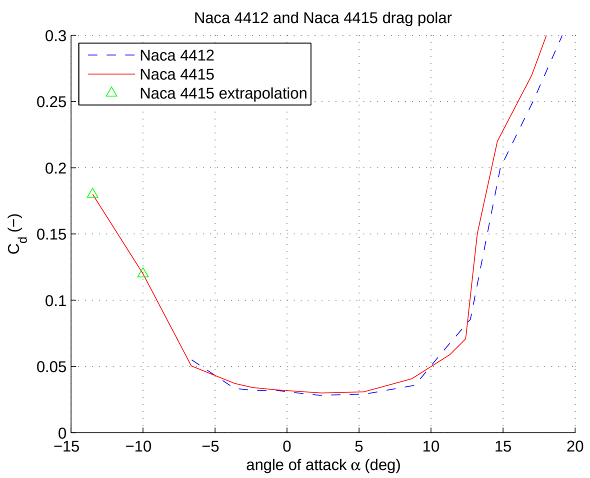

Figure C.1: Naca 4412 and Naca 4415 drag polar, obtained from [Hageman, 1980]

Drag measurements

The measured rotor drag for one blade $D_{blade,m}$ can be obtained from the blade deceleration $a_{rotor,m}$ at zero wind in the following way:

$$D_{blade,m} = m_{blade} \cdot a_{rotor,m} \tag{C.5}$$

$$a_{rotor,m} = \frac{d\omega \cdot r_{drag}}{dt} \tag{C.6}$$

where m_{blade} is the mass of one blade, which is 1 kg. The deceleration of the rotor is $\frac{d\omega}{dt}$, which is measured in the experiment.

In Table C.2 the first (rough) measurements that have been measured in between experiment 1 and 2 is shown. For this measurement only a stopwatch and a tachometer are used, so accuracy is limited.

To match the experimental results and BEM theory, an extra measured drag of approximately 1.6 times the calculated drag would be required. In terms of deceleration of the rotor this would mean a deceleration of 0.72 m/s^2, using Equations C.6 and C.5. Looking at Table C.2 the measurement results are within the same range. Considering the accuracy of the drag measurement, it can be assumed that it is likely that this extra drag is the main cause of the difference between BEM and the measurements. The drag measurements are within the same range of the expected drag. Therefore the BEM model can be used as a design tool in the rest of the thesis.

Table C.2: Rough deceleration measurement of the Hugh Piggott rotor

ω_1 [rpm]	ω_2 [rpm]	Δt [s]	a [rpm/s^2]	a [m/s^2]
195	125	5.2	13.5	0.77
192	140	4.2	12.4	0.71
185	130	4.7	11.7	0.67
198	135	4.6	13.7	0.78
160	108	5.1	10.2	0.58
165	120	4.0	11.3	0.64
170	110	5.8	10.3	0.59
185	98	8.1	10.7	0.61
190	112	6.3	12.4	0.71

During experiment 2 the deceleration of the rotor was measured more accurately, using the measurement set-up of experiment 2. The result of several measurements is presented in Figure C.2. From this figure the deceleration at 300 rpm can be extrapolated and amounts 14.1 rpm/s^2 or 0.8 m/s^2 at r_{drag}. This would mean an extra drag of 1.75 times the calculated drag in BEM.

The static drag in the bearings is measured by hanging a weight at the tip of the blade and finding the distance to the root at which the blade just starts rotating. This start up torque amounts $Q_{start-up} = 0.05$ Nm, or drag force on 1 blade of 0.03 N, using r_{drag}. When this drag also included in the comparison, the extra drag is 1.8 times the drag calculated in BEM. This value will be used in Chapter 5 to compare the results of the measurements and calculations.

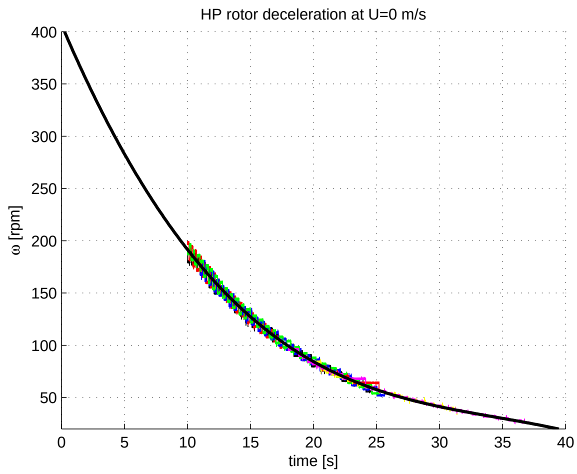

Figure C.2: Deceleration measurement of the Hugh Piggott rotor during experiment II

Appendix D

Effect of changes in experimental set-up

In this appendix the effects of small changes in measurement set-up that are applied throughout the experiments are shown. From the figures below it can be observed that none of the changes in measurement set-up has a significant effect on the power output.

In Figure D.1 the effect of the presence of the tail is shown. During the prony brake measurements (to test rotor performance) and dummy load measurements at fixed wind speeds (to test generator efficiency) the tail was not present. This could have caused a change in output power due to the blockage effect of the tail vane in the wind, but the results show that the effect is not significant.

In Figure D.3 the effect of the blockage due to the presence of the prony brake pipes that protect the rope against the wind is shown. These measurements are performed with the dummy load measurement set-up, at fixed dummy load resistances.

Figure D.4 shows the effect of the difference in position of the rotor in the tunnel jet between experiment 1 and 2. In experiment 1 the tower was centered in the tunnel exit, whereas in experiment 2 the rotor axis was centered, which creates a change in position of 11 cm. The results show that this does not have a significant effect on power output.

The effect of the use of two different prony brake pulley sizes is shown in Figure D.5.

In Figure D.6 the effect of heating up the bearings on the power output is shown. When the bearings are heated up due to the rotation of the rotor, the friction in the bearings could decrease and therefore output power could increase. Therefore the difference in power output at the start of rotation and after 15, 30 and 60 minutes is measured. There is no significant effect measured.

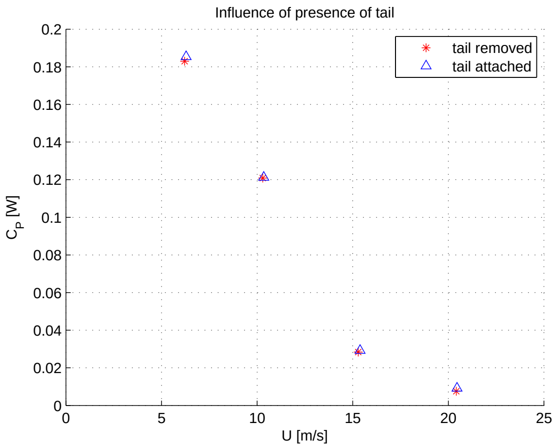

Figure D.1: influence of tail at different wind speeds and yaw angles

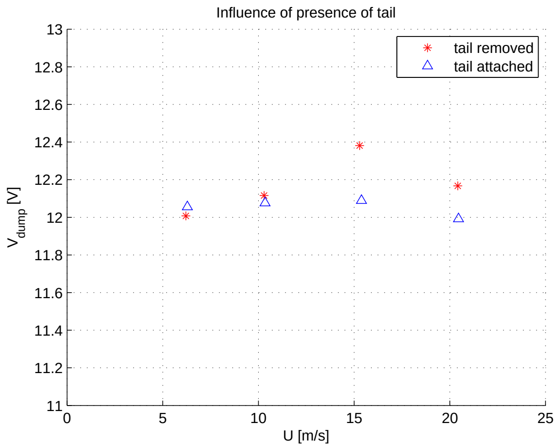

Figure D.2: influence of tail at different wind speeds and yaw angles

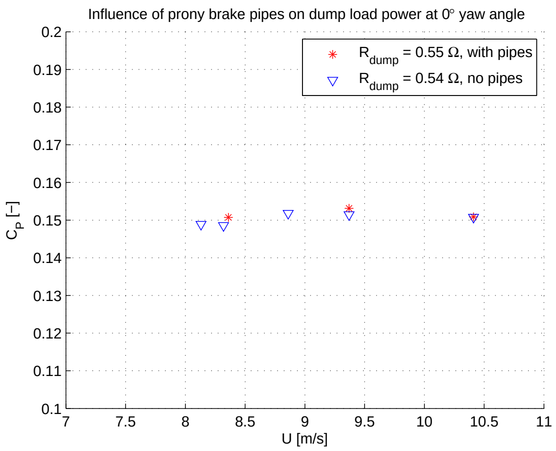

(a) $\gamma = 0$ deg

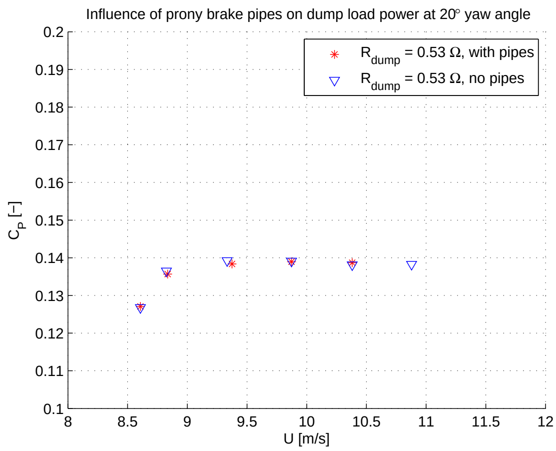

(b) $\gamma = 0$ deg

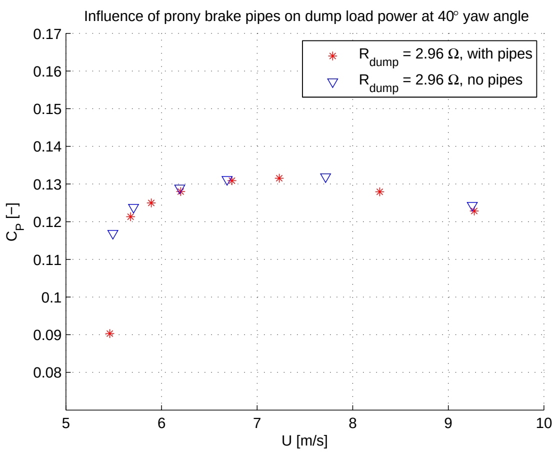

(c) $\gamma = 0$ deg

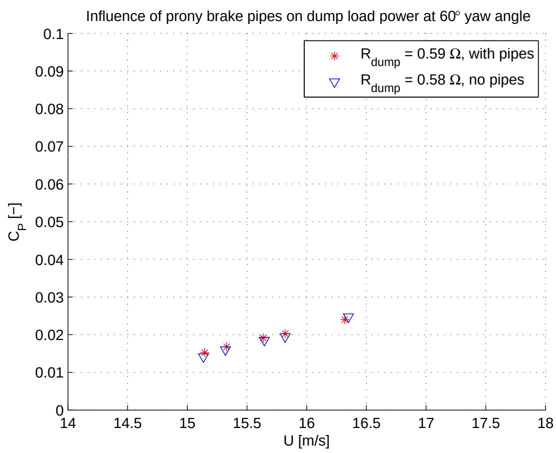

(d) $\gamma = 0$ deg

Figure D.3: Influence of rotor blockage due to presence of prony brake pipes at different yaw angles, C_P is derived from dump load power P_{dump}, measured at fixed resistances R_{dump}

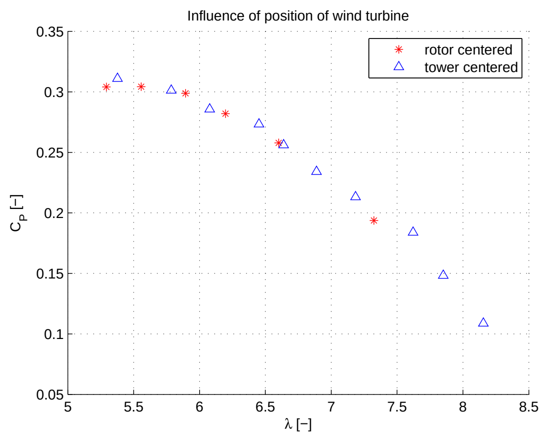

Figure D.4: Influence of position of wind turbine

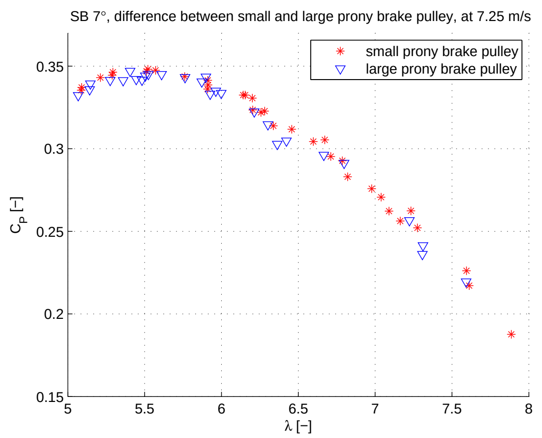

Figure D.5: Comparison of measurement sets using the small and large prony brake pulley

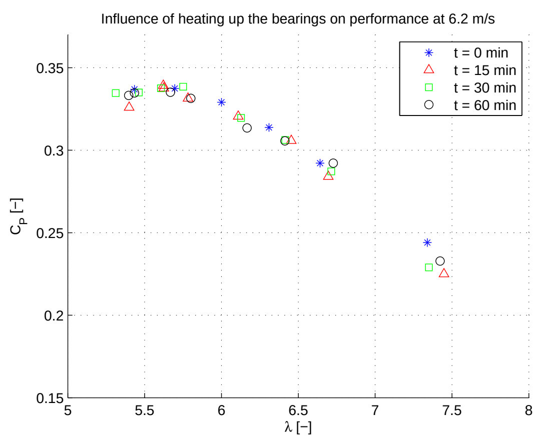

Figure D.6: Influence of heating up the bearings

Appendix E

Remaining results

In this chapter the remaining results, not discussed in the rest of the report, are given.

In Figures E.1 and E.2 the maximum aerodynamic performance at each yaw angle is presented as a function of wind speed. These figures are supplement the measurement results shown in Figures 4.8 and 4.9 and show that power is increasing for decreasing yaw angle.

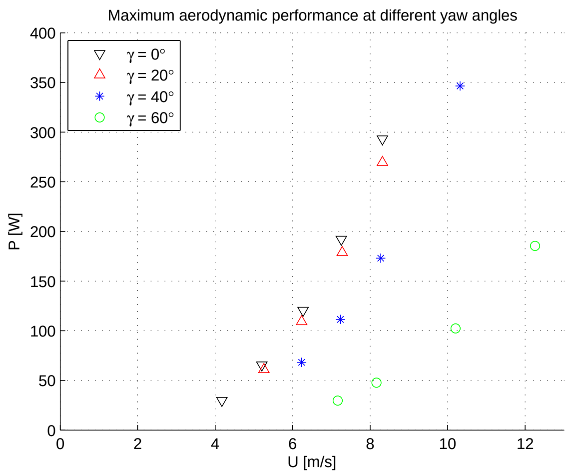

Figure E.1: maximum $P - U$ at for different yaw angles

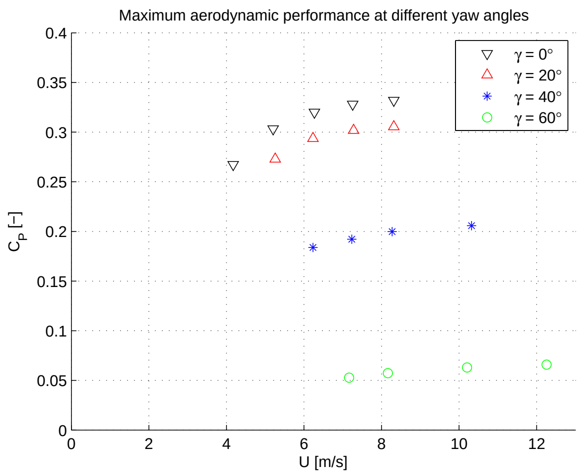

Figure E.2: maximum $C_P - U$ for different yaw angles

During experiment 1 the total performance of the wind turbine at fixed yaw angles was also measured for constant dump load resistances. This imposes a different load on the wind turbine, so the power curves have a different shape.

In Figure E.3 the $C_P - \lambda$ of the dump load at 0° yaw for different resistances is shown. From this figure it is clearly visible that different resistances represent different wind turbine loadings.

From Figures E.4 to E.7 the difference in behaviour for different loads (resistances) is clearly visible. From this it can also be concluded that a battery load, which changes in resistance for different ω, is a more efficient load for the wind turbine. Because of the change in resistance the power curve follows the optimum λ much better.

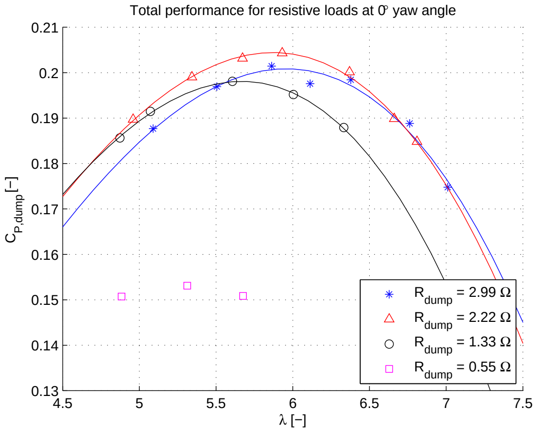

Figure E.3: $C_{P,dump} - \lambda$ at constant dump load resistances for $\gamma = 0°$

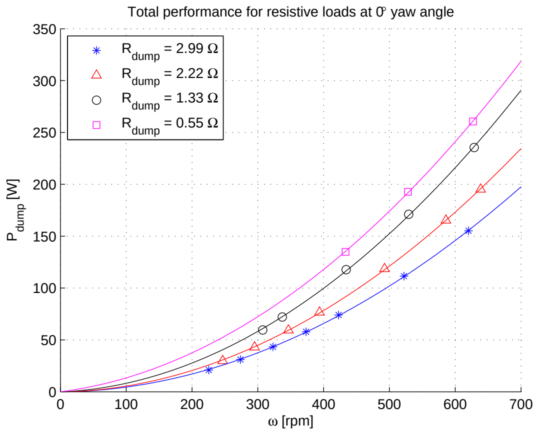

Figure E.4: $P_{dump} - \omega$ at constant dump load resistances for $\gamma = 0°$

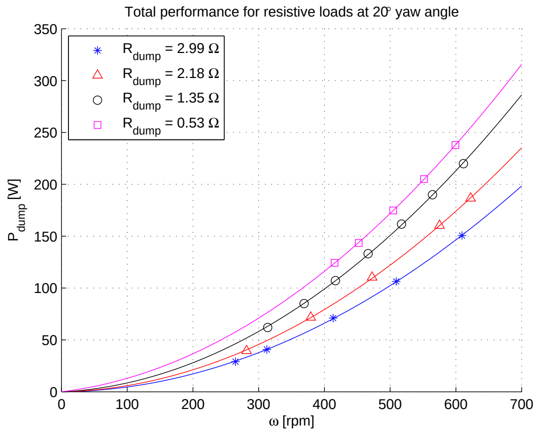

Figure E.5: $P_{dump} - \omega$ at constant dump load resistances for $\gamma = 20°$

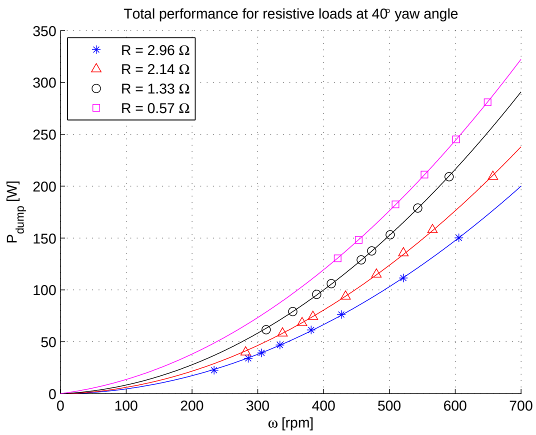

Figure E.6: $P_{dump} - \omega$ at constant dump load resistances for $\gamma = 40°$

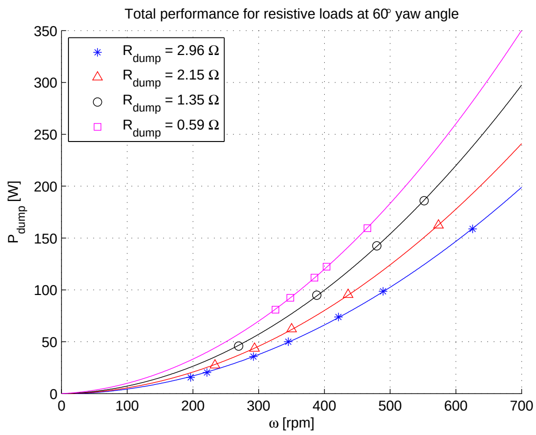

Figure E.7: $P_{dump} - \omega$ at constant dump load resistances for $\gamma = 60°$

Appendix F

Sound measurements

This appendix contains a description of the sound measurements that are performed on the original rotor and the new rotor design. First a general explanation of sound issues on wind turbines is given. After that the sound measurements are described and the results are given.

Wind turbine noise

When a wind turbine is to be placed in the proximity of human activity, it is important to consider the sound caused by the turbine. Noise is defined as any unwanted sound. For small wind turbines in rural areas of developing countries noise is not expected to be a major issue. However, for the completeness of this study and to ensure the relevance to other locations in higher populated areas, sound measurements are part of the study.

There are several sources that generate sound of the small wind turbines that are subject of this study, that can be divided into two categories:

1. Mechanical sounds, from the interaction of turbine components
   These sources include the bearings in the hub, the yaw bearing and tail bearing

2. Aerodynamic sounds, produced by the flow of air over the blades

For small wind turbines noise is largely a function of tip speed and blade shape. Especially near the tip the shape of the wind turbine matters, since here the speed is highest. Like many other wind turbines this wind turbine operates at variable tip speed ratio. Therefore, as wind speed increases so does the tip speed and the noise.

It is important to distinguish between the various measures of the magnitude of sounds: sound power level and sound pressure level. Sound power level is a property of the source of the sound and it gives the total acoustic power emitted by the source. Sound pressure is a property of sound at a given observer location, which can be measured by a single microphone [Rogers et al., 2006].

For this thesis only the sound power level will be considered. The sound level will be expressed in dBA, which is a standard weighting filter used to emphasize the freqencies where the human ear is most sensitive. Figure F illustrates the relative magnitude of common sounds on the dBA scale [Rogers et al., 2006]. In the Netherlands a sound pressure level of 40 dBA outside a house is an acceptable sound level during the night.

To determine the sound level at a certain distance from the wind turbine, a hemi-spherical spreading with a correction for atmospheric absorption is usually assumed [Burton et al., 2001]. This spread gives a reduction of 6 dBA per doubling of distance, when the turbine is located in flat open field.

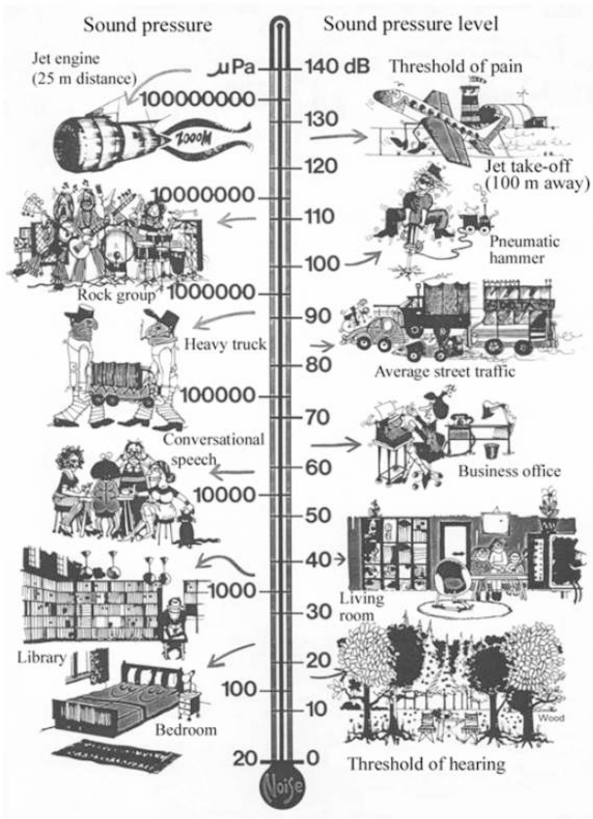

Figure F.1: Common sound pressure levels [Rogers et al., 2006]

Sound level measurements

During experiment 2, described in Chapter 8 the sound pressure level of both the Hugh Piggott (HP-round) turbine and the straight bladed (SB) turbines are measured under several operational conditions. In this section the measurement-set up and results of the experiments are described.

The measurements are performed with a Bruel and Kjaer (type 2231) Modular Precision Sound Level Meter. This meter gives the RMS values of the sound pressure level at the location of the meter in dBA.

The sound measurements are performed during seperate wind tunnel tests in the Open Jet Facility (OJF) wind tunnel, in which the rotor is operated at different conditions, ranging from U =4 to 8 m/s and from ω =400 to 600 rpm. The measurements are performed at different locations in the wind tunnel, at 2, 4 6 and 8 m distance from the rotor center. See Figures F.2 and F.3 for the locations of the measurements.

The sound measurements for the Hugh Piggott rotor are performed on the HP-round rotor. For the straight bladed rotor the sound measurements are performed on different configurations. However, regarding the very small differences in performance that were shown in Figure 8.5, the differences in sound production between these configurations are assumed to be negligible.

In the measurement set-up not only the wind turbine produces sound, but also the wind tunnel itself. This background noise should be cancelled out to make a fair comparison at different wind speeds. When incoherend sound sources are assumed, the total sound pressure level (in dBA) is calculated by using Equation F.1 [Burton et al., 2001].

$$L_p = 10 \log_{10} \sum_{i=1}^{N} 10^{L_{pi}/10} \tag{F.1}$$

In Figures F.2 and F.3 the sound pressure levels at different locations of the wind turbine, corrected for background noise, are shown. The background noise of the wind turbine is shown in Figure F.4.

To be able to compare the sound levels of the different turbines and operational conditions with each other, the measurements at the center positions downwind and upwind of the turbine are shown in Figure F.5. The results of this figure are discussed in Section 8.5.4.

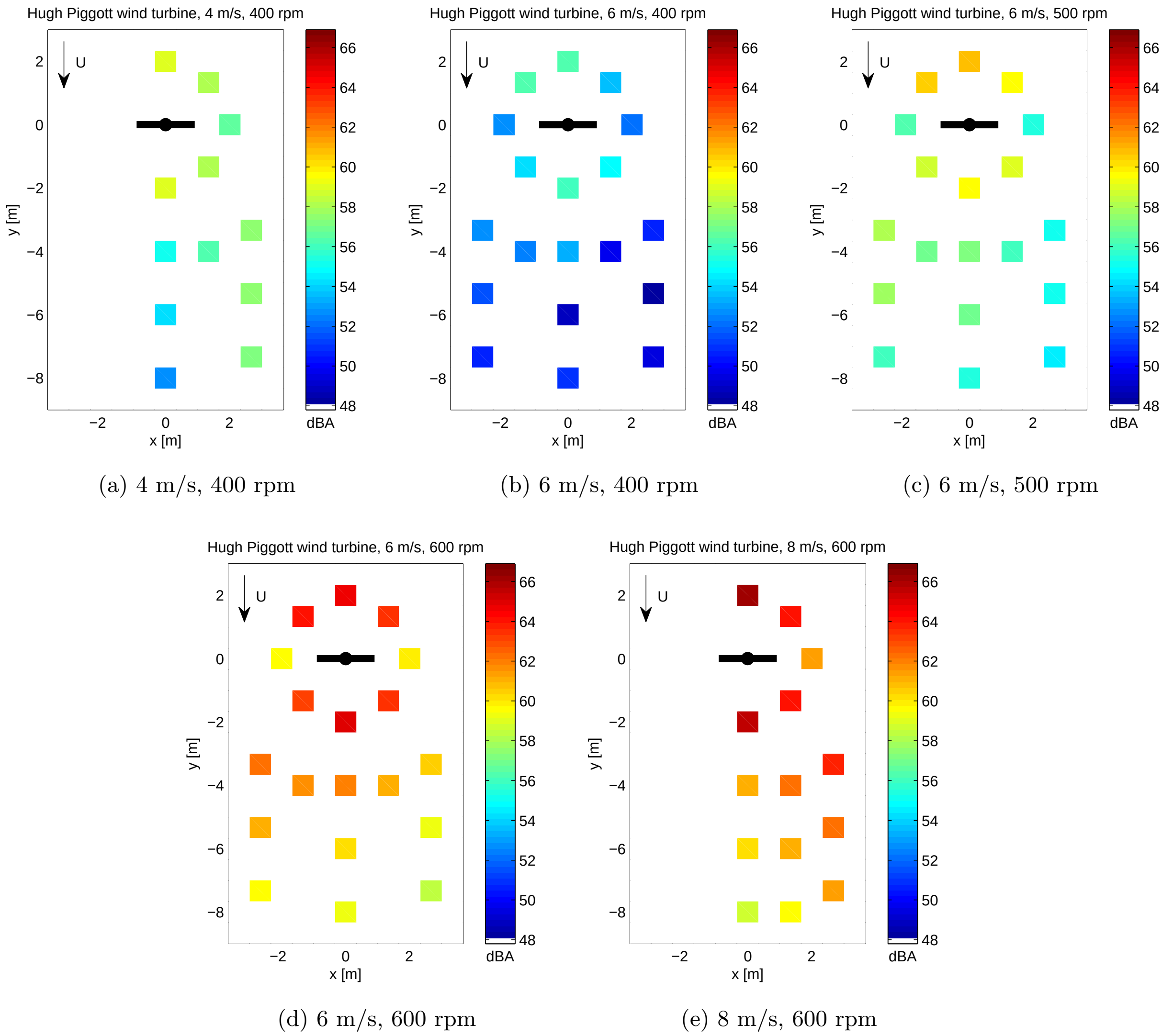

(a) 4 m/s, 400 rpm (b) 6 m/s, 400 rpm (c) 6 m/s, 500 rpm

(d) 6 m/s, 600 rpm (e) 8 m/s, 600 rpm

Figure F.2: Sound level measurement for the HP-round rotor, corrected for background noise

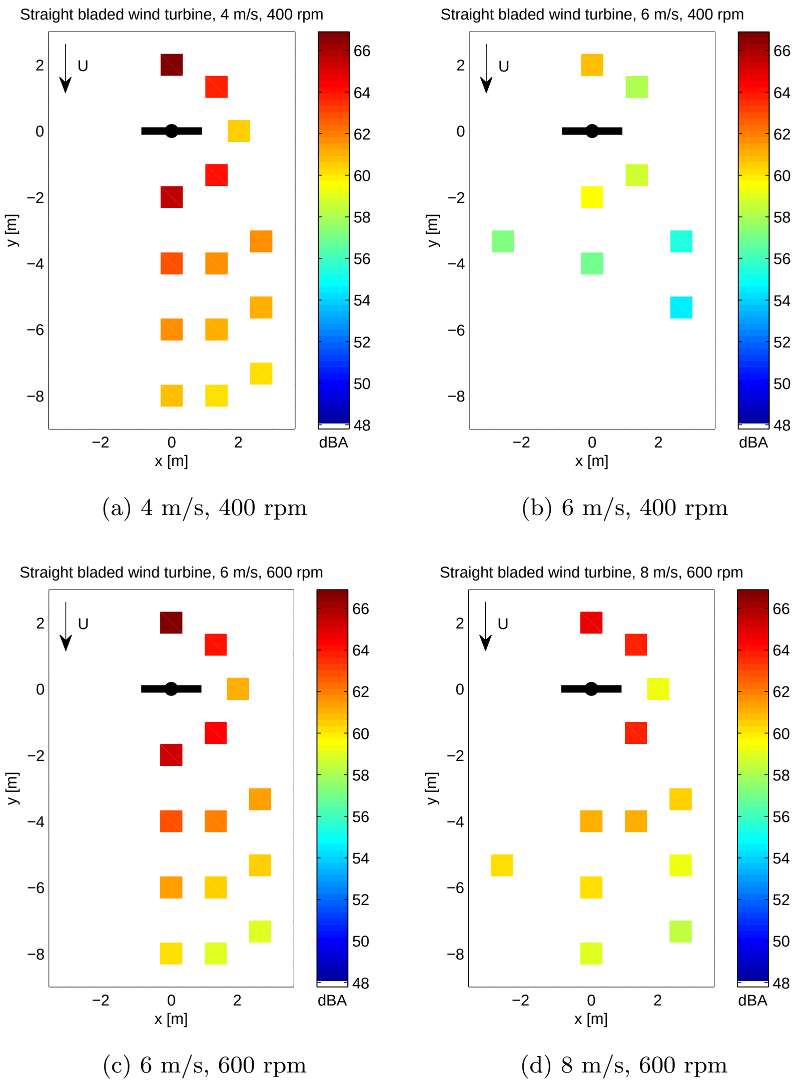

(a) 4 m/s, 400 rpm

(b) 6 m/s, 400 rpm

(c) 6 m/s, 600 rpm

(d) 8 m/s, 600 rpm

Figure F.3: Sound level measurement for the SB rotor, corrected for background noise

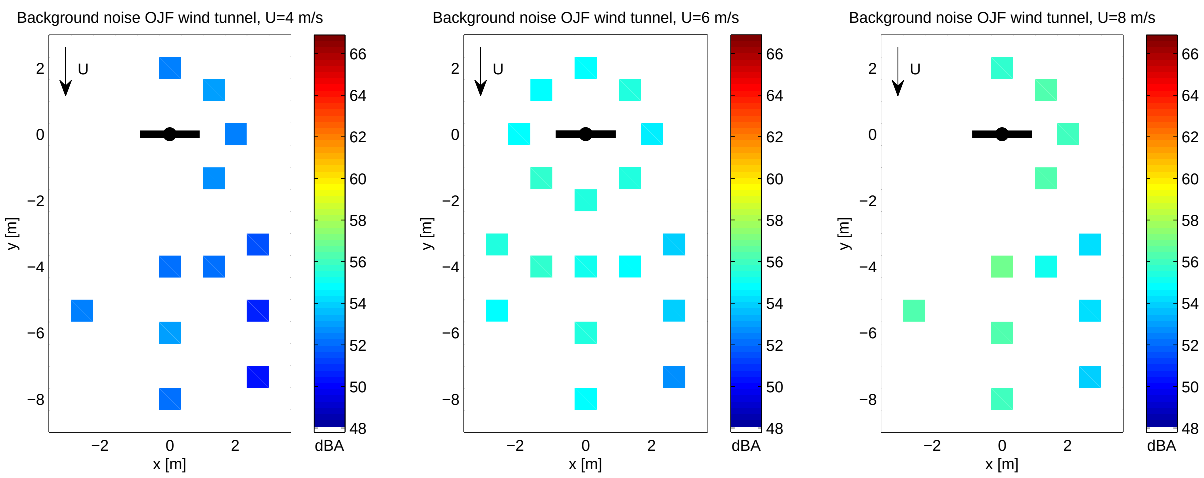

(a) 4 m/s (b) 6 m/s (c) 8 m/s

Figure F.4: Background sound measurements for the OJF wind tunnel (wind turbine present but not rotating)

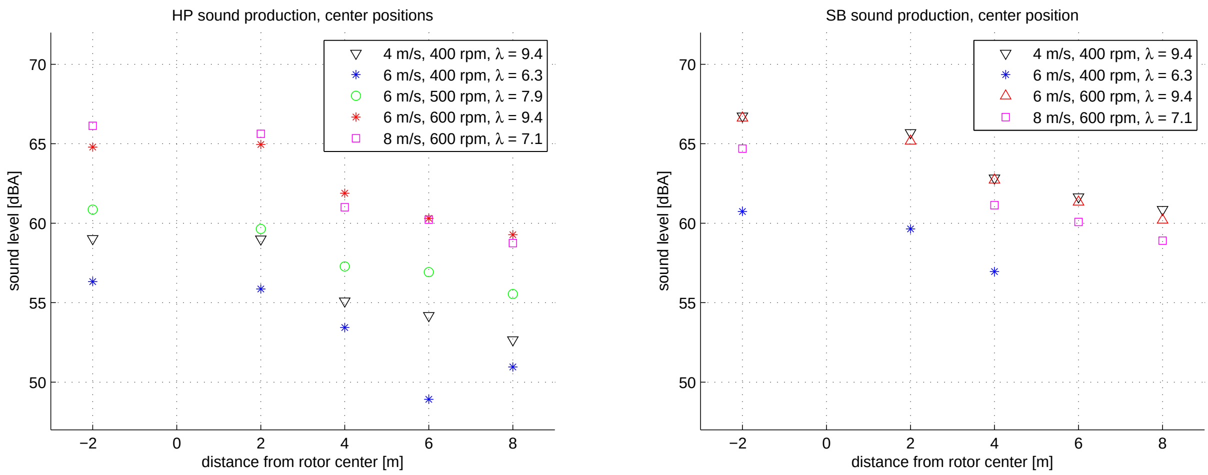

(a) HP rotor (b) SB rotor

Figure F.5: Sound level measurement at center positions upwind and downwind of rotor axis, corrected for background noise

Appendix G

Blade manufacturing manual for the new rotor design

In this appendix the blade manufacturing manual for the new rotor design presented in this thesis is given. This rotor is an alternative for the Hugh Piggott rotor that can be found in the manual [Piggott, 2008]. The dimensions for the 1.8 m and 3.0 m rotors are given in Table G.1

In the manual only the symbols for the distances are given. The values, corresponding to a the 1.8 m rotor that was constructed for this thesis, can be found in the next section. In Table G.1 the dimensions for both a 1.8 m and a 3.0 m turbine are given. The manual given in this appendix is made for the 1.8 m rotor. The only difference in the production process for the 3 m rotor is that the extra blade width at the root is not necessary. For the 1.8 m rotor this was necessary to be able to make the 4 holes for the hub in the 3 blades. Since for the 3.0 m design the chord length is already 110 mm, making the 4 holes will not give a problem. Therefore the blade can have this chord length over the entire blade length, which saves wood and therefore reduces costs.

To make the Naca 4412 airfoil profile shape in the blade, the template that is given in the manual can be used.

Table G.1: Straight blade rotor dimensions for different rotor diameters, all dimensions are given in [mm]

turbine diameter	1800	3000
blade length R	900	1500
wood length L	950	1550
blade width W	100	110
minimum wood thickness H	25	30
chord C	80	110
M	150	150
N	75	75
B	67	73
A	33	37
D	10	12
airfoil thickness T	10	14
a1	10	14
a2	3	4
a3	24	33
blade angle θ	7°	6°

1

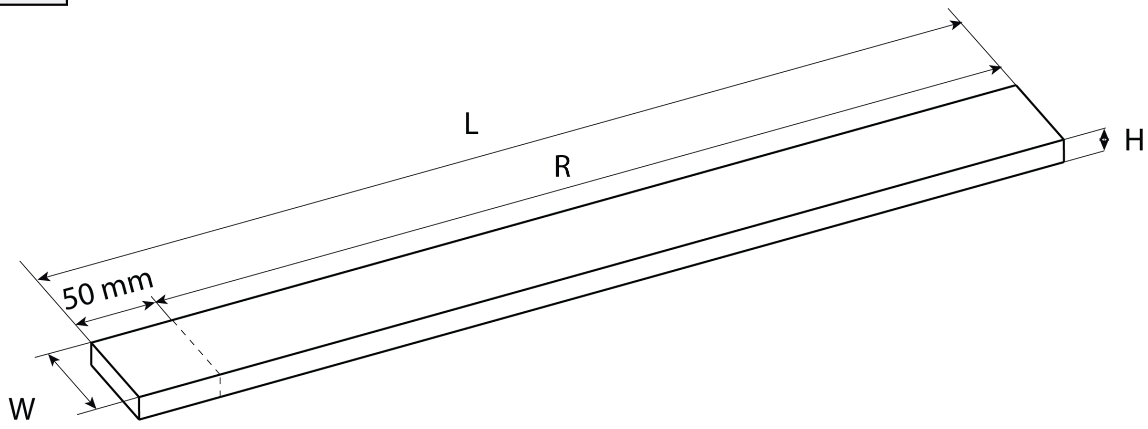

2

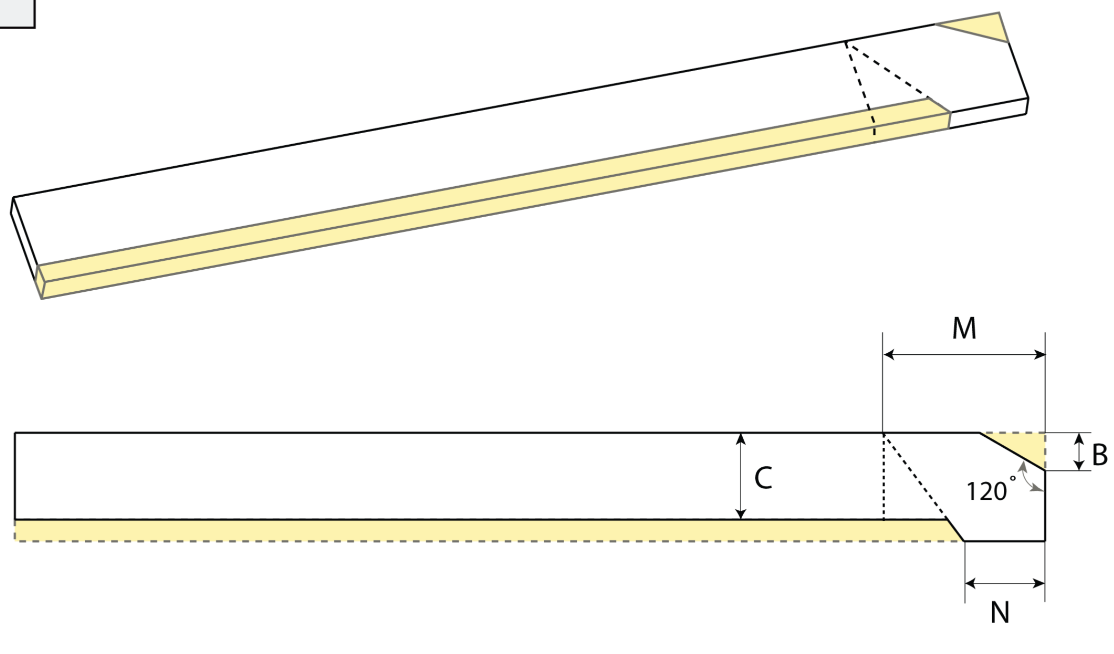

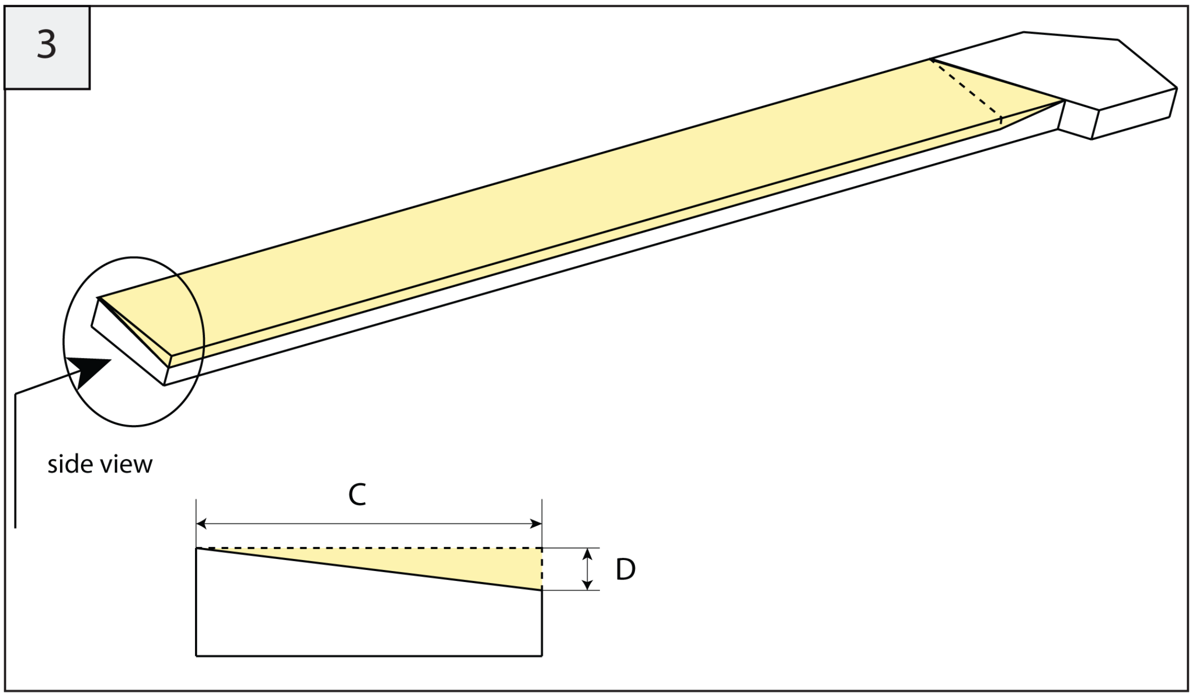
3
side view
C
D

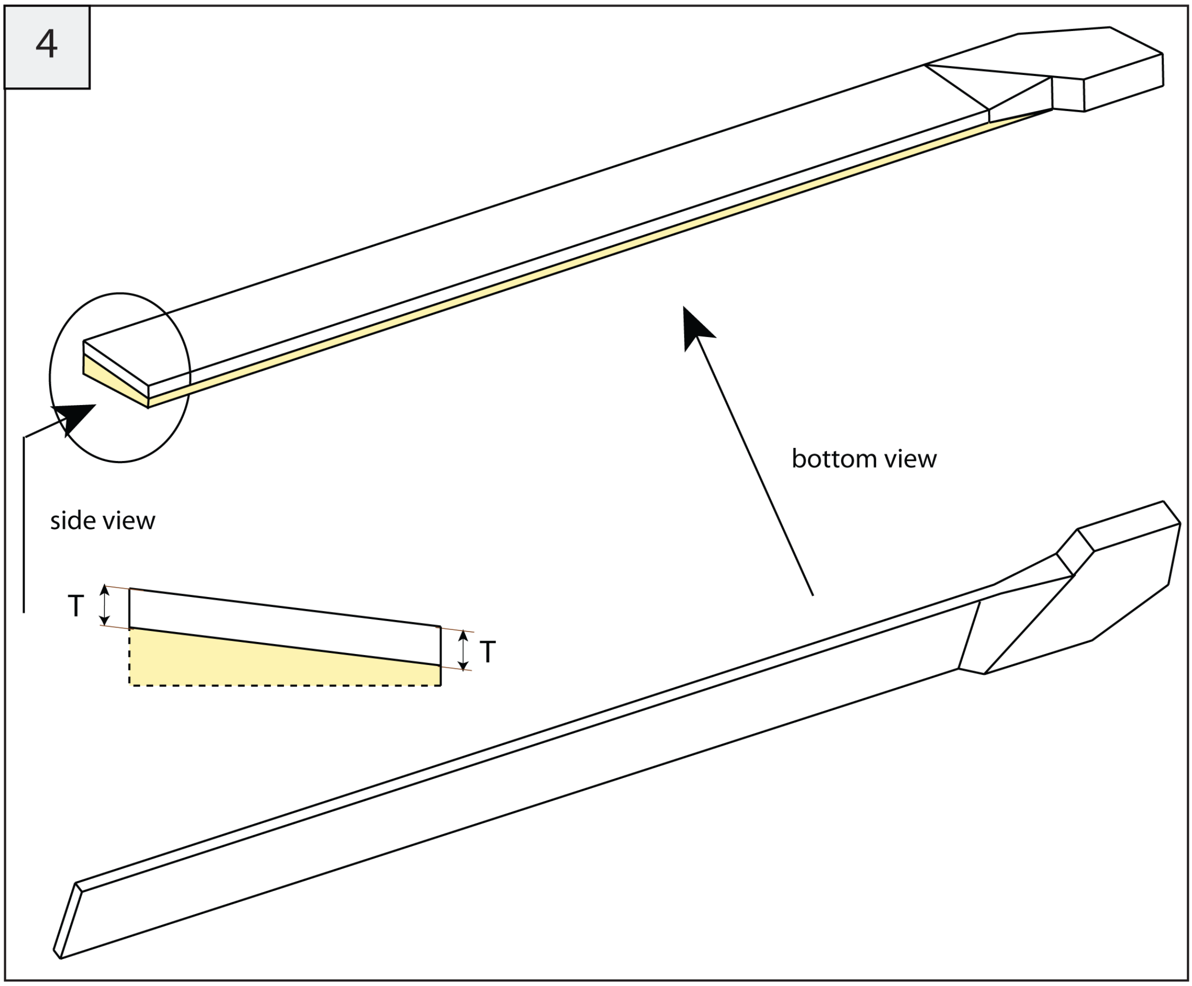
4
side view
T
T
bottom view

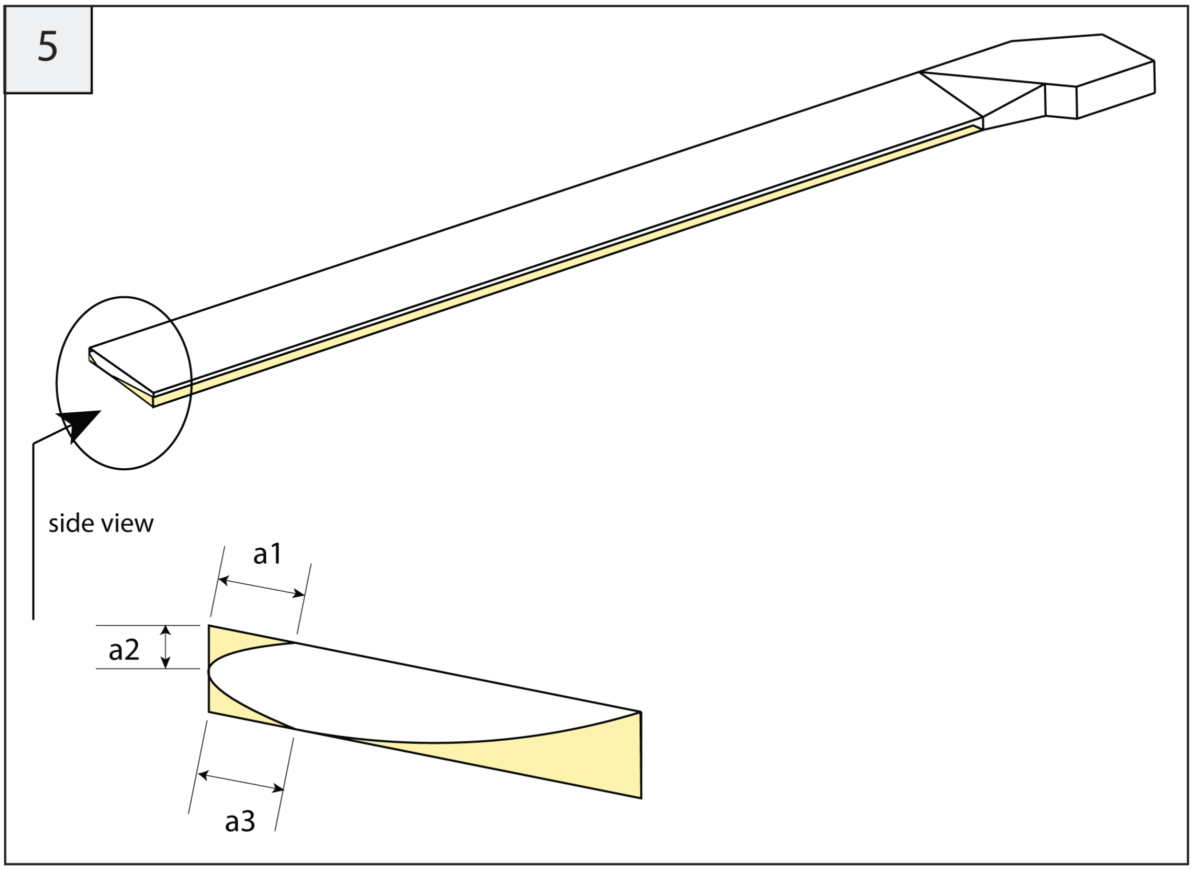
5
side view
a1
a2
a3

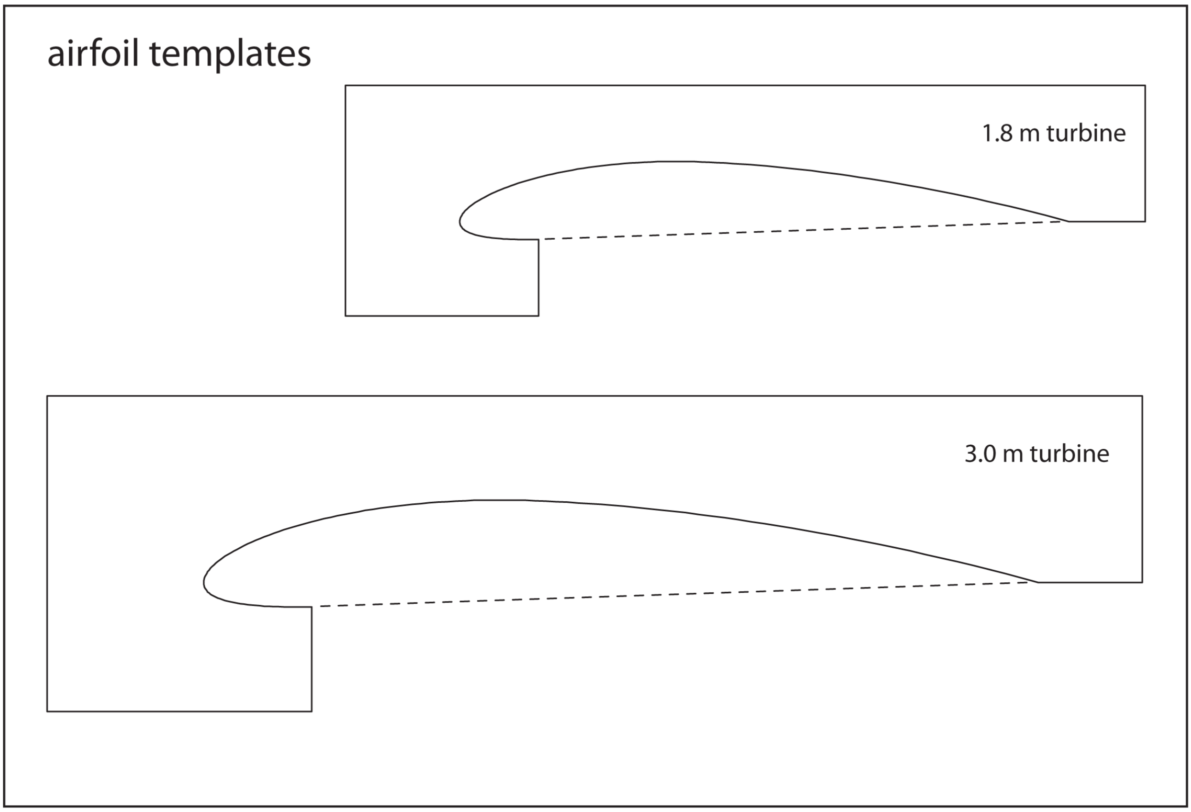
airfoil templates
1.8 m turbine
3.0 m turbine